PREDICTION OF THE VARIABILITY OF SOIL DEPTH USING QUALITATIVE AND QUANTITATIVE GEOMORHOLOGICAL INFORMATION: SIERRA NEVADA, CA, USA

A Dissertation

by

ANIELA ORIANA CHAMORRO LOPEZ

Submitted to the Office of Graduate and Professional Studies of
Texas A&M University
in partial fulfillment of the requirements for the degree of

DOCTOR OF PHILOSOPHY

Chair of Committee,	John R. Giardino
Co-Chair of Committee,	Bradford Wilcox
Committee Members,	John Vitek
	Burak Guneralp
Head of Department,	Michael Pope

May 2016

Major Subject: Geology

ABSTRACT

The variability of soil depth at the catchment scale is an essential input for environmental modeling. If the model requires high resolution inputs, the inherent variability of soil depth in granitic and forested regions poses a challenge to capture representative values. To help to address this problem, I propose that, in soil studies, qualitative and quantitative geomorphological information at the catchment scale should be used as inputs of soil-landscape models. Qualitative information is presented as a geomorphological map, and quantitative data are generated by algorithms applied to the high resolution digital elevation model.

In this dissertation, the term soil depth is used to mean the weathered subsurface layers composed of mobile regolith and saprolite. Measurements of soil depths obtained from 204 hand drillings until refusal, and 6,645 estimations of depths collected using ground penetration radar (GPR) were compared, Alone, the hand drilling data showed lack of autocorrelation, however, a significant correlation was found between GPR and auguring measurements ($r=0.9$, $p<0.001$), validating this method to capture the spatial variability in a continuum. Therefore, GPR resulted to be a valid, inexpensive and quick tool to survey soil depth in this complex environment.

Contrasting several geomorphological variables and measurements of soil depths, significant correlation with lineaments, slope and wetness index suggest that geomorphology is a significant factor in the distribution of soil depths at the catchment scale in this environment. This relationship was then assumed for modeling the soil

depth in a catchment scale. Because the linear regression model and geostatistical methods are not valid approaches for the available sampling design, the use of a simple soil-landscape model, based in the work of Dahlke et al. (2009), is proposed to map the measurements of soil depths to a catchment scale. Indeed, the main strength of this model lies in its independence of sampling design. The resultant prediction maps at different resolutions showed the importance of selecting an appropriate scale of work and adjust the density of GPR survey in the performance of predictions.

ACKNOWLEDGEMENTS

I owe special thanks to my committee chair, Dr. John R. Giardino. He supported my ideas, keeping me on track, but respecting my independence. His academic and personal advices were invaluable. I am also very grateful to my co-chair, Dr. Bradford Wilcox, by his critical advice and stimulating discussions. Special thanks go to my committee members, Dr. John Vitek and Dr. Burak Guneralp for their academic guidance and innumerable reviews. I also want to thank Dr. Mark Everett for sharing his practical and academic knowledge of geophysics, and Dr. Hongbin Zhan for including me as one of his team.

I am very grateful to CZO Southern California, especially to Matt Meadows, whose team drilled 200 soil samples by hand. Matt was also crucial in field-work logistics. Field work would have not been possible without Carol Chamorro. I also thank Brad Weymer and Tim De Smet for technical support with GPR tools. I also would like to thank Phil Rumford and his group at IODP for their support and friendship. I also thank to all Chileans, who sponsored my work thought CONICYT; and I also grateful to the Fulbright program for making all this experience possible.

I would like to acknowledge all the support received from my family and friends during these years, and especially to my husband, my parents and sisters for all their wisdom. I would like to thank all my friends in College Station and Chile for their unconditional support, especially Alejandra, Priscilla, Marcela, Betty and Leslie. I would also want to thank Sevgi Cavdar, Kehua You, Bree McClenning, Tyler Depke, Carolyn

Sexton, Netra Regmi, Heo Joonghyeok, Jacob Hundl, Anna Ahlstrom, Tim Brunk, Adam Lee, Jinia Islam, Raquel Granados and Amy Price for being amazing fellow students. Finally but not less important, I would like to thank all my dharma friends, and specially David Khalil, Brett Warneck, Kim Diaz, Cathy, Lama Thinley, and Catherine Carrasco.

NOMENCLATURE

CZ	Critical Zone
CZO	Critical Zone Observatory
SSCZO	Southern Sierra Critical Zone Observatory
GPR	Ground Penetrating Radar
LIDAR	Light Detection and Ranging
DEM	Digital Elevation Model
GM	Geomorphological Map
USGS	U.S. Geological Survey
NED	National Elevation Dataset
GPS	Global Positioning System

DEFINITIONS

Weathering Zone	Group of subsurface layers that present some grade of weathering.
Weathering Front	Boundary separating solid, unweathered rock and rock that has already been weathered but remains still in situ (Migon, 2006).
Landform	A feature related to a process (or process-complex), usually composed of several elementary forms (Pike et al., 2009).
Landscape	Comprise human and physical attributes of a determined area (Pike et al., 2009).
Bedrock	Parent rock composed mainly by solid, unweathered rock.

Residual Soils	Soils formed from the weathering process of the parent bedrock.
Grus	Products of granite in situ, from the granular disintegration of coarse-grained rocks. Grus is a type of weathering mantle.
Saprock	Rock that has begun to weather, but only about 20-30% of the primary minerals are chemically altered Goudie, 2004, page. 909). Saprock is a fuzzy boundary between unweathered and weathered rock.
Terrain Attributes	Terrain properties computed from elevation values in a defined neighborhood of DEM points. Primary terrain attributes are derived from derivatives of the topographic surfaces, whereas secondary terrain attributes derived from primary attributes.
Soil Attributes	Physical and chemical properties of soil.

TABLE OF CONTENTS

LIST OF FIGURES

Page

LIST OF TABLES

Page

CHAPTER I

INTRODUCTION

Soil is a crucial portion of the structure of the critical zone, being the place where critical zone processes occur, and itself a product of these processes (Anderson and Anderson, 2010, page 164).

In this dissertation, the term soil refers to the subsurface material composed of mobile regolith and saprolite layers (Figure 1). Mobile regolith is the upper portion of the weathered mantle, where hillslope transport of regolith occurs. Correct differentiation of mobile regolith is especially important in mountain and forested regions because the processes of erosion and bioturbation are active in these environments. Saprolite is an unaltered material that forms from weathered rock but keeps its original rock structure (Anderson & Anderson, 2010, p.163). In other words, saprolite has not been displaced or mobilized by weathering, but it is sufficiently soft to be augured.

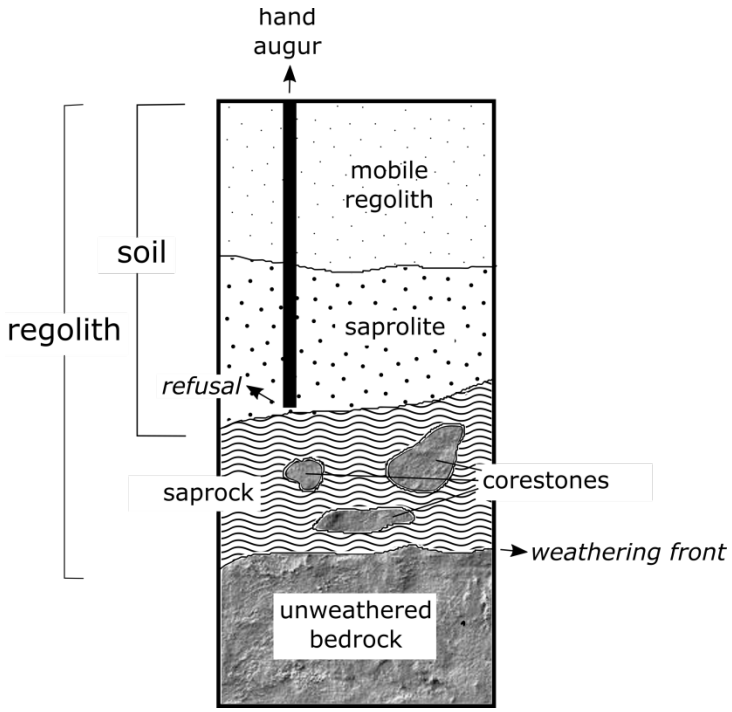

Figure 1. Definition of soil and other important terminology used in this dissertation. Based on Anderson & Anderson (2010, p. 164) and Migon (2006, p.57).

Problem Statement

Information about the spatial distribution of depths of soil is an essential input variable for environmental models, such as estimating water storage and water routing though the unsaturated zone (Quinn et al., 1991; Weiler and McDonnell, 2004), as well as determining soil-water capacity, deep drainage, preferential subsurface flow and linkage of hillslope- riparian flow (Katsuyama et al., 2005). Also, from a geomorphological point of view, depth of soil is a relevant variable to obtain the rate of the advance of weathering front (Anderson and P.Anderson, 2010; Dietrich et al., 1995; Heimsath et al., 1997), studies of slope stability and prediction of shallow landslides (Regmi, 2010; Yamakawa et al., 2012). At last, soil depth is key to studies about site

productivity, nutrient availability, root distribution and biomass production (Krüger et al., 2013).

Despite its importance, insufficient attention has been given to the thickness and position of soils because to obtain values of soil depth at the catchment scale is a challenge (Dahlke et al., 2009). Traditional auguring methods are laborious and expensive, whereas geophysical methods present a statistical constraint in the application of geostatistical methods, such as kriging. I hypothesized that a relationship between surface and subsurface patterns exists; and consequently, geomorphological information can be used to predict depth of soils at the catchment scale. The availability of airborne Light Detection and Ranging (LiDAR) as a free source, covering several areas of the United States, makes geomorphological analysis possible.

Therefore, the goal of this dissertation is to provide an understanding of the spatial variability of soil depth at the catchment scale based on the premise that soils are landscapes (Verstappen, 2011). Two main challenges were addressed: (1) the difficulty of direct measurement by drilling and (2) finding the appropriate spatial method of interpolation of data.

The area of study chosen to address these research problems was not selected at random. Providence is part of the Kings River watershed, a basin of 438,500 ha (Figure 2). Kings River is an important watershed for the San Joaquin Valley that in turn, is part of the Great Central Valley of California. Since irrigated agriculture began in the 1800s (Bolger et al., 2011), the Joaquin Valley system has been supplied a large value of surface and groundwater derived from Sierra Nevada Mountains. Although the

proportion of water supply derived from either groundwater or surface water has varied throughout time (Bolger et al., 2011), surface water flowing from the Kings River and the other watersheds is very important for agriculture and mining. Today, the San Joaquin Valley has significant water management concerns given the high-water demand for an increasing state population and for intense irrigation (Bolger et al., 2011).

Providence is located between 758 to 2,094 m in elevation, in a transitional altitudinal zone that experiences precipitation in form of snow and rain. In elevations higher than 1,700 m, precipitation is dominated by snow rather than rain (Bales et al., 2011a). This snowpack provides an important seasonal storage of water that Bales et al. (2011b) calculated to be in excess (30 cm) to the storage capacity of soils (20 cm) (i.e. the soil storage being 2/3 of the snow-water-equivalent). It is thought in this area that reducing forest cover by 40% could increase water yield by about 9% (Bales et al., 2011b). More specifically, Bales et al (2011) suggest that the increment of the water yield could result in a higher fraction of the precipitation, particularly snowmelt, leaving the mountain as runoff because forest thinning would reduce evapotranspiration (Bales et al., 2011b). What is not known, however, is which fraction of the water-pathways in the subsurface are dominant in this landscape: near-surface or deep drainage. If deeper drainage is an important fraction of the water retention in the catchment, the importance of evapotranspiration would be minor compared with the water storage and would release deep underground. To solve this puzzle, the location of the interface between soil, high and low permeable bedrock is key (Tague, 2008). Liu et al. (2012) found that

near-surface runoff contributes from 45% to 65% of annual streamflow, variation that depends of differences in soil depth in the different sub-catchments.

In this dissertation, the tools of geomorphological mapping and ground penetration radar are combined to predict depths of soil in Providence Catchment. This catchment is part of the National Science Foundation (NSF) network of the Critical Zone Observatories (CZO), who's goal is to contribute to understanding the surface processes occurring in the CZ. In particular, CZO Southern Sierra (SSCZO) primary research focus is the understanding of how the water cycle drives CZ processes. The position of the catchment in a snow-rain borderline in the elevation profile of the Southern Sierra Nevada also makes this place a laboratory to recognize the potential impacts of a climate warming.

Goals and Objectives

The goal of this dissertation is to obtain a spatial representation of depths of soil of the Providence Catchment and then to provide data for further hydrological studies. The focus of this dissertation is to evaluate the use of quantitative and qualitative geomorphological information to extrapolate point measurements of soil depth to a catchments scale. In addition, the use of GPR is tested as a valid tool for collecting information on soil depth.

The following specific objectives were established to reach this goal:

1. Construct a geomorphological map of the area of study;

2. Determine if a relationship exists between terrain attributes and direct measurements of soil depth;
3. Use and validate GPR as a tool for collection of data on soil depth; and
4. Construct and evaluate prediction maps of variations soil depths at different spatial scales.

Description of Dissertation

Under the scope of geomorphology, this dissertation presents a summary of regolith studies in the Critical Zone Observatory of the Southern Sierra Nevada. This work also pointed out the direction of future research and the current gaps of knowledge of the subsurface critical zone.

The four chapters of this dissertation are interrelated. Chapter I introduces the topic of this dissertation, and establish the problem statements and objectives. Chapter II begins with a description of the area of study, not a usual general description, but a visual and holistic assessment using geomorphometry and process geomorphological analysis. The results of Chapter II are then used in Chapter III to explore the relationship between surface expression and soil depth. Chapter IV includes a discussion of the use of GPR for collecting soil depth data. Finally, the last chapter summarizes the main points of this investigation and future directions of research.

CHAPTER II

GEOMORPHOLOGY OF PROVIDENCE CATCHMENT

This chapter describes the geomorphology of the area of study, which is used to conduct a geophysical survey in Chapter IV and in the construction of the model of soil depth in Chapter V. Some of the terrain attributes computed in this Chapter are also used in Chapter III.

Synopsis

The geomorphology of the Providence Catchment follows its regional trend, characterized by the presence of a repeated pattern of steps and treads, along with an abundant number of lineaments in the N and NE directions. The catchment is formed by three headwater catchments that show subtle differences in aspect, relief, foliation of the granodiorite present and patterns of vegetation. These differences are translated in the differences in the potential for erosion and susceptibility for mass movement.

As a descriptive tool, a combination of automated and manual classification of landforms is proposed to obtain a geomorphological map that identifies features and processes. The product of such a combination does not ignore the heterogeneity of the landscape to address complexity. This comprehensive approach is useful for prediction of soil attributes in soil-landscape models and the investigation of the critical zone in the horizontal direction.

Introduction

Reconnaissance of geomorphological units with relatively homogeneous geomorphological processes is the first step towards the spatial characterization of soil profiles. Quantitative soil-landscape methods are regularly applied to predict soil parameters from point observations to a landscape scale (McBratney et al., 2003; Minasny and McBratney, 2006). The spatial representation of geomorphic features and processes through geomorphology maps facilitates the applications of such methods.

Techniques employed to create geomorphological maps are becoming increasingly sophisticated (Dramis et al., 2011). The availability of high-resolution DEMs has enhanced the development of geomorphological studies towards the automated classification of landforms and the use of the capabilities of Geographic-Information-Systems (GIS) software (Gustavsson et al., 2008). Automated classification of landforms reduces the cost and time of production of maps compared with manual interpretations (Bue and Stepinski, 2006), but the disadvantage is the omission of the analysis of processes (Verstappen, 2011). Analysis of processes such, as diffusive transport of colluvial materials, are important for the investigation of the relationship between soil attributes and landscape position (Dietrich et al., 1995).

In the Providence Catchment and its surroundings, geomorphological descriptions are scarce. DeGraff (1994) has documented the physical geomorphology of debris flows in the Kings River drainage and Jessup et al. (2011) have discussed the origins of the stepped topography in the Southern Sierra. Although other studies have described weathering patterns (Holbrook et al., 2013) and mechanisms of landscape

evolution (Hahm et al., 2014), a simple, geomorphological description of features and processes present is missing.

Providence Catchment is highly instrumented and is the object of investigation of several Earth science disciplines (Anderson et al., 2012; Bales, 2011; Bales et al., 2011a; Field et al., 2015; Holbrook et al., 2013; Hunsaker et al., 2012; Johnson et al., 2011; Musselman et al., 2012). As a mental tool to synthesize geomorphic data, a geomorphology map may facilitate interdisciplinary or transdisciplinary efforts (Bocco et al., 2001).

The available high resolution, LiDAR- DEM provides an opportunity to detail field mapping and geomorphological description at a detailed scale (i.e, 1:15,000). This is especially relevant considering that the catchment, with an area of 2.5 km^2, is highly vegetated (Smith and Pain, 2009). This research develops a simple method of combining the benefits of automated and manual classification of landforms with the aim of producing a detailed geomorphology map that does not ignore features and processes at the scale necessary for soil and hydrological predictions. The map also is legible and simple enough to constitute a tool for scientific discussion in the Southern Sierra Critical Zone Observatory (SSCZO). To achieve these goals the following objectives must be met: 1) identify geomorphic units using an automatic system of classification; 2) build a geomorphological map of the area of study; 3) obtain terrain attributes from the LIDAR data set; and 4) describe the geomorphology of the area of study.

Area of Study

Providence Catchment is located along the Southwestern slopes of the Sierra Nevada, CA (37.068^{o}N, 119.191^{o}W), 53 km northeast from the city of Fresno (Figure 2). Minimum elevation in the catchment is 758 m whereas its maximum is 2,094 m. The dominant aspect direction is south-west (Hunsaker et al., 2012) and its area is approximately 2.8 km^2 (~380 ha).

Providence catchment contains three sub-catchments, identified by the SSCZO as P301, P303 and P304 with respective areas of 99, 132 and 49 ha. P302 is named in this work as the confluence of the three small sub-catchments.

Geology

The Sierra Nevada Mountains were formed in the Nevadan orogeny during the Jurassic Period (Chernicoff and Venkatakrishnan, 1997). Nonetheless, the uplift of the region began in the mid-Tertiary, with the greatest rate of uplift occurring during the Pliocene, thereby exposing the mountain to great erosion processes. Evidence of ages of erosion shows that the uplift was differential, being greater in the Merced River region, where Providence Catchment is located (Thornbury, 1965). The morphology of Providence and its surroundings is explained as the progression of erosional stages of the Sierra Nevada and by the product of unique weathering properties of granite (Clark et

al., 2005). Also, periglacial processes[1] from past glaciers, approximately 24 km away, influenced the morphological character of the catchment.

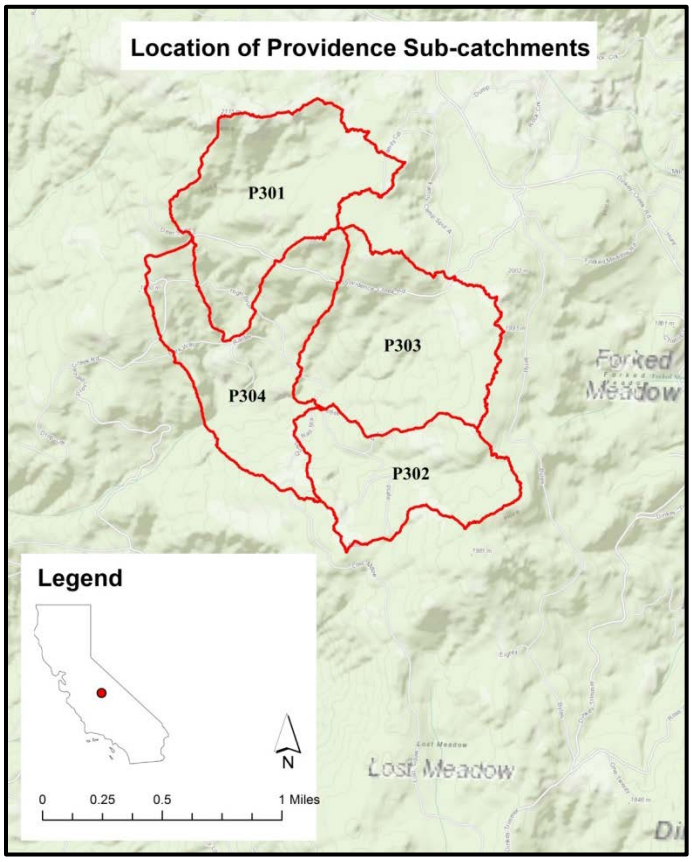

Figure 2. Providence Catchment, the area of study, is divided in four sub-catchments: P301, P302, P303 and P304. Providence Catchment is located in the Southwest of the Sierra Nevada, East from the City of Fresno.

Providence is relatively homogeneous in its geological made up that makes this area suitable to understand the local variability of soils as products of geomorphological and climatic gradients. Providence and its surroundings are mantled by deeply weathered

[1] Geomorphic environment located at the periphery of past Plio-Pleistocene glaciation.

granite with occasional outcrops of intact bedrock (Clark et al., 2005) (Figure 2) . These granite bodies are part of the Sierra Nevada Batholith of Mesozoic Age (Bateman and Wones, 1972; Thornbury, 1965; Twidale and Romaní, 2010) in which 75% of its area is mantled by glacial till (Bateman and Wones, 1972). The entire catchment is formed by the Granodiorite of Dinkey Creek, foliated to the north of Providence and absent of foliation to the south. The unit contains granodiorite with abundant disc-shaped mafic inclusions composed of hornblende, biotite, sphene, plagioclase and opaque minerals. Age is estimated by Rb-Sr whole-rock isochron as 110+/- m.y (Bateman and Wones, 1972).

Just above the Providence Catchment another geologic unit, Quartz diorite of Blue Canyon, influences the area. This unit is formed by granodiorite that is equigranular and well foliated and part of the weathered products are deposited by erosion in Providence Catchment.

Figure 3. Photo showing the catchment from North to South. Providence is highly forested, with occasional outcrops of intact bedrock, mainly granodiorite.

Soils

Providence Catchment is dominated by soils classified as Shaver family in its southern part and Gerle-Cagwin family in the south (Giger and Schmitt, 1993) (Figure 4). The Cagwin family of soils is a mixed, frigid Dystric Xeropsamments, residuum weathering from granite. The Gerle family is a coarse-loamy, mixed, frigid Typic Xerumbrepts, residuum weathering from granodiorite, and the Shaver family is a coarse-loamy, mixed mesic Pachic Xerumbrepts, residuum weathering from quartz-diorite (Johnson et al., 2011; USDA, 2012).

Vegetation

Providence Catchment is covered by a Sierran mixed-conifer forest (76-99% of total coverage) and mixed-chaparral (Bales et al., 2011a) (Figure 3). The forest is composed of White Fir (*Abies concolor*), Red Fir (*Abies magnifica*), Incense Cedar (*Calocedrus decurrens*), Jeffrey Pine (*Pinus jeffreyi*), Ponderosa Pine (*Pinus ponderosa*), Sugar Pine (*Pinus lamberiana*), and California Black Oak (*Quercus kellogii*) (Bales et al., 2011a; Woodward et al., 2013). The height of mature trees ranges from 20 to 60 m. The mixed chaparral is composed of mountain gooseberry (*Ribes roezlii*), western wild ginger (*Asarum caudatum*) among others (Woodward et al., 2013).

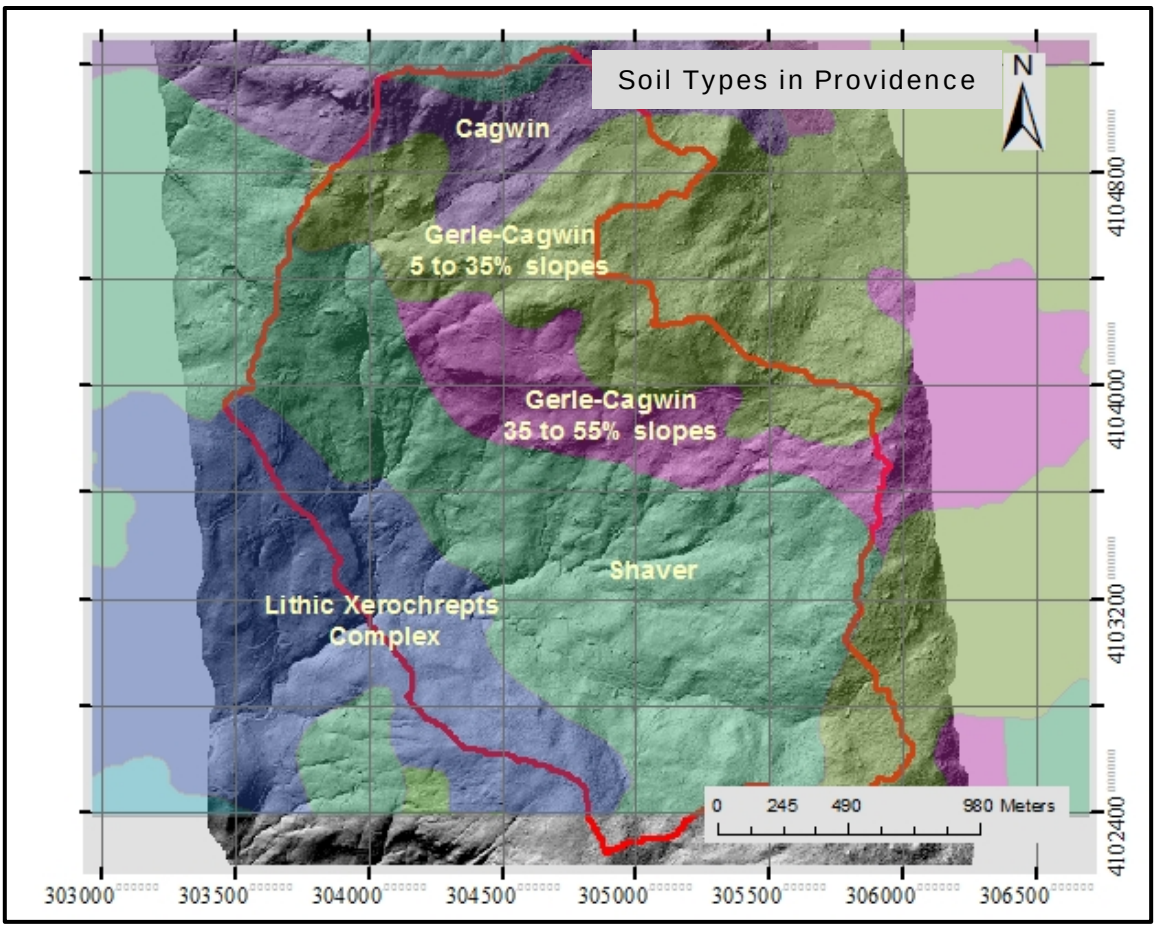

Figure 4. Soil types present in Providence catchment according to USDA_NRCS, 2012. The limits of the catchment are in red.

Climate

According to the Köppen-Geiger classification, Providence is located at the intersection between a Mediterranean (Csb) and Boreal/Microthermal (Dsb) (Kottek et al., 2006) regional climate zones. At the local scale, the catchment is positioned in a rain-snow transition zone of the Sierra Nevada, where at lower elevations 40 to 85% of total precipitation is rain (Hunsaker and Neary, 2012; Hunsaker et al., 2012). Currently, local conditions are characterized by seasonal snow, followed by spring melt and a

relatively dry state. Changing climate, however, is expected to affect the amount and seasonal distribution of rainfall and snowpack in the future. This scenario has implications for the water supplies in the lower section of the Basin that depends on runoff originating as snowmelt (Hunsaker et al., 2012).

Landuse

The main economic activities in the area are extensive livestock and timber harvest, and they are present in all the sub-catchments. These activities have a long-term history in the watershed, and logging is a practice that started in 1995 after a few decades of cessation (personal communication with Matt Meadows, Summer 2012).

Evidence of Native Americans occupation (basins on archeological materials) shows land use before European Settlement in this watershed (as many other watersheds in the Sierras). Indigenous people have burned and cut forests to improve wild crops and facilitate pasturage (McKelvey & Johnston, 1992). After colonization, in the early 1900s, the forest floor and regeneration structure were impacted repeatedly by intense grazing. Many of the trees were established in the 1600s or before, and grew during a period characterized by extended droughts (1750 to 1860 and from 1860 to 1880)(Mc Kelvey & Johnston, 1992). Drought, combined with grazing and fire, created a forest dominated by very large, old trees and with very little ground cover.

Logging in the Sierra Nevada started in 1900 and increased steadily over time until, reaching a peak after World War II and a low period during the 1982 recession. Logging typically removed only the largest and oldest trees. This explains the change of

the forest from one dominated by large, old, widely spaced trees to one characterized by dense, fairly even-aged stands in which most of the larger trees are 80-100 years old (McKelvey & Johnston, 1993).

Materials and Methods

The geomorphological analysis is based on the construction of a geomorphological map of the area of study. A combination of automated and traditional identification of landforms was used for this purpose, using the approach shown in Figure 5.

Materials

Two digital elevation models (DEMs) at different scales were used. At the catchment scale, Light Detection and Ranging (LiDAR) resolution was applied, whereas the USGS - National Elevation Dataset (NED) was used for analysis at the regional scale. The airborne LiDAR survey was acquired by SSCZO during August of 2010. For the purposes of geomorphological analysis and interpretation, the August survey allows a proper representation of the surface, because at this time, snow present during the wet season was complety melted. The sensor used in the survey was LiDAR Gemini 06SEN/CON195 and digitizer 08DIG017 system installed on the PA-31 tail number N931SA. The preprocessing of the DEM was done by the National Center for Airborne Laser Mapping (NCALM). Interpolation of elevation data was made by kriging, using a

linear variogram model with a 0.15 m of nugget variance. The DEMs were free of voids and errors with a 1 m node spacing (Guo, 2011).

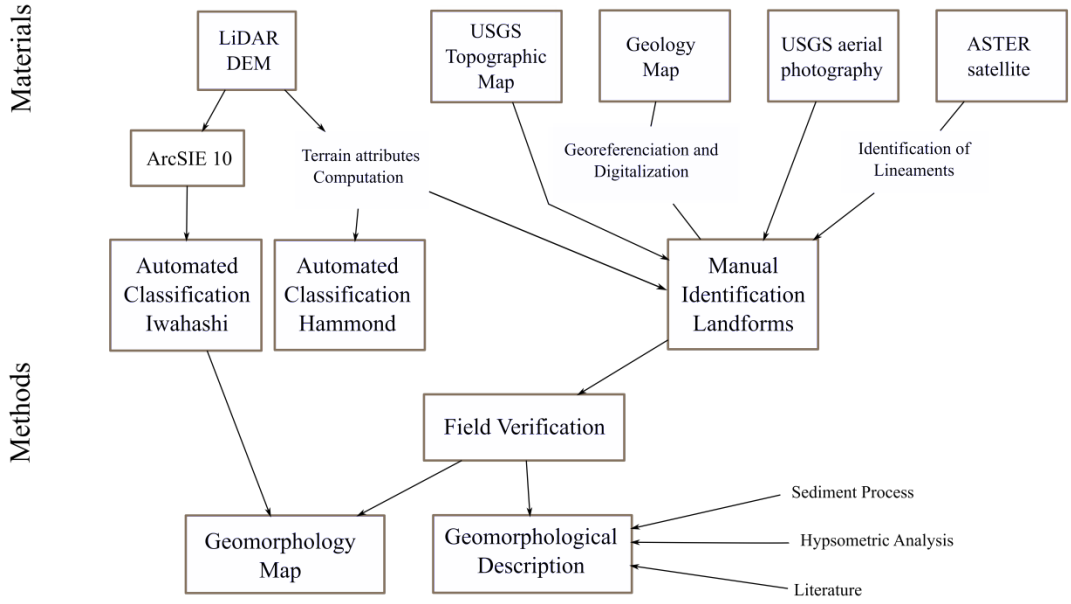

Figure 5. Diagram of materials and methods used in the geomorphological analysis of the area of study.

The LiDAR-DEM has an accuracy of 1m in the horizontal direction and 50 cm in the vertical direction (James et al., 2007). The average, point density of LIDAR flight over Providence Catchment is 12.55 points per m^2. In the center of the image, the average density increases to 16 to 17 points per m^2. Because the Providence Catchment is highly vegetated a higher density of points is found above bare areas, vegetation openings and meadows. Precision tends to be less near channels because of thick riparian vegetation and steep scarps (James et al., 2007). Surface and vegetation information was extracted from the ground and second return point clouds of LiDAR, respectively.

The second DEM was obtained from the National Elevation Dataset (NED) data set available from the USGS at http://earthexplorer.usgs.gov. NED has a resolution of one third arc-second (approximately 10 m) composed of multiple data sources and production methods.

In addition to elevation data, aerial photographs from the USGS (scale 1:10,000, year 2011), the geology maps of Huntington Lake and Shaver Lake at the scale 1:62,500 (Bateman and Wones, 1972), and ASTER satellite images from 2013 were examined. All spatial information was managed and computed in ArcMap 10® (ESRI), using the system of coordinates Datum D_North American _1983 and Spheroid GRS_1980 and Transverse Mercator Projection).

Automated Classification of Landforms

Automated classification of landforms is an alternative to the classical manual classification (Dragut and Blaschke, 2006), in which computational operations replace manual procedures. In this work, however, automated classification of landforms is only one of the several inputs of the classical geomorphological map. Although one of the benefits of the automated classification is the consistency and reproducibility, eliminating the interpreter's bias (MacMillan and Shary, 2009), the use of landscape position and topographic situation alone ignores that processes in the dynamic landscape influence of the spatial variability of soils (Verstappen, 1983). Therefore, process is incorporated in the geomorphological analysis to correlate with soil depth.

Several automatic-mapping methods exist and the scope and results differ in the selection of appropriate terrain attributes for calculations. The goal is to obtain geometric signatures or derivative maps that describe important attributes of topographic form avoiding redundancy (Iwahashi and Pike, 2007). Therefore, simplicity is preferred in the search of attributes. In this work, two methods were tested: the one proposed by Iwahashi & Pike (2006) and the Hammond landforms mapping (Dikau et al., 1991; Hammond, 1964; Morgan and Lesh, 2005).

The Hammond semi-quantitative method (Hammond, 1964) is considered in the category of supervised classification. In other words, it is designed to map recognized training samples. Implementation in GIS was adapted from Dikau et al. (1995). The classification of landforms was derived from the DEM, using a moving window of 2x2 pixels instead of the original moving window of 9.8 x 9.8. Also, the moving window technique, as proposed by Dikau et al. (1995), has the disadvantage of an inherent "edge effect". Cells along the edge of the window do not get the full benefit of all surrounding neighbors creating an edge in the products (Figure 6). One way to minimize this effect is to overlap of areas using fuzzy logic and circular neighborhood to reduce directional bias. This was accomplished by using the ArcMap 10® extension ArcSIE10 (Soil Inference Engine) (Shi, 2013). ArcSIE is designed for soil mapping and its independence of cell size has positive implications on high-resolution DEMs.

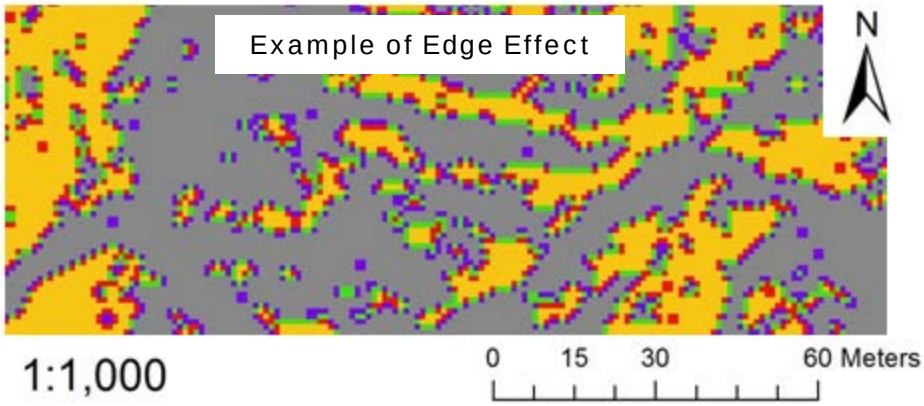

Figure 6. Example of edge effect after applying moving window technique using Hammond classification framework.

Inputs of the classification are: slope gradient, local relief and profile type. Profile type, however, was omitted. The scale and resolution of this work makes the variable redundant because the Hammond technique is designed for regional scale. The algorithm defines the predominant type of profile in terms of percentage of coverage, assigning specific classification for the dominant type of profile. In this case, the entire catchment belongs to the category hills and mountains (Dikau et al., 1995). The six landforms units contained under the category 'hills and mountains' are shown in Table 1.

Inputs were computed from the LiDAR- DEM using Spatial Analyst, Focal Statistics and Reclassify toolboxes of ArcGIS 10®. The ranges for each one of these variables are designed by threshold values according to what was described in Morgan and Lesh (2005). Outputs are units that represent qualitative descriptions of the surface (Dikau et al., 1995).

Table 1. Classification of landforms according to Hammond (1964). Modified from Dikau et al., 1995.

Type of Profile	ID	Landform Class	Slope (% area)	Local Relief (m)
Hills and Mountains	**110**	**Very low hills**	**< 20% gentle sloping**	**0 – 30**
	120	**Low hills**	**< 20% gentle sloping**	**30-91**
	130	**Moderate Hills**	**< 20% gentle sloping**	**91-152**
	140	**High Hills**	**< 20% gentle sloping**	**152-305**
	150	**Low Mountains**	**< 20% gentle sloping**	**305-915**
	160	**High Mountains**	**< 20% gentle sloping**	**>915**

The second method applied, proposed by Iwahashi and Pike (2006), uses slope gradient, surface texture and local convexity as inputs to obtain terrain classification (Iwahashi and Pike, 2007). This classification technique is a combination of threshold-divided variables. Table 2 summarizes the codes and values used in the classification. The dividing threshold for each variable is its mean value. In contrast with the Hammond (1964) method, this is an unsupervised classification, unconstrained by pre-set conditions. Thus, the geomorphological meaning of categories must be interpreted by the researcher. The advantage of this method is the applicability to areas differing in extent, spatial scale, and topographic variety (Iwahashi and Pike, 2007). Whereas Dikau (1995) uses moving windows operations, Iwahashi and Pike (2006) combine moving windows techniques with neighboring aggregates analysis. To overcome the limitations

of a moving window operations, computations were also made using the software package ArcSIE®, which has a module incorporated for Iwahashi and Pike method.

Table 2. Classification according to (Iwahashi and Pike, 2007). The threshold values for each one of the parameters correspond to the mean.

Class	ID	Slope%	Texture	Convexity
Steeper, high convexity, fine texture	1	> 13.81	< 0.50	> 9.61
Steeper, high convexity, coarse texture	2	> 13.81	> 0.50	> 9.61
Steeper, low convexity, fine texture	3	> 13.81	< 0.50	< 9.61
Steeper, low convexity, coarse texture	4	> 13.81	> 0.50	< 9.61
Gentler, high convexity, fine texture	5	< 13.81	< 0.50	> 9.61
Gentler, high convexity, coarse texture	6	< 13.81	> 0.50	> 9.61
Gentler, low convexity, fine texture	7	< 13.81	< 0.50	< 9.61
Gentler, low convexity, coarse texture	8	< 13.81	> 0.50	< 9.61

Aggregation Technique

Although it is possible to visually identify semi-homogeneous areas from the results, the level of detail hinders the possibility of obtaining enclosed patterns at a certain desired scale. Testing the best upscaling factor is necessary to adjust the input of results in a hydrological model. In addition, the accuracy and error of GPS forces the

need of aggregation. Consequently, to construct the geomorphology map, aggregation was performed to identify abrupt boundaries where slope, texture, relief change. The details are replaced by the identification of these boundaries, which in GIS means gathering patterns in vector objects.

A median-aggregation technique was applied because it retains median values at scales within the ranges of spatial autocorrelation of data (Bian and Butler, 1999). Compared with the average-aggregation technique, the representation of the group of pixels by median values maintains the true values of the classification, instead of creating an average, diffuse cell value. Four windows sizes were tested: 3, 5, 10 and 15.

To evaluate the correct window size, sample points were obtained from each one of the aggregation results of Iwahashi classification in an area corresponding to ¼ of the entire area of study to optimize computational time. This was accomplished observing the autocorrelation of sampled points by ordinary kriging algorithm using the Geostatistical Analyst Tool in ArcMap10®. The nugget effect (i.e., percentage of variation in the data that is not spatial) was set to zero.

Finally, results of the classification from the LiDAR-DEM were compared with the original coarser resolution NED-DEM (i.e., 10 m) downloaded from www.glovis.usgs.gov.

Field Methods

Field work was completed during August 2011 to validate remote-sensing analysis and refine ambiguous boundaries and interpretations. The catchment was

surveyed to locate, describe and map mass movements (i.e., rock fall areas, landslides, boulder creeks, and debris flow), landforms, bank erosion and the presence of terracettes. Data were georeferenciated using a GPS (Global Positioning System).

Geomorphology Map

The goal of the geomorphology map is to describe the area to provide general information on the spatial variability of processes (Goudie et al., 1990). The map is accompanied by a description of identified features, which are organized in sub-categories. The legends follow the manual of geomorphology mapping of Demek (1972) and the symbols established by (Kneisel et al., 1998). Symbols were adapted to ArcMap® environment by (Otto and Dikau, 2004) available at http://www.geomorphology.at/symbols.html.

Identification of features, such as meadows and debris flows, were made manually, discriminating color and pattern using terrain attributes, aerial photography and field mapping notes. The high resolution of ground point returns of LiDAR was very valuable because ambiguity of shadows present in the aerial photography were clarified using terrain attributes derived from the DEM, as well as 3D visualizations (Smith, 2011) (Figure 7). Main breaks of slope were defined using contour lines, profile and gradient curvature (Smith, 2011).

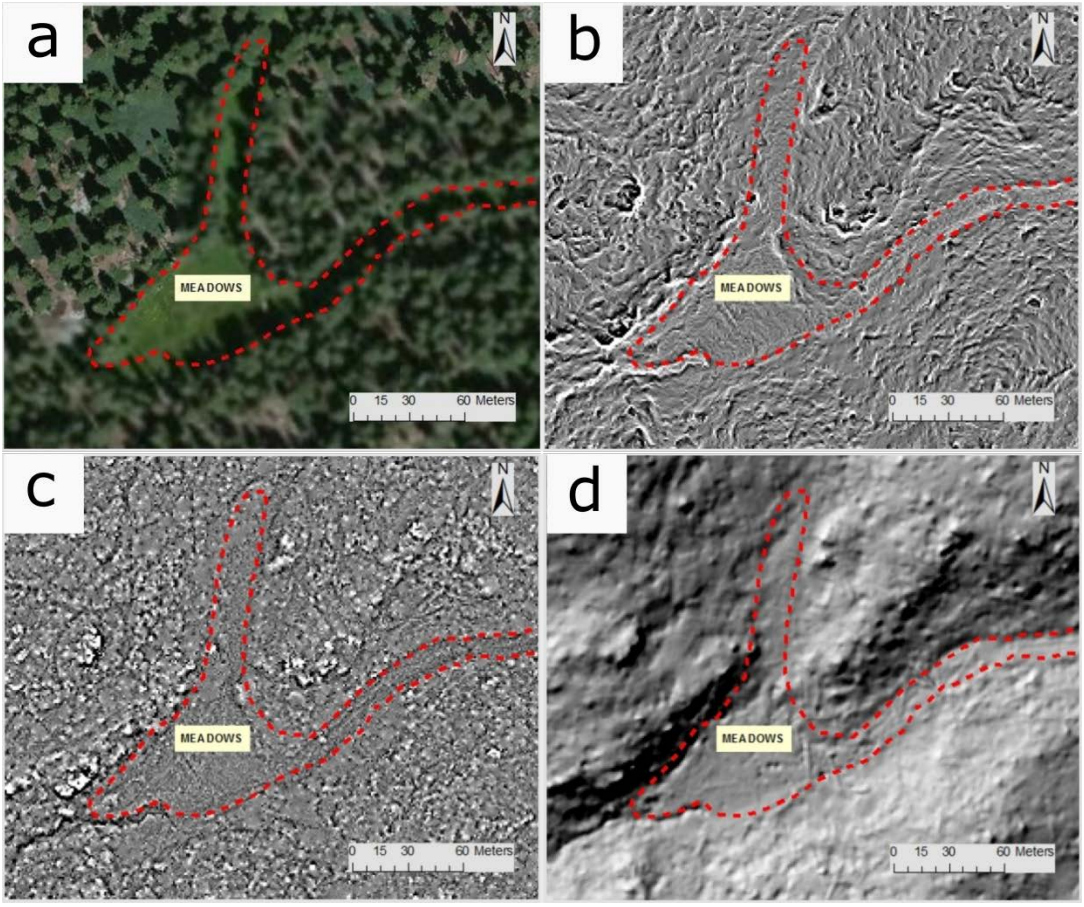

Figure 7. Example of the importance of combining different terrain computations and aerial photography to visually discriminate boundaries of features. Meadows were identified using (a) aerial photography, (b) profile curvature (c) mean curvature and (d) hill-shaded visualization of DEM. Scale 1:2,000.

Sediment transfer processes are mapped by adapting the method proposed by (Theler and Reynard, 2011). First, sediment sources were identified and delineated. Second, the catchment was classified according to the intensity of the susceptibility to mass movement by intersecting slope and vegetation. Slope areas with steeper slope gradients and high convexity are assumed to have a higher potential for mass movement (Wu and Sidle, 1995) in a landscape that is prone to slope instability (DeGraff, 1994).

The exceptions are areas with more than 70% of vegetation cover because vegetation stabilize slopes by root cohesion (Gyssels et al., 2005). Computation of slopes was made using a DEM built with the ground-points returns of the LiDAR, whereas vegetation coverage was obtained from the second returns. Percentage of vegetation cover was calculated using the sum of the 10 m neighborhood, whereas slope classes were computed using the mean in a 10 m radius.

Second, sediment storages where classified as high, latent or inactive levels of susceptibility for erosion (Figure 8). Only high and latent intensities were included in the geomorphology map.

Finally, high and latent areas were then analyzed according to the hydrological connectivity, under the assumption that in forested zones, channel erosion dominates slope erosion (Dedkov and Moszherin, 1992). A buffer 20 m from the center of the channels were computed, and only sediment stores intersecting the buffer were included.

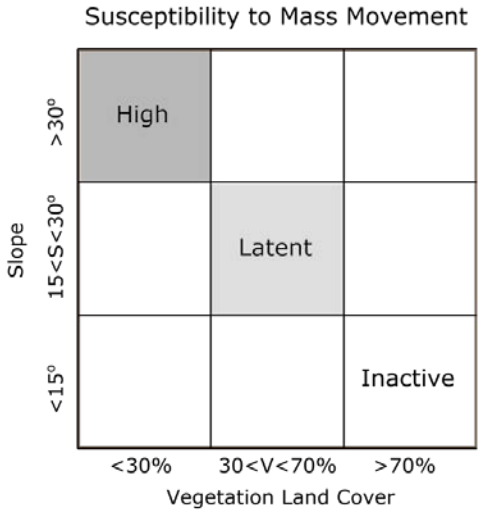

Figure 8. Matrix of the calculation of the level of susceptibility to mass movement by intersecting vegetation and slope. Slope classification thresholds are 15° (angle of repose) and 30° (i.e., general slope of a fan) (Theler and Reynard, 2011).

Classes with high susceptibility to mass movement indicate active slopes, with high dynamism (i.e., steeper slopes, lower percentage of vegetation cover and high fluvial connectivity), whereas low values indicate passive slopes, more stable areas.

Hypsometric Analysis

To know if erosion and deposition processes are relevant for this watershed, a hypsometric analysis (Strahler, 1952) was performed. This analysis was developed for large watersheds by Langbein (1947) and application to small scales along with its relationship with erosion stage of certain catchments was developed by Strahler (1952), among others (Chow, 1964). The method developed by Strahler shows the potential erosion of each one of four sub-catchments of Providence by characterizing the topographic relief within the drainage basins (Pérez-Peña et al., 2009). Knowing the hypsometric indices of each one of the sub-catchments allows comparison among them.

The hypsometric curve was obtained by graphing elevation versus cumulative area. Convex hypsometric curves are typical of a relatively new area; s-shaped curves are related to an area of considerable age, and concave curves are indicative of an area that has been stable for a long time (Pérez-Peña et al., 2009; Strahler, 1952). Values near 1 are typical of convex curves and indicate a new basin.

To calculate the hypsometric integral values the following equation was used:

$$Hypsometric\ Integral(HI) = \frac{Mean\ incision}{Total\ Relief} = \frac{E_{mean} - E_{min}}{E_{max} - E_{min}}$$

Where mean incision and total relief were calculated using the LiDAR-DEM.

Lineaments

Lineaments represent linear surface structures, like faults or fractures as well as geomorphological features such as as ridges or torrents (Rutzinger et al., 2007). In granitic landscapes, lineaments are joints that mark a tendency of differential weathering, consequently contributing to the heterogeneity of weathering profiles in the subsurface.

Lineaments were identified following the methodology of Gleeson and Novakowski (2009). Linear tonal and /or topographic features were identified manually at scales of 1:10,000, 1:30,000 and 1:50,000. Automatic identification would lead to error by the presence of anthropogenic features, such as internal pathways and roads. LANDSAT 5 has `a raster resolution of 20 m with a false-color composite RGB using bands 7, 5 and 4 to highlight tonal differences (Gleeson and Novakowski, 2009; Papadaki et al., 2011). Also LANDSAT 8 with the same resolution and false-color composite using bands 7, 6 and 5 was used to identify the lineaments at the scale of 1:50,000. For the smaller scales, a hillshaded-enhanced LiDAR-DEM with a raster resolution of +/- 4 m was used.

Results

Automated Classification of Landforms

Hammond versus Iwahashi Technique

Map results of Hammond classification (Figure 9) and Iwahashi classification (Figure 10) show similar patterns. The number of classes differs (i.e., 7 versus 8 classes) but main lineaments and scarps can be easily visualized in both classifications. In general, the catchment is divided into three main units: high areas with low relief, areas with intermediate relief and variable curvature, and escarpments.

In the Iwahashi classification the size and the level of discrimination of the patterns is higher compared with the Hammond technique. A higher level of discrimination means that units of relatively homogeneity are revealed, and identification of such units are desired for using the map for soil prediction (Moore et al., 1993) and ecohydrological modeling (Tague and Band, 2004).

Better discrimination in the Iwahashi classification is the result of the ability of the method to adapt the scale of work from regional to local scales unlike the Hammond method. Therefore, when Hammond and Iwahashi techniques are adapted from a regional scale (i.e., 1:200,000) to a local scale (i.e. 1:10,000), the variable type of profile became unnecessary. Therefore, at a local scale the Hammond generates the classes only using two inputs: local relief and slope gradient, reducing the number of classes generated.

Determination of the right upscale aggregation factor

Aggregation results are summarized in Figure 12. Considering a scale of 1:2,000 as a useful scale for field work and investigation of the CZ in the watershed (Blöschl and Sivapalan, 1995; Grayson et al., 2002; MacMillan et al., 2005), discrimination of patterns is possible if aggregation of 15x15 pixels is applied to the 1 m resolution DEM. A factor bigger than 15 increases noise, producing a smoothing effect that blurs break-of-slopes and scarpment edges. A semivariogram analysis applied to the DEM data (Figure 11) shows that the range of spatial autocorrelation (i.e., spatial similarity) occurs before the 20 cm lag. This graph confirms that the application of median aggregation technique beyond the factor of 15 may not reveal any new actual patterns (Bian and Butler, 1999). Therefore, in this particular area and scale the window size of 15x15 pixels, corresponding to 15 cm, is a threshold value to keep dominant information of patterns.

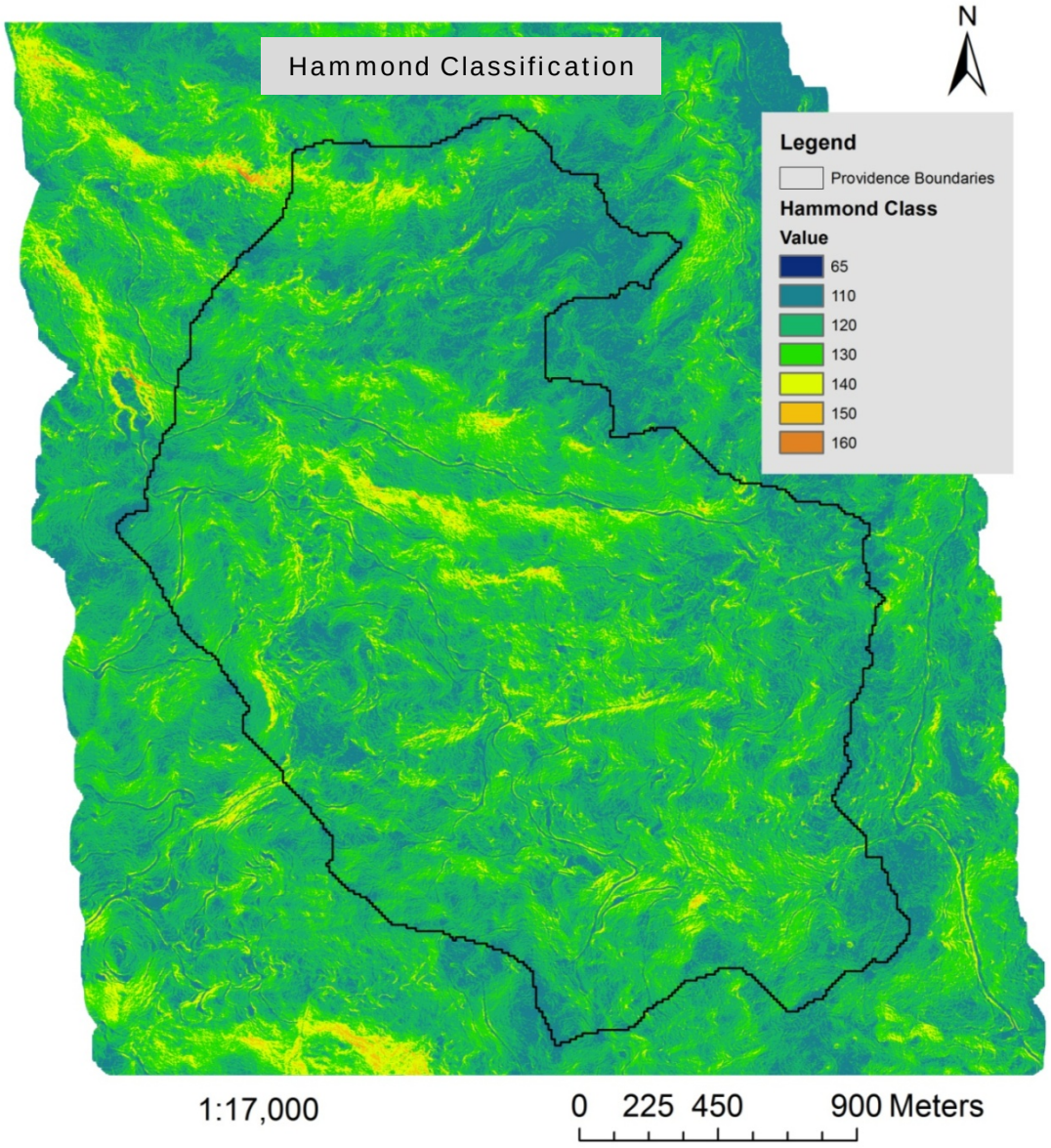

Figure 9. Results of Hammond classification, using 1 m horizontal resolution DEM. Numbers indicates the classification according to Hammond supervised themes: (110) Very low hills (120) Very low hills (130) Moderate Hills (140) Low Mountains (150) (160) High Mountains.

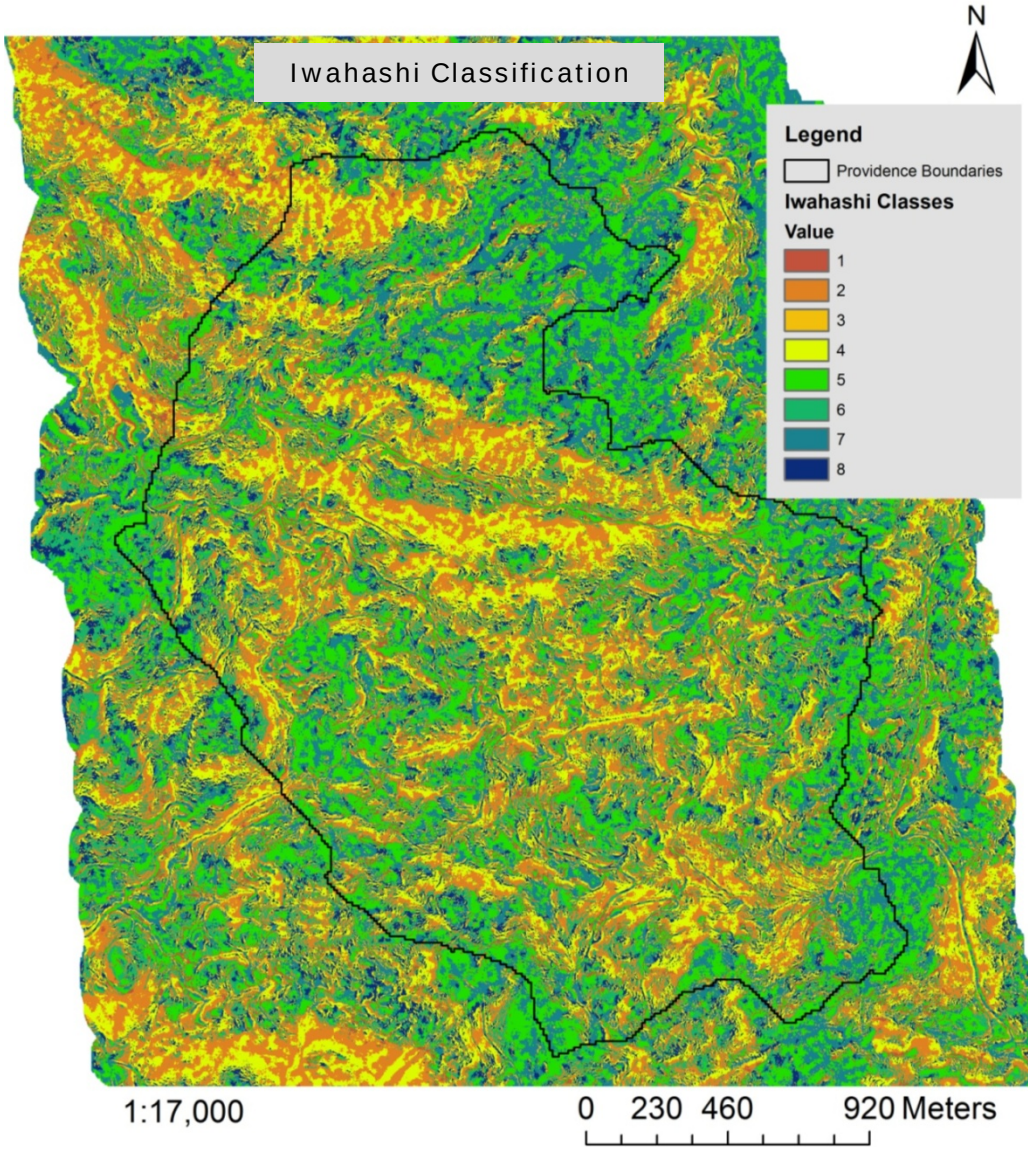

Figure 10. Results of Iwahashi classification using 1 m horizontal DEM resolution. Numbers indicate the classification according to texture, gradient and curvature combinations: (1) Steeper, high convexity, fine texture (2) Steeper, high convexity, coarse texture (3) Steeper, low convexity, fine texture (4) Steeper, low convexity, coarse texture (5) Gentler, high convexity, fine texture (6) Gentler, high convexity, coarse texture (7) Gentler, low convexity, fine texture (8) Gentler, low convexity, coarse texture

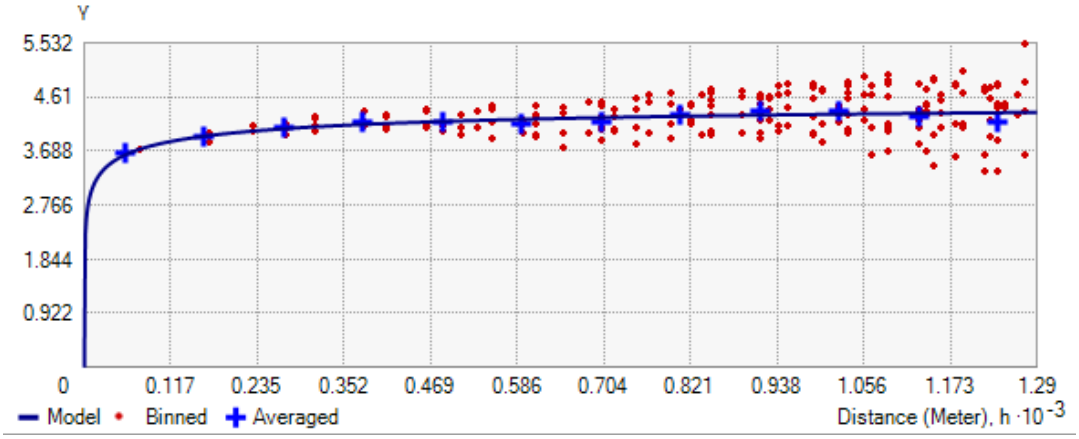

Figure 11. Semivariograms of the different levels of median aggregation method applied in Iwahashi classification. The blue line shows a spherical model applied to the data.

Considering that the GPS has an average error of 7 m as a result of the screen-effect of trees, upscaling through aggregation is a must. Therefore, the classification, with the aggregation factor of 10 for further analysis, which contains the peripheral error from GPS was used. The upscaling with the median factor of 10, however, only includes the central tendency of the neighborhood cells around a defined center. Therefore, the graphical results, shown in Figure 13B, have a tendency towards the class 3 (Steeper, low convexity, fine texture) and 4 (i.e., steeper, low convexity, coarse texture). Also, if the aggregation results are contrasted with the classification using the DEM of 10 m from the NED-USGS, the latter drops off the predictive power of landform differentiation (Figure 13C). Therefore, although a high resolution DEM is not always necessary (MacMillan and Shary, 2009), landform classification through the Iwahashi technique is affected by the resolution of the source of the elevation data.

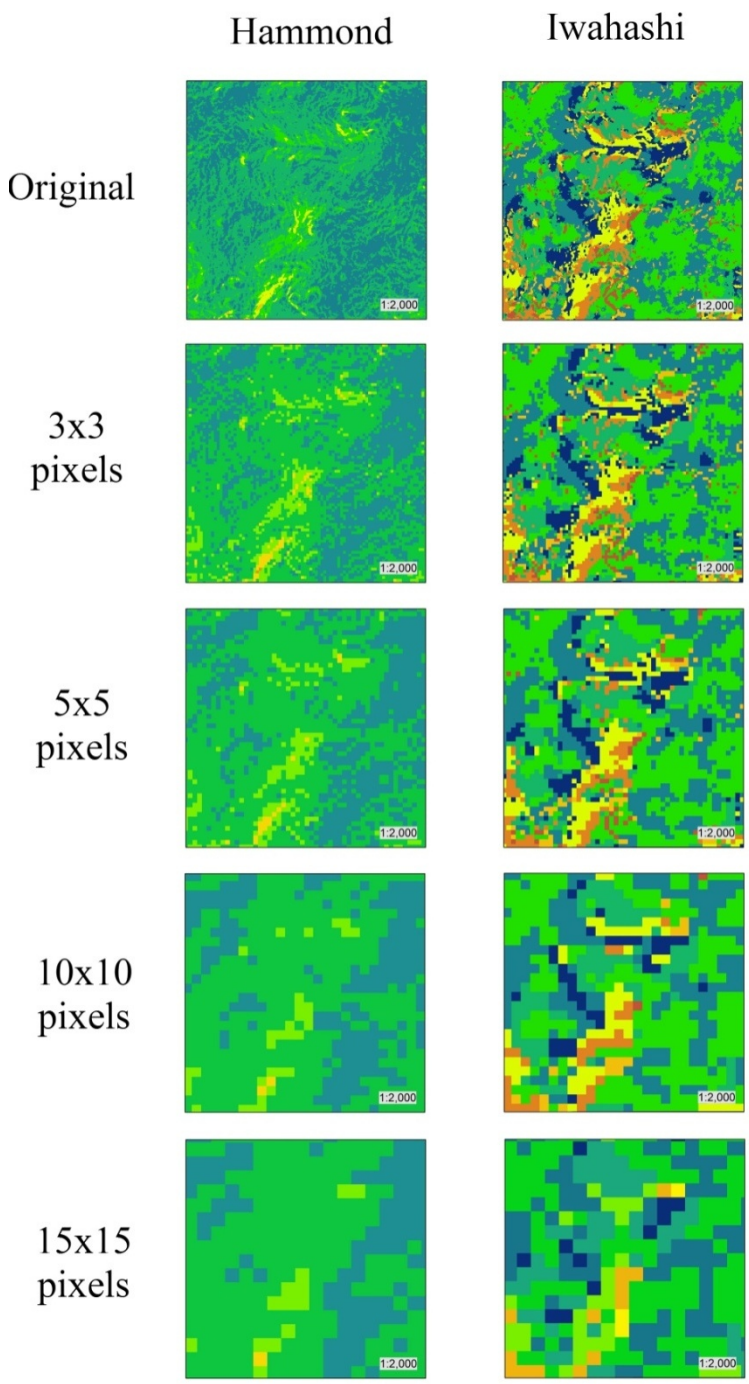

Figure 12. Results of median aggregation technique. (a) Hammond and (b) Iwahashi classifications using different window sizes.

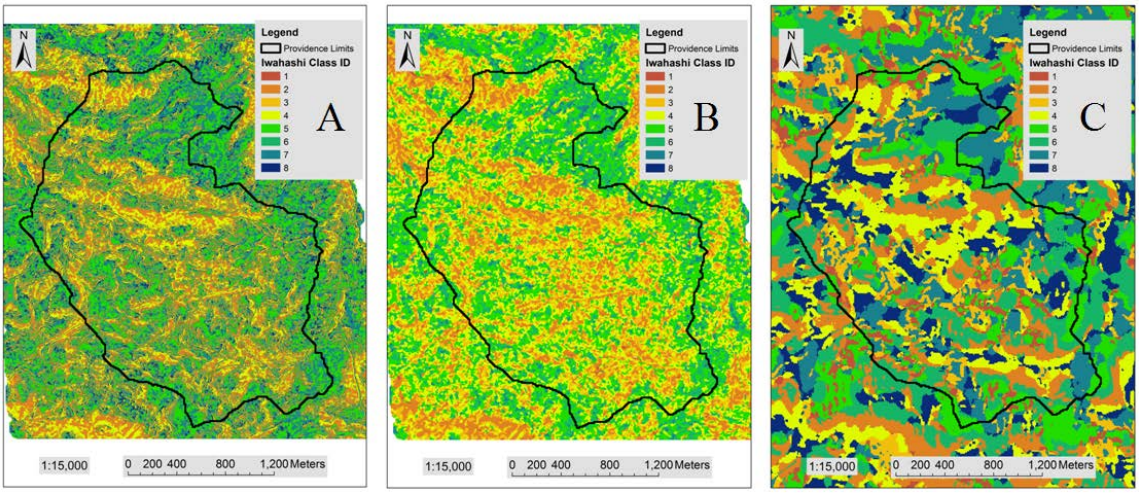

Figure 13. Comparison among Iwahashi classifications applied to: (B) a 10 aggregation factor from a 1 meter resolution LIDAR-DEM and (C) original data from a 10 meter resolution NED from USGS. (A) shows the classification of the original LIDAR-DEM without upscaling.

Geomorphology Map

The geomorphology map presented in Figure 4, covers an area of approximately 3 km^2 at a scale of 1:15,000. The map integrates manual and automated identification of landforms and contains morphometry, fluvial, process, structural and anthropogenic spatial information of Providence. The geomorphological data base of the map in ArcGIS 10® can be seen in the Appendix.

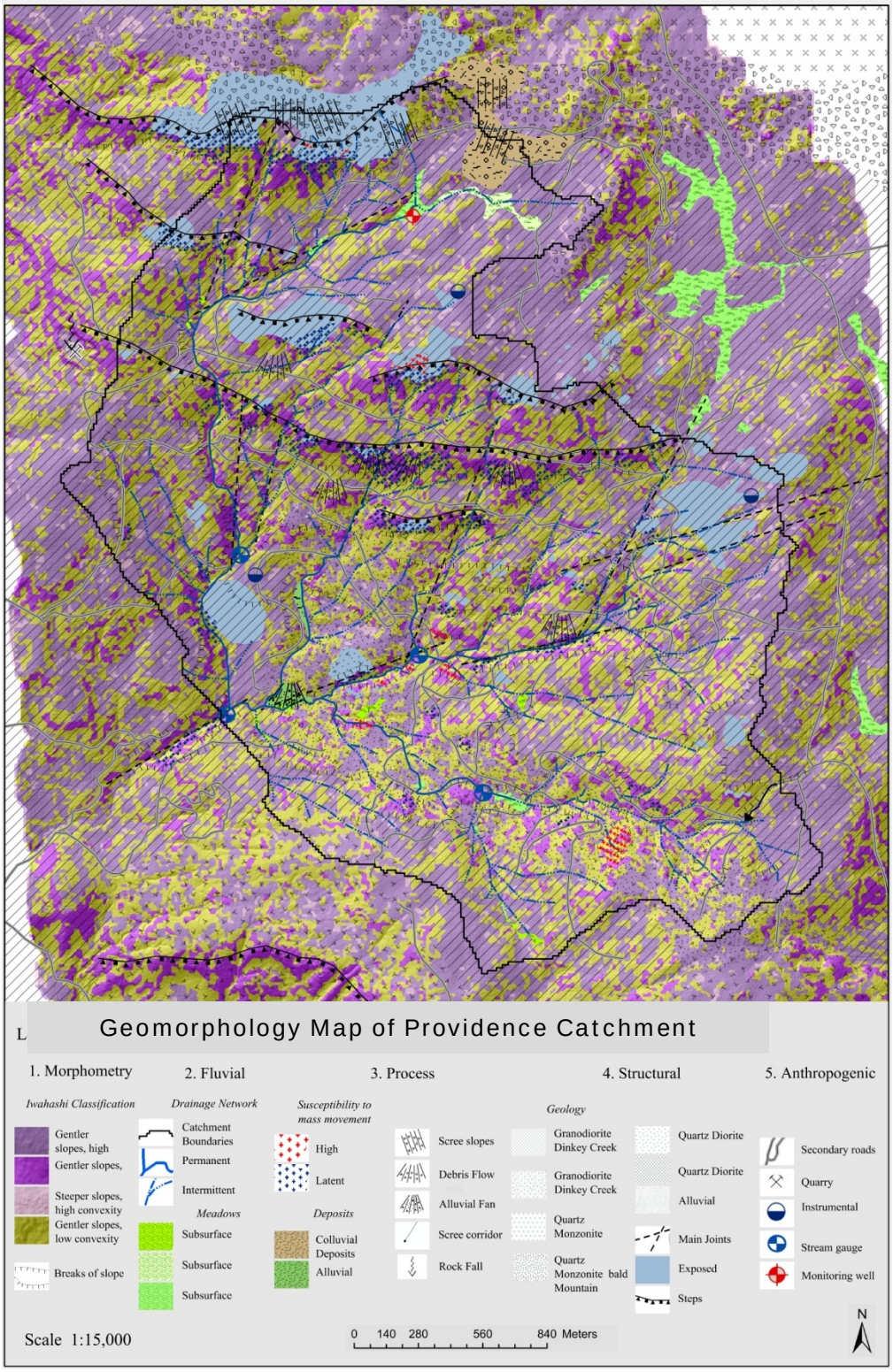

Figure 14. Geomorphology Map of Providence Catchment.

1. Morphometry

This layer is a derivative map, in a vector form, the result of the application of the Iwahashi automated classification of landforms. The variable texture of the Iwahashi technique was omitted for two reasons. First, processes of erosion and deposition that are related with soil depth are derived from curvature and slope information alone (Dietrich et al., 1995). And second, simplicity was favored (Iwahashi and Pike, 2007). The main breaks of slope coincides with high convexity and steep-slope zones.

2. Fluvial

Drainage networks and meadows comprise the fluvial layer.

Permanent drainage network is defined as a perennial stream that has continuous flow throughout the year. Perennial networks have higher drainage density with approximately half of the total channel length located in the headwaters (Knighton, 2014). Therefore, its structure depends on processes occurring into intermittent headwaters.

Meadows are defined as depositional features and are classified according to gradient (Brinson and Rheinhardt, 1996):

- Subsurface Low Gradient: Meadows of gradients less than 2%.
- Subsurface Middle Gradient: Meadows of gradients between 2% and 4%.
- Subsurface High Gradient: Meadows of gradients higher than 4%.

3. Process

This layer identifies areas of accumulation, transport and deposition. Processes acting on sediment storage are classified as high and latent classes of susceptibility to mass movement. Higher relief is found in the north portion of the catchment; however the south has more patches without vegetation coverage, which explains the high susceptibility of those areas for mass movement (Figure 15).

Three types of stores are present in the study area: structural surfaces (i.e. free faces and rock escarpments on fracturated rocks), fluvial and gravitational stores (Theler and Reynard, 2011; Ventura and Irvin, 2000).

Two types of deposits were observed: colluvial deposits or undifferentiated footslopes and alluvial deposits, both covered by vegetation. Concave colluvial deposits are found at the toeslope of steps and erosional scarps, in which steep topography results in the redeposition of loose material. Examples of debris flows in the watershed considered as sediment stocks are show in (Figure 16). Alluvial toeslope deposits are areas with responses to redeposition from upvalley alluvial materials with 0 to 4^{o} gradient (Ventura and Irvin, 2000).

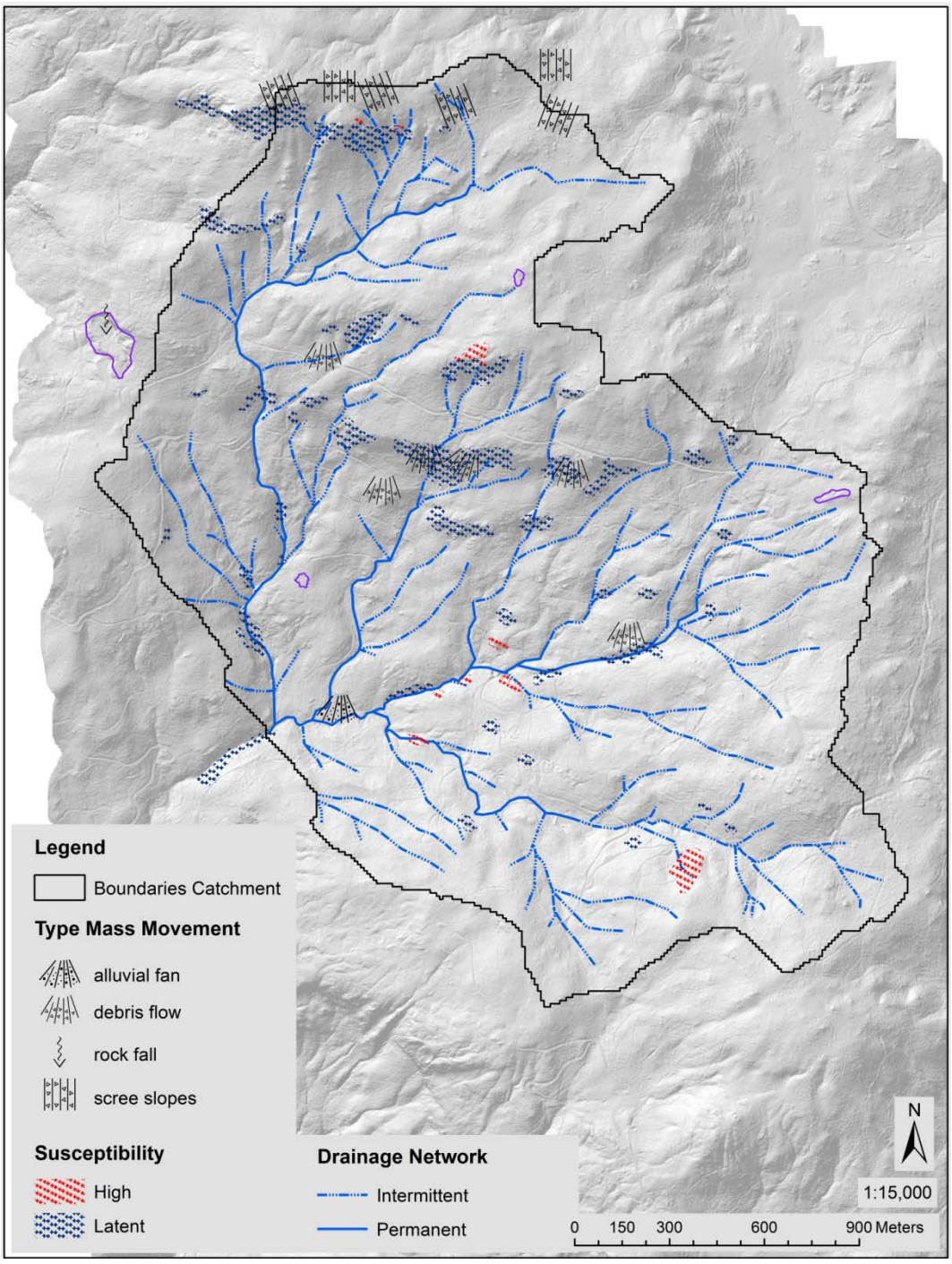

Figure 15. Map of susceptibility for mass movement along with mass movement observed in the catchment.

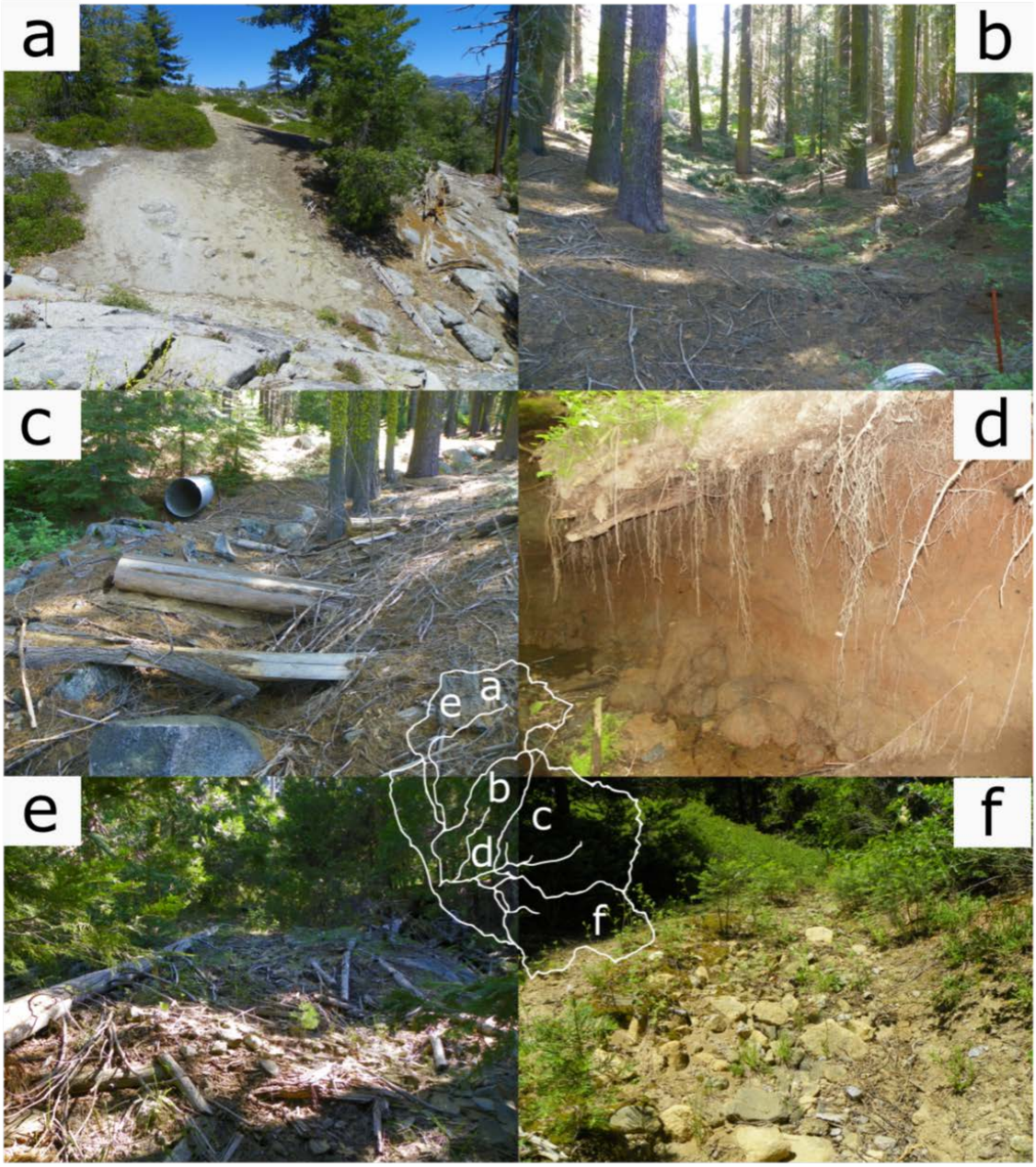

Figure 16. Examples of sediment stores present in Providence. Letters indicate the place where the examples are located in the catchment. (a) grus formation on the granite exposed in the north interfluve (b)intermittent channels connects sediment storages with deposition sites during the wet seasons (c) debris slide (d) bank erosion (e) deposits accumulated along erosional scarps (f) scree corridor. Photographs taken on August 2012.

4. Structural

This layer contains geological information. Although Providence has a relatively homogenous geology, subtle differences are noticeable among sub-catchments. The absence of foliation in the unit of Granodiorite Dinkey Creek (Bateman and Wones, 1972) correlates with lower relief, more active sediment dynamics and more sparse patches of vegetation in the sub-catchment P304. Contrast this with sub-catchment P301 where the presence of steps, patches with exposed bedrock, and a sub-rectangular drainage pattern relate with strongly foliated granodiorite. Furthermore, analysis of sediment load showed that P304 has the highest volume of sediment and load of mineral mass, whereas P301 has the lowest (Hunsaker and Neary, 2012).

5. *Anthropogenic*

This layer shows the current, secondary roads that are used mainly for logging (Figure 17). Places with instrumental clusters consist of a meteorological station, a 60 m tall flux tower, sensors for volumetric water content, matric potential, sap-flow and snow-depth sensors (Bales et al., 2011a). The position of the monitoring well as well as stream gauges are indicated on the layer.

Figure 17. Secondary roads for logging purposes. Photos taken in July 2013.

Geomorphology of Providence Catchment

Providence Catchment is part of the north headwaters of one of the tributaries of Pine Flat Reservoir, which impounds the Kings River (Figure 18). The entire area and its surroundings are dynamic from the point of view of processes. The hummocky topography, with low hills and rises towards the south and east of the area, is evidence of the presence of landslides. Providence Creek contributes to the alluvial deposits located at the outlet junction with the Big Creek, with a total sediment load of 6 m^3/yr (record 2003-2009) (Hunsaker and Neary, 2012). Hypsometric analysis reinforced the idea that the catchment is an active source of sediments, with subtle variations among sub-catchments. Providence Catchment has a dendritic and rectangular drainage pattern that matches regional patterns. Those patterns are explained by the underlying granodiorite and the presence of abundant right-angle lineaments, which are oriented North (Figure 20).

Steps and threads are characteristic in this area. In details, such steps are formed by corestones and erratic boulders, which are the main landforms found in the region along with several meadows. Details are discussed below.

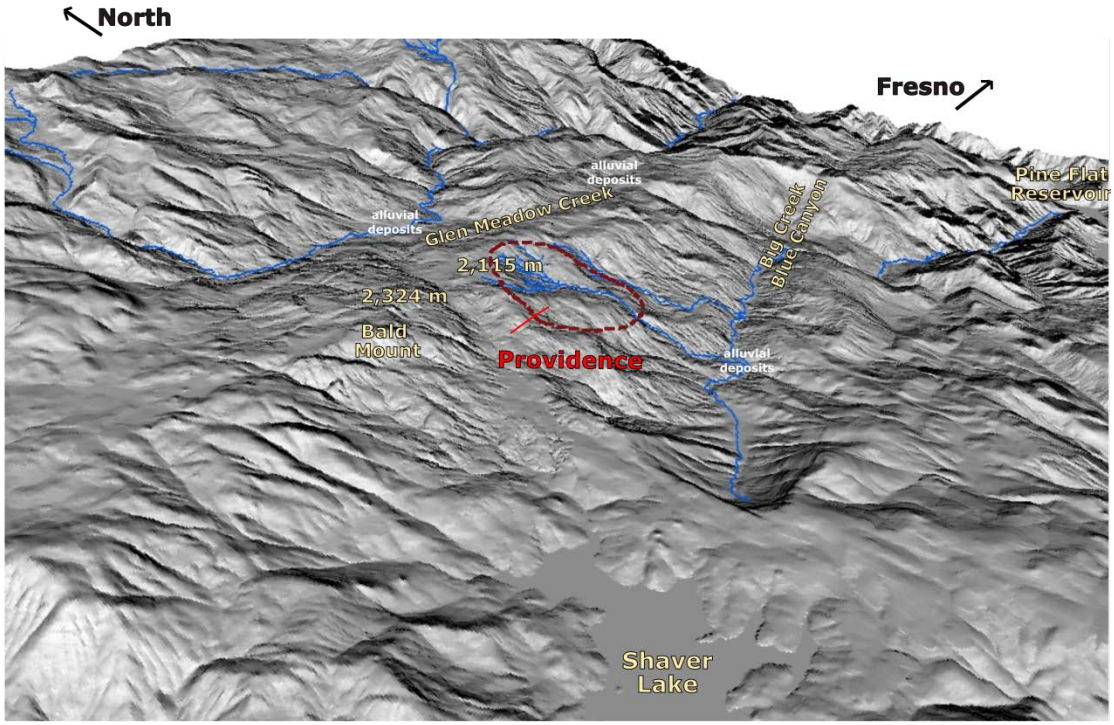

Figure 18. A tree dimensional, hillshaded representation of the surroundings of Providence catchment (in red). Providence is part of the Big Creek Basin which feed the Pink Flat Reservoir downstream. The area is enclosed to the North and East by several meadows formed throughout the Glen Meadow Creek. Elevation of the catchment is approximately 2,000 m. All the area covered in the figure is part of the Sierra National Forest.

Hypsometric Analysis

The hypsometric curve (Figure 19) shows that the sub-catchment P304 (HI=0.34) has an s-shaped curve and a low value in the hypsometric integral (Table 3). The s-shape of the hypsometric curve is related with the stage of geomorphic development of the

basin (Goudie et al., 1990) and it is also a indicator of the presence of relatively homogeneous rock (Strahler, 1952), or in other words, a more uniform distribution of relatively low elevations exist. Therefore, the sub-catchment P304 has less potential for erosion compared with P302 and P303 (Pérez-Peña et al., 2009). Sediment loads, however, indicate that P304 has the highest values (i.e., 3 m^3/yr., record 2003-2009) compared with P301 and P303 (Hunsaker and Neary, 2012). Also, auguring measurements (see Chapter III) shows that P304 is the sub-catchment with deeper soils (Bales et al., 2011a) and less rock content to the one meter depth (Hunsaker and Neary, 2012). Field observations found that P304 has less exposed granite, a higher number of meadows and smaller corestones.

The low value of HI of P304 indicates the action of fluvial aggradations. P302 and P303 have a dissected topography, and although the curves do not present dramatic convexity. The shapes indicate the role of diffusive hillslope processes and the higher potential for erosion (Pérez-Peña et al., 2009). The concavity of the sub-catchment P301, (HI=0.59), however, is explained by the presence of more resistant material and steps of granitic rocks in its northern area. The convexity of P303 indicates more material is held higher in the sub-catchment. Thus, diffusive hillslope processes are dominant processes. Overall, the hypsometric curve and HI of the entire catchment indicate potential for erosion in a stage of non-equilibrium.

Table 3. Results of hypsometric analysis for each one of the sub-catchments of Providence.

Catchment	HI	Mean Incision	Total Relief	Emean	Emin	Emax
P301	0.59517426	222	373	1956	1734	2107
P303	0.57654723	177	307	1894	1717	2024
P304	0.33711048	119	353	1790	1671	2024
P302	0.576	144	250	1870	1726	1976
Providence	0.47706422	208	436	1879	1671	2107

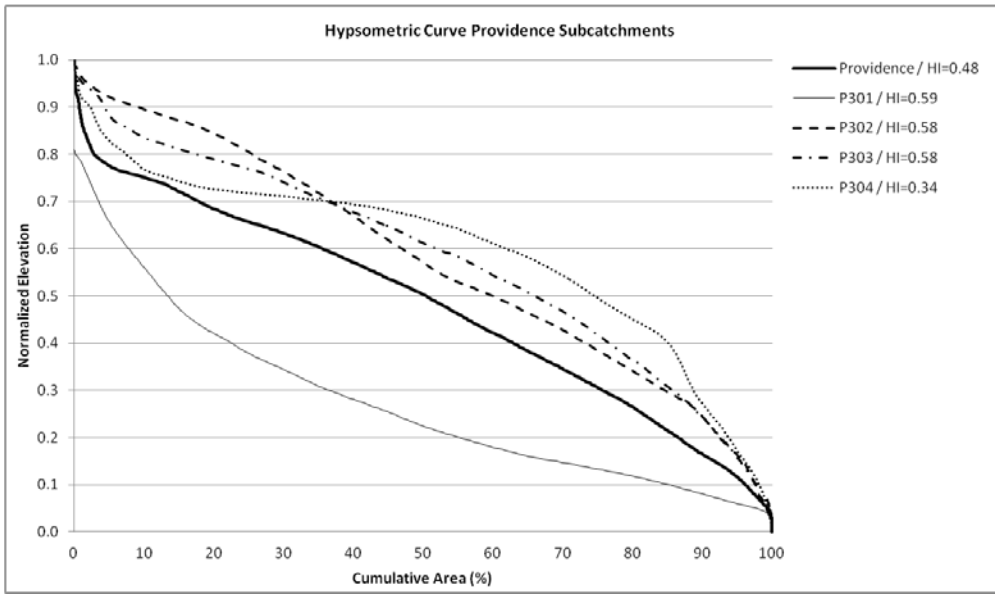

Figure 19. Hypsometric Curve for all sub-catchments and the entire Providence. HI (Hypsometric Integral) was calculated according to (1). The normalized form of the hypsometric analysis proposed by Strahler (1952) was used.

Lineaments

Lineament is a term that includes joints (i.e., displacement associated with the opening of the fracture) and faults (i.e., lateral displacement in the plane of fracture). Important faults are lacking in the area of study. Previous field investigations found that

many of the lineaments abundant in granitic rocks in the Southern Sierra are joints (Lockwood and Moore, 1979; Ross, 1989). Joints developed after emplacement of the Sierra Nevada batholith but before the extensive weathering period that followed, because joints themselves are deeply weathered (Migon, 2006).

Lineaments in the Providence Catchment are shown in Figure 21. Colors are related with the scale of work used during the visual identification. Dominant strikes of lineaments are N-NE (Figure 20). This result is in agreement with studies in other sites of the Southern Sierra (Lockwood and Moore, 1979; Ross, 1989). Thus, the lineament analysis of the area matches closely with the regional trends of the area studied.

Main drainage of all sub-catchments follows the direction of important lineaments. This may be evidence of differential weathering that contributed to initiation of channel incision (Knighton, 2014).

Steps and Threads

Steps and treads are characteristic of the southern Sierra, and Providence is a representative area of this stepped topography (Jessup et al., 2011; Wahrhaftig, 1965). As shown in Figure 22, if a hillshade effect is applied to the DEM, steps and threads can be seen as parallel bands from 300 m to 1.5 km apart. The presence of these features are explained by a phenomenon called back weathering. Differences of water retention (Wahrhaftig, 1965) cause a contrast of erodability between bare and soil-mantled granite (Jessup et al., 2011) confirmed by direct measurements using cosmogenic nuclides (Bierman, 1994). Generally, steps are formed by random, granitic tops, whereas threads

are zones of deposition of the disintegrated material, with gentle slopes (Wahrhaftig, 1965). In Providence, however, steps are composed by bare rock and are soil-mantled as well. Because soil-mantled steps erode fastest, steps appear to be wearing back into the treads at several meters per million years (Jessup et al., 2011).

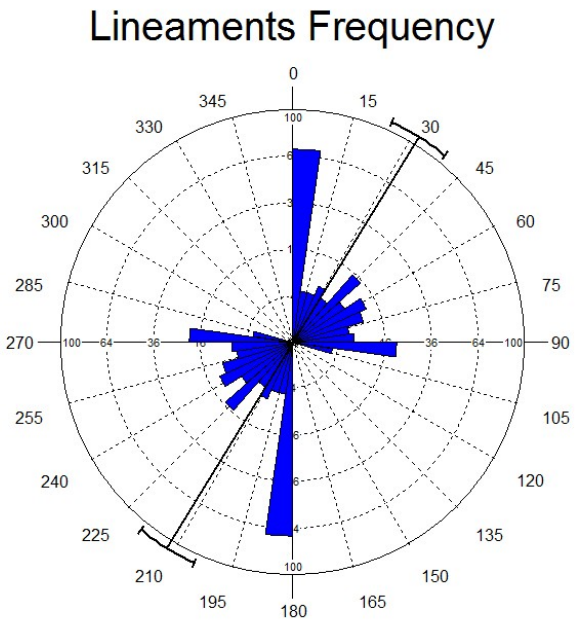

Figure 20. Rose diagram of lineaments identified in Providence catchment. (N=172). Frequency shown as area of wedge. 0 represents North, 90 the East, 180 South and 27 the West.

Corestones

Corestones and erratic boulders are found throughout the catchment as isolated blocks or tors (Figure 23). Corestones are remnants from the weathered residues removed locally primarily by erosion (i,e., wash, rills and channels) and solifluction (Twidale, 1982). Big isolated corestones (more than 5 m high) are present in the

northern part of the catchment as isolated rises of hard bedrock. They are formed by differential rock outcrop exposition, which implies that the outcrop is less saturated in comparison with the areas around it, where weathering and erosion occurs more rapidly (Bremer and Sander, 2000).

Meadows

In the Providence Catchment and its surroundings, meadows are areas of deposition, with alluvium or valley fills characterized by the existence of a shallow water table (i.e., less than one meter). The soil material (gleysol) is fine textured and only covers the upper centimeters of the profile (i.e., approximately 30 cms) (Weixelman et al., 2011).

Meadows of low and middle gradient (Figure 14) are fed by a combination of surface and groundwater flow. Those meadows are outflow systems driven by gravity, with a continuous out-flowing of groundwater and surface water (Weixelman et al., 2011), strongly affected by bedrock permeability (Burcar et al., 1994) and, therefore, important from a geomorphology point of view. Some of them, however, lack a stream channel and are fed by subsurface groundwater without significant surface water inputs, commonly occurring with meadows found in gradients higher than 4%. Meadows occurring on alluvium or in valley bottoms or swales become dry during summer, indicating that they are dominated by seasonal precipitation and snowmelt.

The persistence of a shallow water table facilitates the existence of hydric herbaceous species, limiting the conditions for the establishment of trees and most shrubs (Figure 24).

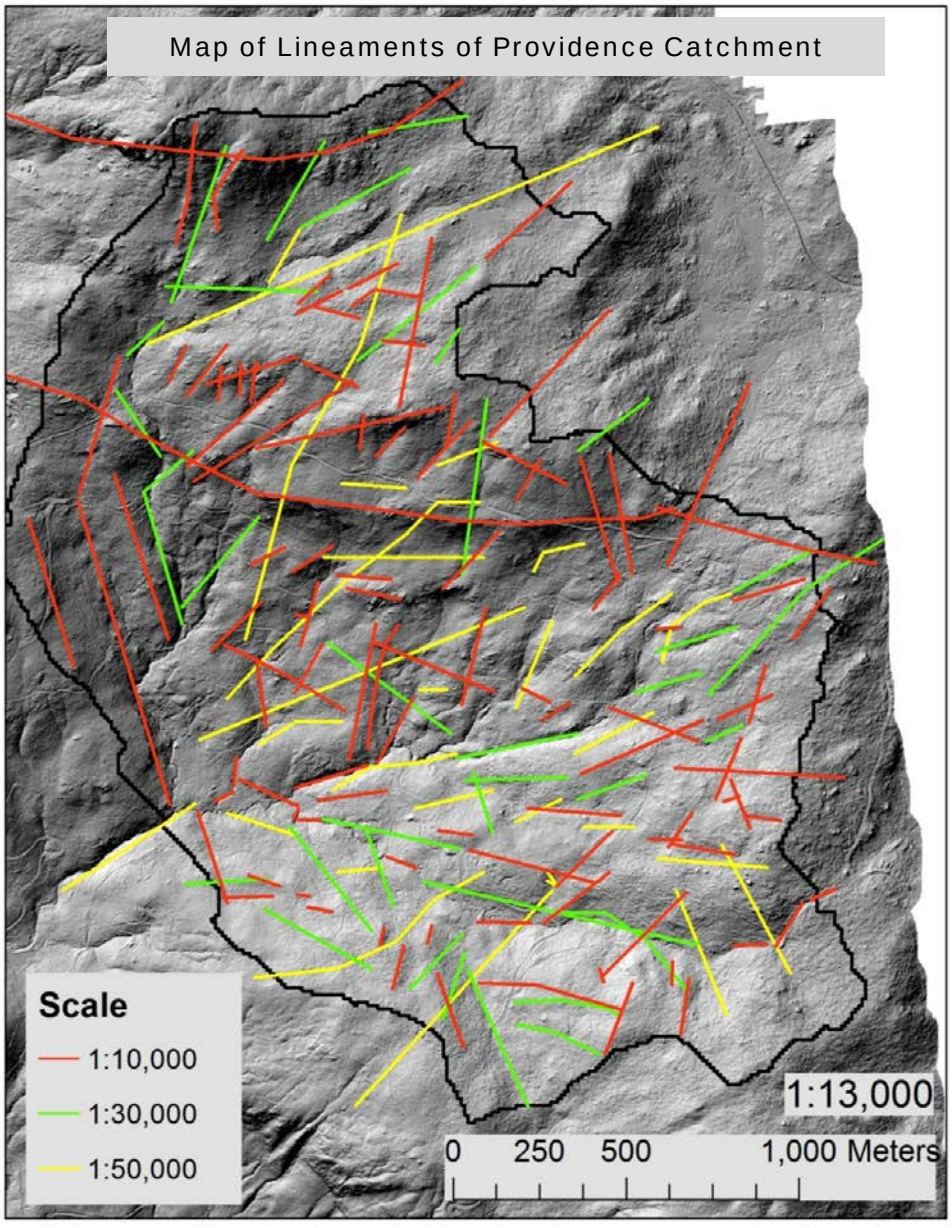

Figure 21. Lineaments were identified manually in three scales of work: 1:10,000, 1:30,000 and 1:50,000 represented in lines with colors red, green and yellow respectively.

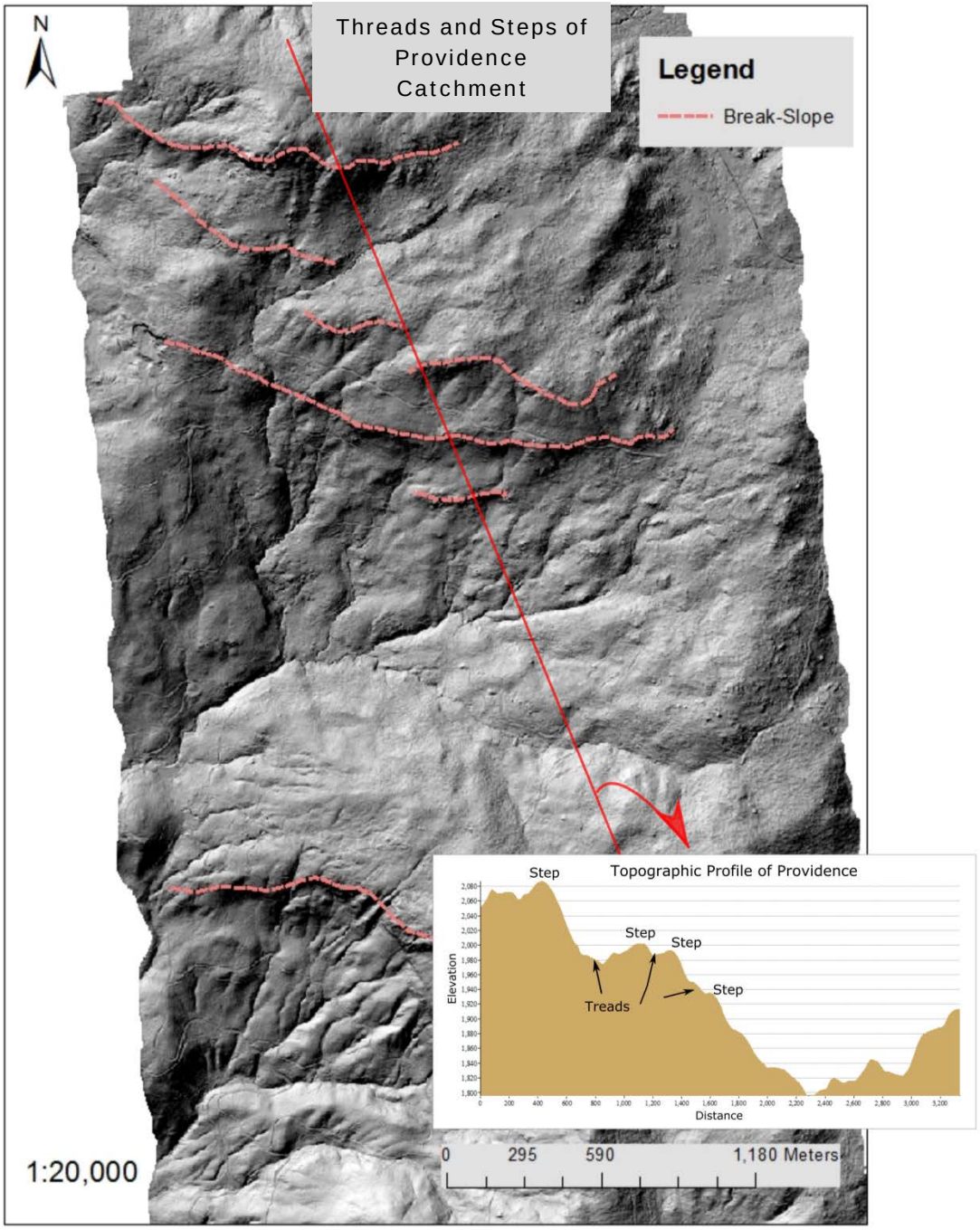

Figure 22. Treads and Steps observed in the Providence catchment. Hillshade effect was applied to the LIDAR elevation data.

Figure 23. Examples of Corestones found on Providence. (a) All-round attack of boulders by soil moisture in a scarp foot zone has produced a mushroom rock (Twidale, 1982), (b) big fractured corestones (c) secondary fractures (not involved in delimiting the joint blocks) within the original mass have been exploited by moisture attack either in the subsurface or after exposure forming a split rock (Ollier, 1971), and (d) granular disintegration and flaking boulder.

Figure 24. Example of a meadow with herbaceous species showed in the picture as a green mantle. Picture taken in the north of the catchment (sub-catchment P301) on July 2013.

Discussion and Conclusions

Discussion

Although the Iwahashi method is more suitable for this area of study, it is not possible to affirm that the Iwahashi is superior to the Hammond; however, the Iwahashi has the advantage to adapt at different scales of analysis. This adaptability makes the method valuable when spatial heterogeneity is the scope of the investigation. But in general, methods of automated classification need to be locally adaptive because no single fixed-window size fits all landscapes (MacMillan et al., 2005).

Another advantage of the Iwahashi over the Hammond automated classification is that threshold values for each one of the input variables are set as the mean value from the complete range. On the other hand, the Hammond method establishes a fixed value,

and ignores the natural spatial variation of the data and overlooks its heterogeneity. This can be visually noticed by comparing the results of classification (Figures Figure 9 andFigure 10): the number of the Iwahashi classes in a given space is greater than the Hammond classes.

Results can be used for predictions in soil studies because homogeneous units correlate well with soil attributes such as soil depth, organic matter and pH (Gessler et al., 2000; Hengl et al., 2004; McKenzie and Ryan, 1999; Moore et al., 1993).

In both methods of classification, results with fine resolution impede the vectorization of homogeneous units. Vectorization is desired in object-base analysis, or in other words, manipulation of objects instead of pixels. Vector objects give topographic meaning to recognizable landforms, allowing further analyses, such as aggregative statistics (Gustavsson et al., 2008; Stepinski et al., 2006). Thus, upscaling through aggregation was performed to obtain landform vectors. Choosing the right aggregation factor is important because fine resolution is not always needed and actually may be counterproductive if less computation time or simplicity of modeling (e.g., hydrological modeling) is sought.

To choose the right aggregation factor three elements were taken into account: the GPS error (i.e., $\pm$ 7 m), spatial autocorrelation of data, and the desired 1:15,000 scale of the geomorphological map. The aggregation factor that best fits the goal of this work is 15. Smaller or bigger grids may be more useful in other cases, but the predictive power of the DEM drops off after about 30-50 m grid resolution (MacMillan and Shary,

2009). To support soil mapping, a geomorphological map with 1:50,000 is adequate for a 1:25,000 scale soil survey (Verstappen, 1983).

Results of automated classification overlap with features identified in the manual approach. Steps are easily recognizable (i.e., warm colors in Figure 10) and areas with arbitrary patterns are the counterpart treads. Some of the main drainages coincide with major joints, and geological differences in the materials more resistant to weathering can also be visualized by observing areas of higher convexity and higher relief in the northern portion of the catchment. Automated classification facilitates the manual recognition of features and likewise, manual classification along with field mapping brings the classes with recognizable landforms. This turns the unsupervised Iwahashi method into a supervised method; or in other words, a method that assign landform class-labels to each class.

The benefits of the automated classification is its repeatability, independence from the user interpretation, and the reduction of cost and time of production (Dramis et al., 2011). At the scale of work of Providence (1:15,000), however, the defined units that share the same combination of slope, texture and convexity miss details that are relevant for study of the critical zone: areas of deposition, active processes, and anthropogenic structures. Therefore, the combination of automated and manual classification convey in a more realistic spatial representation that address somehow the complexity of the landscape. Process is actually often ignored in the construction of geomorphology maps (Dramis et al., 2011; Otto and Smith, 2013). The adaptation of the method of Theler and Reynard (2011) resulted in adding dynamism to an otherwise static map and the

incorporation of vegetation as an geomorphological variable. The layer of process could not be obtained without identification of deposits by remote sensing and validating the observations in the field. Hillshade effect, derived from the DEM, has an azimuth bias (Smith et al., 2011) and the differentiation among bare rock, debris accumulation deposits, and grus is not possible with solely cluster analysis applied to the images. Meadows also could not be differentiated in the automated classification. Similarly, identification of lineaments had to be made manually because an automated approach would erroneously detect roads as lineaments in this area.

The downside of the construction of a manual geomorphic map is the need of expertise and field work, both important and indispensable tools for interdisciplinary studies in the critical zone. Geomorphology maps give the horizontal perspective to complement the vertical context of the current operational procedures of the Critical Zone (Chamorro et al., 2015). It is suggested that geomorphological mapping and its description be part of the background data of critical zone observations to plan sampling, field activities and facilitate the first approach towards the investigation of the catchment. The advantage of a simple geomorphology map as a common tool is obtaining an instant overview of the dynamics occurring in the common area under investigation.

Conclusions

The combination of automated and manual classification of landforms converges to a more comprehensible description of the features and processes occurring in a

watershed. The method of classification of the Iwahashi method resulted as a better fit for the goal of this work. Therefore, Iwahashi classification was superpose to the spatial results from the application of the manual classification, complementing the advantages of supervised and unsupervised methods of identification of landforms. The final geomorphology map summarizes processes and identifies fluvial, structural and anthropogenic features.

Distinct characteristics of Providence and its surroundings are the presence of steps and threads that can be seen as parallel bands from 300 m to 1.5 km apart. The presence of these features are explained by a phenomenon called back weathering (Jessup et al., 2011). Also, lineaments are abundant with dominant strikes in the N-NE direction. At the local scale, corestones are common throughout all the catchment, and some of them show differential weathering by higher soil moisture at the foot of scarps, forming mushroom rocks (Twidale, 1982). Debris-flow deposits, found mainly in the P301 and P302, originated from sediment stores (i.e., grus) abundant in the northern interfluves.

Areas of high and latent susceptibility for mass movement were defined. Areas with high susceptibility are defined as areas where deposits of sediment are prone to movement because of the scarce vegetation cover and the presence of channels in a radius of 10 m of distance. Compared with sub-catchments P301 and P303, P304 had more areas with high susceptibility despite that higher relief is found in the former sub-catchment. This finding is reaffirmed by the differences in sediment load in the channels (Hunsaker and Neary, 2012) and results of the hypsometric analysis.

CHAPTER III

RELATIONSHIP BETWEEN TERRAIN ATTRIBUTES AND DEPTH OF SOIL FROM AUGURING ESTIMATIONS AT THE CATCHMENT SCALE

In this chapter terrain attributes are calculated to explore the correlation of each one of them with measurements of soil depth obtained from hand auguring. Terrain attributes computed in this chapter are also used in Chapter IV and correlation analysis is used in the development of the model of soil depth in Chapter V.

Synopsis

The relationship between the thickness of the first horizon of soil and measurements of soil depth is explored using univariate and multiple linear regression. As a quantitative approach, the correlation between auguring measurements and terrain attributes obtained from DEM were tested and field observations supported the results. Among all the terrain attributes that were tested, exploratory analysis has shown that A Horizon is correlated with wetness index (R^2=0.47), slope (R^2=0.33) and plan curvature (R^2=0.32). Total soil depth is significantly correlated ($p<0.01$) with wetness index (R2=0.37), mean curvature (R2=0.24) and plan curvature (R2=0.19). Slope is poorly correlated (R2=0.15, $p<0.05$) with total depth unlike the Horizon A. The available number of samples is insufficient to valid results using multiple-linear regression. Therefore another type of soil-landscape model is necessary to explain the spatial variance of depth of soils in the catchment.

Introduction

Depth of soil in a specific location are the result of a combination of several geographical factors (Birkeland, 1999), and consequently, at the catchment scale, the spatial representation of this variable is far from being uniform. Some of the factors affecting soil depth are related to the geomorphological characteristics of the landscape, making the relationship between soil depth and terrain attributes relevant for the purposes of upscaling point measurements to a higher, desired scale.

The degree of correlation between soil and terrain attributes varies from site to site. In lands with historical or present agricultural uses a moderate to strong relationship between soil and terrain parameters exists (Akumu et al., 2015; Gessler et al., 2000; Gillin et al., 2015; Goovaerts, 1999; Hengl et al., 2004; Martin and Timmer, 2006; McKenzie and Ryan, 1999; Moore et al., 1993; Odeh et al., 1995; Young and Hammer, 2000; Zebarth et al., 2002). On the other hand, in natural landscapes the relationship is less clear. In native forests, erosion and deposition processes may cause the lack of a spatial structure, where pedogenetic processes dominate over geomorphic ones (Vanwalleghem et al., 2010). Geomorphological processes, in contrast, usually occur at rates many times higher than the formation of soils (Verstappen, 1983).

Natural lands with few interventions by human impacts have been reported with a high degree of randomness in the values of horizons thickness, and weak (Martin and Timmer, 2006; Pennock, 2003; Vanwalleghem et al., 2010) and strong (Gillin et al., 2015) relationships between soil and terrain attributes. Therefore, a generalization cannot be held, considering that native landscapes are less studied compared with

cultivated areas. Existing studies limit the focus on the A and B horizons because these are the most important for agronomic purposes (Vanwalleghem et al., 2010), and undisturbed landscapes are often related with poor accessibility, limiting sampling. This work, therefore, aims to contribute to this research gap.

The goal of this chapter is to analyze the correlation between point measurements of soil depth made by hand auguring and terrain attributes in the Providence Catchment. The following objectives were established to fulfill this goal: (1) compute terrain attributes from the LiDAR-DEM of Providence, (2) complete the SSCZO collection of the soil-depth measurements in a grid 123 m apart (4), spatially relate soil measurements and terrain attributes at an appropriate resolution, and (5) perform an exploratory analysis of the statistical relationship between soil and terrain attributes.

Area of Study

For this study point measurements and terrain attributes are calculated for the entire Providence Catchment. Details about the geology, soils and geomorphology of the area of study can be found in Chapter II.

Materials and Methods

Auguring Measurements

CZOSS samples of soil depth were obtained at 204 locations during the dry months of 2011, 2012 and 2013. Auguring measurements were done manually, using a metal-rod auger. The sampling was systematic, in a regular grid spaced 123 m apart. Auguring locations were recorded with a GPS, with an accuracy of an average 7 m under a forest canopy. From the 204 measurements, 152 were taken until refusal (i.e., hard bedrock was reached), whereas 49 reach the saprolite but not a hard contact. In either cases bedrock was reached, either in the form of saprolite or hard rock contact. In eight of the 204 samples, Soil horizons are described following the procedures of USDA-National Soil Survey Center (Schoeneberger, 2002), and using the Munsell color book. The average soil depth is 245 cm and the maximum is 728 cm. Figure 25 shows the distribution of auguring measurements and the patterns of depth in the catchment.

In addition, in 2010, CZOSS sampled 37 locations to obtain detailed information of soil parameters as part of the investigation conducted by Johnson et al. (2011). Among other soil attributes investigated, thickness of the A, B and C horizons were recorded, which are used in this work. Details about field and laboratory procedures can be found in Johnson et al. (2011).

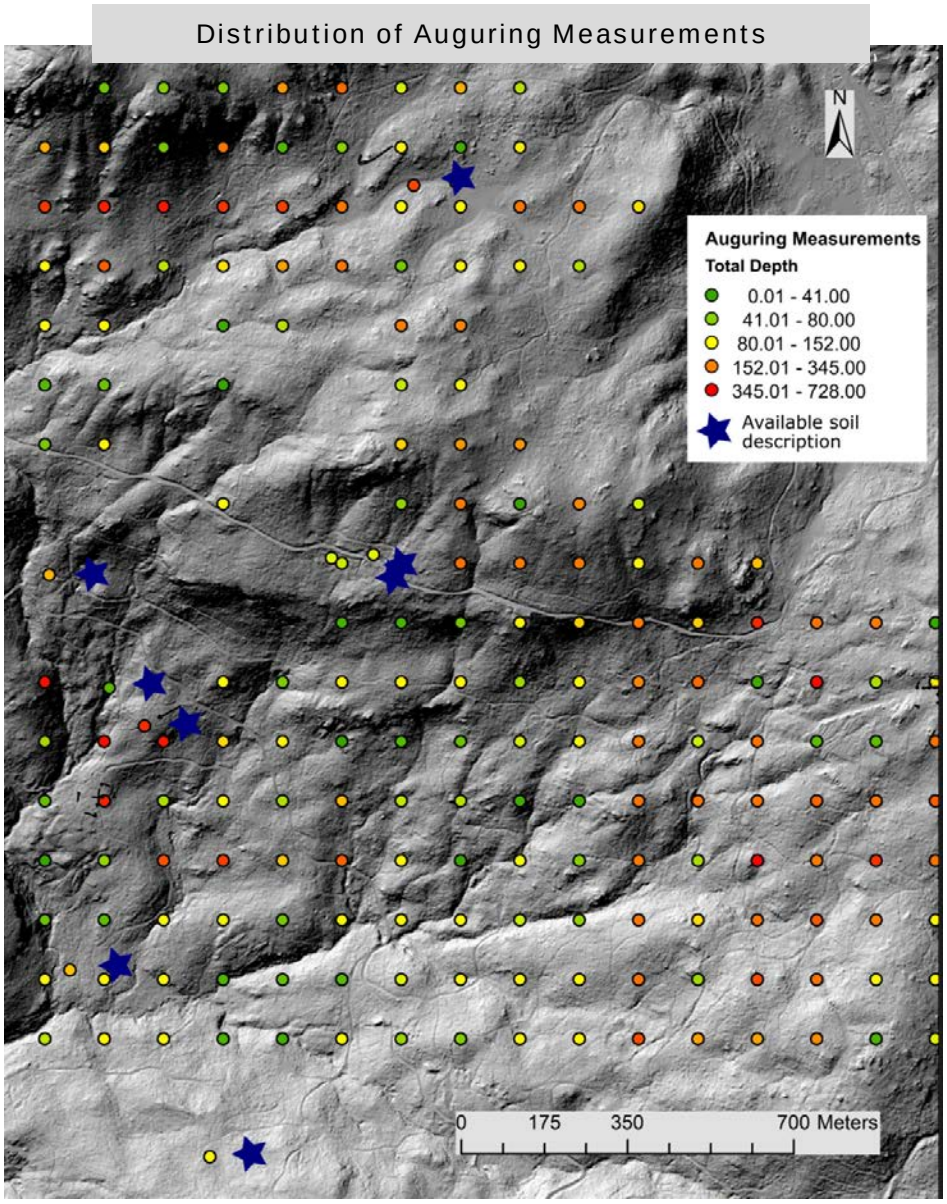

Figure 25. Distribution of auguring measurements. The blue stars indicate augurings where soil profile descriptions were made (N=8). Hot colors indicate deeper soils and green indicated shallower soils (cm).

Calculation of Terrain Attributes

Terrain attributes are morphometric parameters derived from elevation data. Therefore, the ability to distinguish landforms and obtain accurate terrain analysis is directly related with the resolution of DEM data (James et al., 2007). All terrain attributes were calculated using a DEM derived from LiDAR described in Chapter III (Materials and Methods Section).

Primary terrain attributes were computed directly from the DEM whereas secondary attributes were derived from the combination of the primary ones (Wilson and Gallant, 2000). All computations were made using Spatial Analyst® toolbox in ArcMap 10®, and the ArcSIE10® package developed by Xun Shi group (downloaded from http://www.arcsie.com/Download.htm). Terrain attributes algorithms were applied with a 3x3 window size. To match the resolution of the resulting rasters and the level of measurement error from the GPS (i.e., ±7 m), aggregation was performed to obtain a final cell size of 4x4 m. The method of aggregation used was the median of neighborhood cells to maintain the mean and median of the original rasters (Bian and Butler, 1999).

Terrain attributes tested are: slope (S), aspect (A), flow accumulation (FA), plan curvature (PaC), profile curvature (PoC), mean curvature (MC), tangential curvature (TC), vegetation height (VH), surface roughness (SR), stream power index (SPI), wetness index (WI), and Euclidean distance from connectivity of sediment stores (ST), lineaments (L), steps (SN) and break of slope (BS). Table 4 and Table 5 summarize the relevance, references and details about the calculation of the metrics.

Selection of terrain attributes were made based on correlations found in previous works (Gessler et al., 2000; Gillin et al., 2015; Hengl et al., 2004; Martin and Timmer, 2006; Moore et al., 1993). Also, ST, L, SN and BS, obtained from the manual geomorphological map developed in Chapter II, were hypothesized as relevant attributes to determine patterns of soil depth.

Values of terrain parameters were extracted without interpolation using Spatial Analyst on ArcMap 10® and added to the GIS database of soil depth measurements.

Table 4. Primary terrain attributes.

Terrain Attributes		Reference	Description of Calculations
Slope (S)	S drives surface-shaping processes such as erosion and deposition (Iwahashi and Pike, 2007)	(Horn, 1981)	ArcMap 10® uses the algorithm developed by Horn (1981)
Aspect (A)	A influences local microclimate (Zhao et al., 2007)	(Sharpnack and Akin, 1969)	ArcMap 10® uses the algorithm developed by Sharpnack and Akin (1969)
Flow Accumulation (FA)	FA affects weathering patterns	(Jenson and Domingue, 1988)	ArcMap10®
Plan Curvature (PaC)	PC indicates concavity or convexity, which are related with erosion and deposition processes.	(Zevenbergen and Thorne, 1987)	ArcMap 10.1® PC is calculated perpendicular to the direction of maximum slope. Each cell shows the percentage of convex cells in a 3x3 cell radius
Profile Curvature (PoC)	Slope variation in the vertical plane (Wilson and Gallant, 2000)	(Zevenbergen and Thorne, 1987)	Arcmap 10.1® PoC is calculated in the direction (parallel) of the maximum slope.
Mean Curvature (MC)	Medial values of the landform convexity and concavity (Olaya, 2009)		ArcMap 10® Default curvature computation derived from the mean of values between maximum and minimum curvature for each cell from a 3x3 window size.
Tangential Curvature (TC)	TC highlights differences in the land with the same principles of plan curvature	(Mitasova and Hofierka, 1993)	Phyton - Raster Calculator ArcMap 10 Plan curvature is multiplied by the sine slope

Table 4 Continued

Terrain Attributes		Reference	Description of Calculations
Vegetation Height (VH)	Maximum height of vegetation extracted from first returns of LiDAR data.		Phyton - Raster Calculator ArcMap 10
Surface Roughness (SR)	SR emphasizes the fine versus coarse expression of surface. Related with morphogenesis (Anbazhagan and Sajinkumar, 2011)	(Ruszkiczay-Rüdiger et al., 2009)	Phyton - Raster Calculator ArcMap 10

Table 5. Compound terrain attributes.

Terrain Attributes		Reference	Description of Calculations
Stream power index (SPI)	SPI describe a channel ability to move sediment	(Florinsky, 2012)	Phyton - Raster Calculator ArcMap 10®
Wetness Index (WI)	WI gives as a result spatial distribution of water flow and water stagnation (Irvin et al., 1997; MacMillan et al., 2000)	(Beven and Kirkby, 1979)	Phyton- Raster Calculator ArcMap 10®
Connectivity of Sediment Stores (ST)	ST is related with sediment stores mobility through channels (Theler and Reynard, 2011)		Phyton- Raster Calculator ArcMap 10® Euclidean distance from sediment stores and permanent channels
Lineaments Nearness (L)	Lineaments are zones of differential weathering (Anderson et al., 2002)		Phyton- Raster Calculator ArcMap 10® Euclidean distance from lineaments
Step nearness (SN)	Steps are areas of granitic tops in which soil tends to be shallower compared with treads (Jessup et al., 2011)		Phyton- Raster Calculator ArcMap 10® Euclidean distance from steps
Break of Slopes Nearness (BS)	Patterns of bedrock outcrops are related with areas where the depth of soil is at an equilibrium state (Dietrich et al., 1995)		Phyton- Raster Calculator ArcMap 10® Euclidean distance from main breaks of slope

Exploratory Analysis

Finally, to determine if a potential relationship exists between soil and terrain attributes, a partial correlation matrix was performed in R. The matrix summarizes results of scatter plots and single variable regression analysis. Although the number of measurements were not adequate to obtain reliable results with multivariate regression analysis (Li and Heap, 2011), the regression was performed to discuss the results.

Results and Discussion

Descriptions of Soil Profiles

Results of qualitative assessment of the eight soil profiles (Figure 26) show the variability of depth of soils and thickness of the A Horizon in the catchment, even in the same landscape positions. Dominant spectral colors were HUE 10 and 7.5. Change of color was observed from dark brown in the topsoil to yellow-brown (i.e., by the presence of iron-oxides) to a grayish (i.e., parent material) in deep profiles. Change in color is result of pedogenesis, and not the lithological discontinuities observed. Floodplains coincide with deep profiles, where deposition processes are taking place; whereas shallow profiles are present in toe-slopes. It is hypothesize however, that shallow measurements are the product of big intact bedrock pieces deposited by mobile regolith containing bedrock slides and rockfalls that could be easily mistaken by refusal. This limitation of reaching the actual granitic bedrock with hand auguring is reported in previous investigations (Earl et al., 2003; Phillips, 2008) and has been pointed out as one

of the problems to assess the real depth of the critical zone (Riebe and Chorover, 2014). Reaching the bedrock in this setting is difficult and expensive. Auguring can take several hours, and fragments may block and interrupt the drilling which limits the auger from reaching the actual bedrock.

Exploratory Analysis

Different results of correlations were found for topsoil (i.e., Horizon A) and subsoil (i.e., total depth). Univariate correlation found that A Horizon is correlated with wetness index (R^2=0.47), slope (R^2=0.33) and plan curvature (R^2=0.32) (Figure 27). Correlation between slope and the thickness of Horizon A suggests that lateral movement of water and sediment differentiated by the local-slope and upslope contributing area are contributing to the variability of topsoil (Gillin et al., 2015).

Total soil depth is significantly correlated ($p<0.01$) with wetness index (R2=0.37), mean curvature (R2=0.24), and plan curvature (R2=0.19). Slope were poorly correlated (R2=0.15, $p<0.05$) with total depth, unlike Horizon A (Figure 28). Contemporary pedological and geomorphological processes are more active in the surface horizon and may explain the better correlation in the horizon A with slope (Park and Burt, 2002). Vanwallehhem et al., (2010), however, have found non-statistical relationships between terrain and soil attributes of the upper horizon in a forested, natural landscape, but a significant correlation with the attributes of slope and wetness with the horizons B and C (Vanwalleghem et al., 2010). Hence, with more differentiation between natural and cultivated landscapes, the relationship between soil

and terrain attributes is site specific. And, although the wetness index is correlated with the thickness of the first horizon and total soil depth, this coincides with previous studies (Gessler et al., 1995; Moore et al., 1993; Vanwalleghem et al., 2010); discordant findings with respect to other terrain-soil attribute relationships, make a call to avoid generalizations.

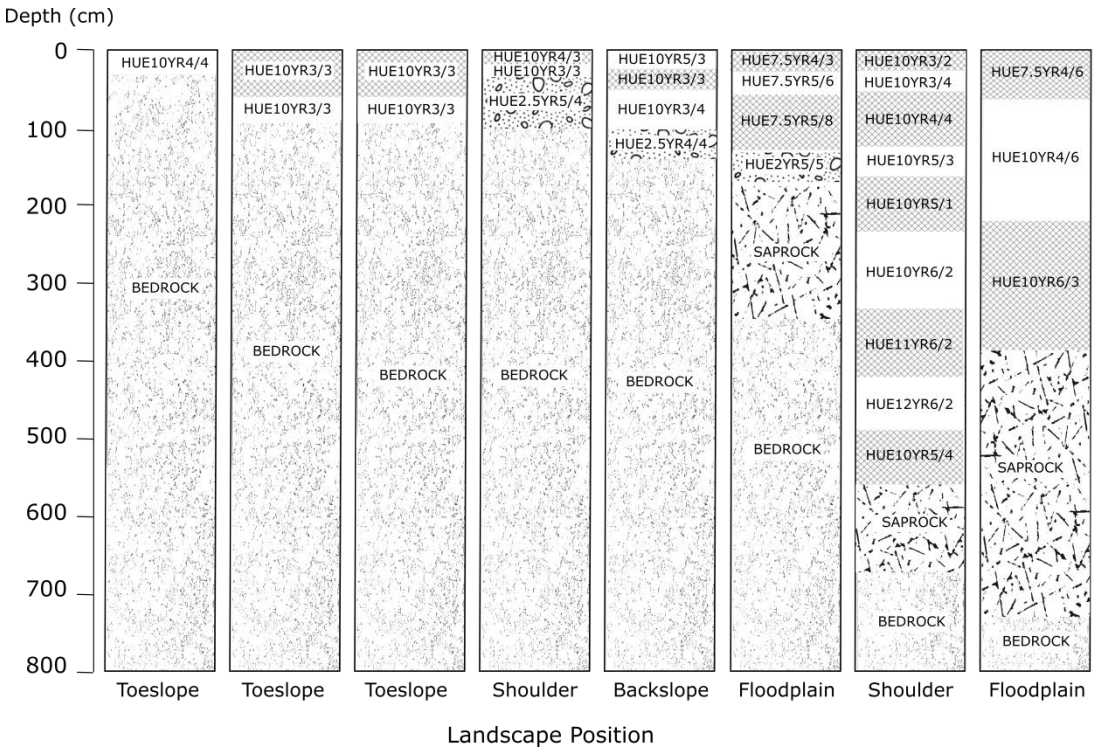

Figure 26. Soil profiles at different landscape positions (Ventura and Irvin, 2000). Each one of the horizon is differentiated by Munsell colors.

Gessler et al. (2000), however, found a strong relationship between soil depth (i.e., Horizon A and Horizon A and Horizon B combined) and some terrain attributes (i.e., slope, wetness index and flow accumulation) because the type of sampling (i.e., excavations to bedrock) is different from the other researchers in native areas. Depth to

bedrock was determined directly in the backhoe and hand-dug pits. In concave positions where the soil material was >3 m in depth, estimations of soil depth were made using a truck-mounted Geoprobe that measures electrical resistivity of lithologic layers (Gessler et al., 2000).

Soils without vertical discontinuities and the significant correlation of topsoil and subsoil with wetness index reinforce the theory that *in situ* pedogenesis is dominant over geomorphological processes in native landscapes (Moore et al., 1993; Skidmore et al., 1996; Vanwalleghem et al., 2010). It is relevant to consider this hypothesis while choosing the method of modeling soil depth in the entire catchment because, for example, kriging ignores pedogenesis (Moore et al., 1993).

Modeling Soil Depth with Linear Multiple Regressions

Results of multiple regression are in agreement with previous findings in Providence Catchment (Bales et al., 2011a). Although Bales et al. (2011a) used a restricted cubic-splines technique in the regression to account for the non-linearity in the relationship between slope and total soil depth (Harrell, 2013), in both cases, the model explains only 16% of the variance. This is because the number of samples of the thickness of the A horizon (N=37) and total depth (N=204) are insufficient to account for the high spatial heterogeneity of the data. Therefore, to obtain valid predictions through multiple linear regression and capture spatial changes, a higher density of samples would be necessary (Li and Heap, 2011). Besides that, the requirement of a normal distribution (Hengl et al., 2004) is not met by the original values of total soil

depth. Even if a cox-box transformation is applied (Figure 29), the result of the normality test (i.e., Shapiro-Wilk) indicates that the data still cannot be used for confident predictions. Therefore, another type of modeling needs to be applied, which is the topic of investigation of Chapter V.

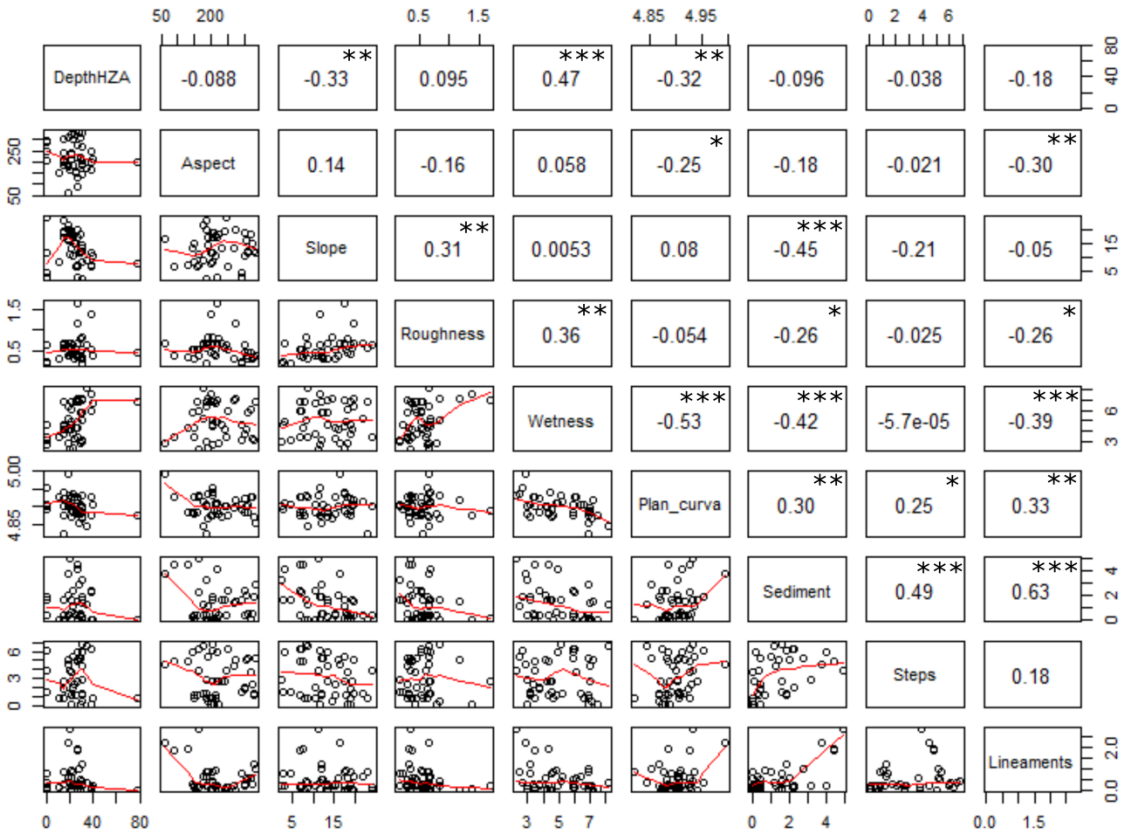

Figure 27. Scatter Plot matrix of depth of horizons A (N=37) and selected terrain attributes. In the top are the results of single variable regression analysis. In the bottom are the scatter plots with a Loess smoother shown in red. P-values of significance are shown as :* if ≤ 0.05, **if ≤0.01 and ***if ≤ 0.001.

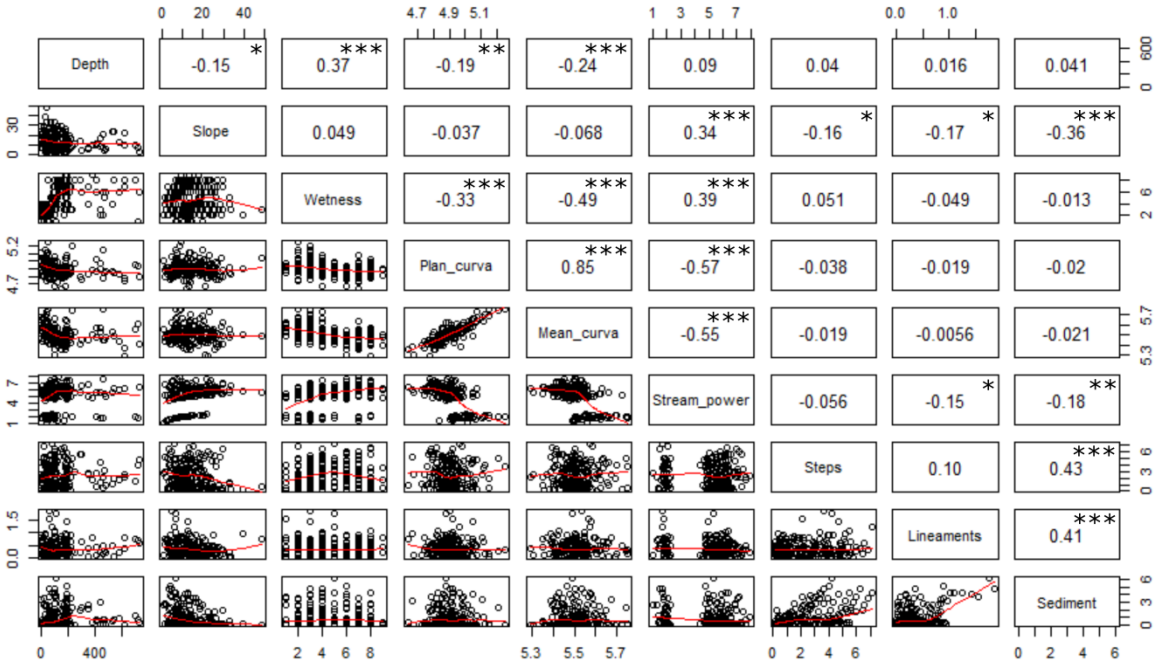

Figure 28. Scatter Plot matrix of total depth (N=203) and selected terrain attributes. In the top are the results of single variable regression analysis. In the bottom are the scatter plots with a Loess smoother shown in red. P-values of significance are shown as :* if ≤ 0.05, **if ≤0.01 and ***if ≤ 0.001.

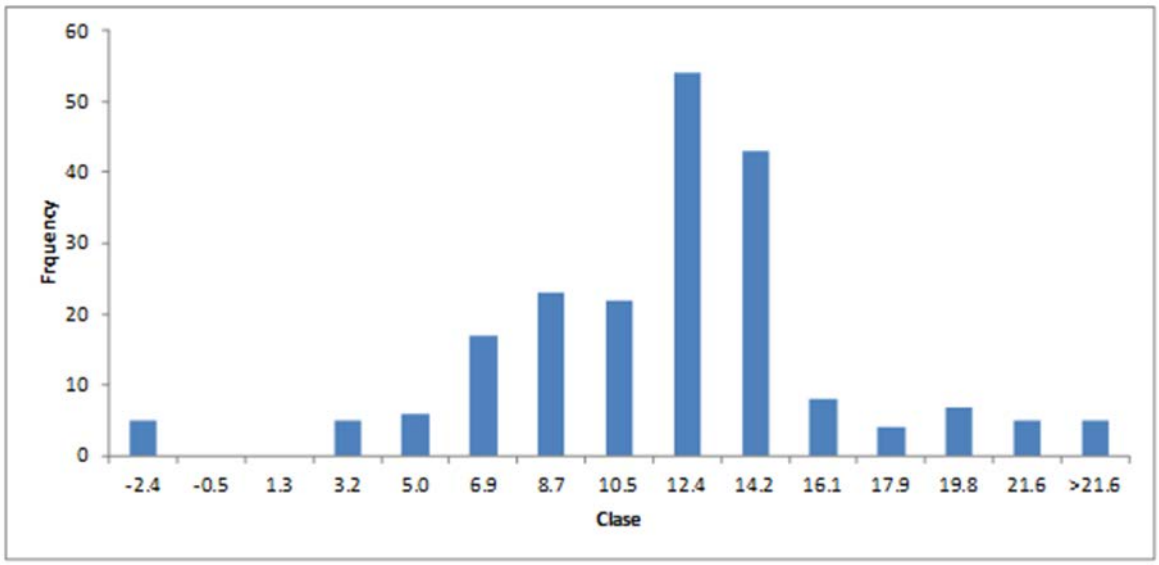

Figure 29. Histogram of the total depth data set after cox-box transformation was applied, resulting in a decrease of skewness and kurtosis.

Table 6. Summary of Statistical Results of Multiple Linear Regression for the A Horizon and total depth using the terrain attributes with the best univariate correlation.

Residuals

	Min (cm)	1Q	Median	3Q	Max (cm)
A Horizon	-31.879	-4.810	-0.493	3.416	41.968
Total Depth	-159.07	-60.82	-36.21	-4.58	693.88

Coefficients

	A Horizon (cm)		Total Depth (cm)	
(Intercept)				
Regression	146.7931		3,836.089	
Wetness	3.3075	***	18.040	*
Slope	-0.8012	**	-	
Mean curvature	-		-809.326	
Plan curvature	-26.0626		136.751	
Adjusted R^2	**0.3026**		0.1573	
F-statistic	11.41	***	13.63	***

Note: ** means P<0.01 and *** means P<0.001. Values without asterisk mean that results are not significant.

Precise location of measurement is necessary to take advantage of the maximum resolution of the DEM (i.e., 1 m). Because all field measurement were taken with a GPS that has a maximum error of 7 m, aggregation was necessary to relate the variables correctly. Also, different coordinate systems and transformation were used during the data collection. Permanent field markers, installed by the SSCZO group, were identified and mapped to ensure that the locations were well-positioned. All the preprocessing of the spatial data is an essential requisite for soil-landscape analysis.

Conclusions

Qualitative and quantitative geomorphological information were used to observe the spatial distribution of depths of soil at the catchment scale. Qualitative description of soil profiles discard lithological discontinuities and support quantitative results. This finding reinforces the idea that field description cannot be ignored (Phillips, 2008).

Among all the terrain attributes that were tested, exploratory analysis has shown that the A Horizon is correlated with wetness index (R^2=0.47), slope (R^2=0.33), and plan curvature (R^2=0.32). Total soil depth is significantly correlated ($p<0.01$) with wetness index (R2=0.37), mean curvature (R2=0.24), and plan curvature (R2=0.19). Slope poorly correlated (R2=0.15, $p<0.05$) with total depth, unlike the A horizon.

Results of multiple regression are in agreement with previous findings in the Providence Catchment (Bales et al., 2011a). Simple multiple regression developed here and the cubic splines technique to the regression developed by Bales et al. (2011), explains only 16% of the variance of depth of soils. This is because the number of samples of horizon A thickness (N=37) and total depth (N=204) are insufficient to account for the high spatial heterogeneity of the data. Besides that, the requirement of a normal distribution (Hengl et al., 2004) is not met by the original values of total soil depth. Even if a cox-box transformation is applied (Figure 29), the result of the normality test (i.e., Shapiro-Wilk) indicates that the data from auguring measurements alone cannot be used for confident predictions. In addition to the inadequate spacing between samples, the presence of random corestones distributed in the subsurface, may mislead them with saprock refusal. Therefore, another type of data collection and

extrapolation method is required to capture the spatial heterogeneity of soil depth in Providence Catchment.

CHAPTER IV

RELATIONSHIP BETWEEN TERRAIN ATTRIBUTES AND ESTIMATIONS OF SOIL DEPTHS FROM GROUND PENETRATION RADAR AT THE CATCHMENT SCALE

This chapter describes the collection of the measurements of soil depth using Ground Penetrating Radar (GPR) and explores the correlation between the results and terrain attributes computed in Chapter III. The results of this chapter are used in the development of the model of soil depth in Chapter V.

Synopsis

GPR was used to obtain depth information of the first horizons of soil in the Providence watershed as an alternative to hand auguring. Obtaining thickness of soil horizons in this forested, granitic region by drilling is laborious and expensive and may lead to inaccurate results by misleading refusal of bedrock by the presence of corestones and roots. Estimations of total depth and thickness of the A Horizon were taken based on the reflection of electromagnetic waves using a 100 Mhz and 200 Mhz antenna. The results were contrasted with hand-auguring measurements. The results suggest that the antenna resolution were not adequate for identifying A horizons, but a good correlation ($r=0.9$, $p<0.001$) was found between GPR and auguring measurements on estimations of total depth. Total depth estimations were then contrasted with terrain attributes from a LiDAR-DEM, suggesting that slope, wetness index and lineaments were the attributes

with better correlation. Multiple linear regression using these attributes show that GPR can explain 36% of variance of data at the catchment scale.

Introduction

Capturing the spatial variability of soil depth is important for models of water transport, studies of productivity (Krüger et al., 2013), and prediction of shallow landslides (Yamakawa et al., 2012). Therefore, estimations of total depth along with descriptions of the structure of soil profile are also necessary for studies conducted in the critical zone. Especially, the thickness of the A horizon in forest landscapes is fundamental for studies of soil drainage, nutrient cycling, nutrient availability (Craigg et al., 2015), model soil respiration (Zribi et al., 2015), C storage (Abella et al., 2013; Johnson and Curtis, 2001; Kristensen et al., 2015), and also studies of environmental assessments, such as the impact of compactation (Craigg et al., 2015), thinning (Abella et al., 2013) and land degradation (Mohawesh et al., 2015).

Among all soil properties, the variable depth of soil continues being the baseline for several studies, but one of the most difficult to define and measure (Riebe and Chorover, 2014). Traditional methods of auguring are expensive, disruptive and laborious. In granitic environments, hand auguring presents the inconvenient encounters with blocks of fresh bedrock and roots through the profile. The malleability of the saturated horizons can also limit the advance of the augur. The auguring campaigns conducted by SSCZO during the years of 2010-2012 provide valuable information, but the spacing between measurements (i.e., 123 m) does not capture the natural occurring

horizontal variability of soil depths. Moreover, drilling does not always reach bedrock or saprock. As in other granitic environments of the world, rock fragments and irregular bedrock topography make the interpretation of the auguring measurements more ambiguous (Doolittle and Butnor, 2009).

An alternative to auguring is the use of geophysical tools, which unlike drilling, are noninvasive and inexpensive. Holbrook et al. (2013) investigated the total depth of the weathering mantle in a peripheral, north area of Providence with seismic refraction and electrical resistivity data. Maximum soil depth appeared to vary from 10 up to 35 m deep in this area, occurring within level surfaces separated by steps (Holbrook et al., 2013; Wahrhaftig, 1965). The weathering thickness of granite reported by Holbrook et al., (2013) are coincident with the reported thickness of weathering mantles in others granite environments of North America (Migon, 2006). Although the geophysical methods used by Hoolbrook et al. (2013) permitted an estimate of the total thickness of the weathering profile, the first soil layers cannot be resolved because of the low resolution of these methods.

Among the geophysical techniques that are able to investigate the subsurface with high resolution is Ground Penetrating Radar (GPR). GPR is able to provide estimations of the depth of soil in a continuum, and, therefore, allows the investigation of the spatial variation of the variable of interest in two and three dimensions.

GPR has been successfully used in granitic environments to obtain the spatial variation of soil depth, reaching up to 20 m deep (Aranha et al., 2002; Davis and Annan, 1989), and the lateral extent of horizons with a few centimeters of thickness (Collins and

Doolittle, 1987; Laamrani et al., 2013). Actually, GPR has been used since 1970 to support soil surveys in the United States. The technology is based on the emission and reflections of electromagnetic waves, and the record of dielectric permittivity changes in the medium (Davis and Annan, 1989; De Benedetto et al., 2012). The velocity and attenuation of waves transmitted into the ground is controlled by the water content of geological materials (Davis and Annan, 1989). Strong radar reflections are produced by soil interfaces with abrupt boundaries and contrasting materials. Contrast between soil horizons is often associated with differences in moisture, texture, bulk density or chemical properties (Doolittle and Butnor, 2009), making the differentiation of horizons possible.

Although GPR has the ability to obtain high resolution information from the subsurface, loss of range of penetration and resolution occurs in the presence of conductive materials like clay, silts or soils with conductive pore water (Everett, 2012). Penetration is also controlled by the frequency pulse of the emitting antenna. For example, an antenna emitting 200 Mhz produces greater resolution compared with a 100 Mhz antenna, but the former is more limited in depth of penetration (De Benedetto et al., 2012).

GPR estimates, however, cannot be used completely independently. Validation with direct measurements is a requirement (Cassidy, 2009). In this work, GPR surveys are collected and contrasted with hand-drilling measurements made by SSCZO to validate the use of this technique in the Providence Catchment. Although GPR has been successfully used to obtain thickness of the soil (Davis and Annan, 1989; Yamakawa et

al., 2012), few studies have been conducted in wildlands, especially on mountain hillslopes (Sucre et al., 2011; Vanwalleghem et al., 2010). This section of the Sierra Nevada, located at an elevation between 800 to 2000 m, is highly heterogeneous (Bales et al., 2011a) and highly forested, with a water table that it is located at less than 2 m deep in the dry season. These characteristics present challenges for GPR surveys, but two factors favor the use of the technique in this setting: (1) the availability of auguring measurements, and (2) the relatively homogeneity of bedrock in the area of study, composed of granodiorite, which allows the radar wave to penetrate and capture changes in the electrical conductivity of the soil (Sucre et al., 2011).

This study contributes to the understanding of the capabilities and limitations of the use of GPR in this type of environment, and discusses the feasibility to use the results in landscape-soil models.

The primary goals of this study are to collect data of thickness of the A horizon and total soil depth in a continuum, to capture the spatial variability of data, and to correlate this information with surface characteristics at a catchment scale. To achieve these goals the following objectives must be met: (1) collect subsurface information of the first 10 m of regolith using ground penetrating radar; (2) validate the remote-sensing measurements, and (3) explore the correlation between the results and terrain attributes.

Area of Study

The area of study is described in Chapter II.

Materials and Methods

Materials

Auguring measurements, obtained from SSCZO and qualitative data collected in eight locations, were used to confirm and validate GPR estimations. Description of field methods used to obtain auguring measurements can be found in Chapter III. The location of auguring measurements is shown in Figure 30.

Terrain attributes were obtained from the LiDAR-DEM described in Chapter II. The original DEM raster with 1 m resolution was aggregated to a 4 m resolution using the bilinear neighborhood interpolation method. The process of mapping GPR profiles and auguring measurements were made using ArcMap 10®. R mode statistical analysis was used.

GPR Survey

The GPR device used in the survey was a pulse EKKO PRO LF®, system connected to a Digital Video Logger (DVL) that allowed real-time observations in the field, manufactured by Sensors & Software Inc® (Canada, 2006). Seventeen transects were collected using a 200 Mhz antenna whereas three transects were collected using both, a 100 MHz and a 200 MHz antennas. The 200 Mhz antenna was preferred because

of the higher resolution compared to the 100 Mhz antenna, and the smaller of the plates, facilitating the carrying of the instrument throughout the field. Lengths of the transects vary according to the accessibility of the locations. Actual lengths of transects were 75 to 362 m. The recommendation of the manufacturer was used for the establishment of step-size distances.

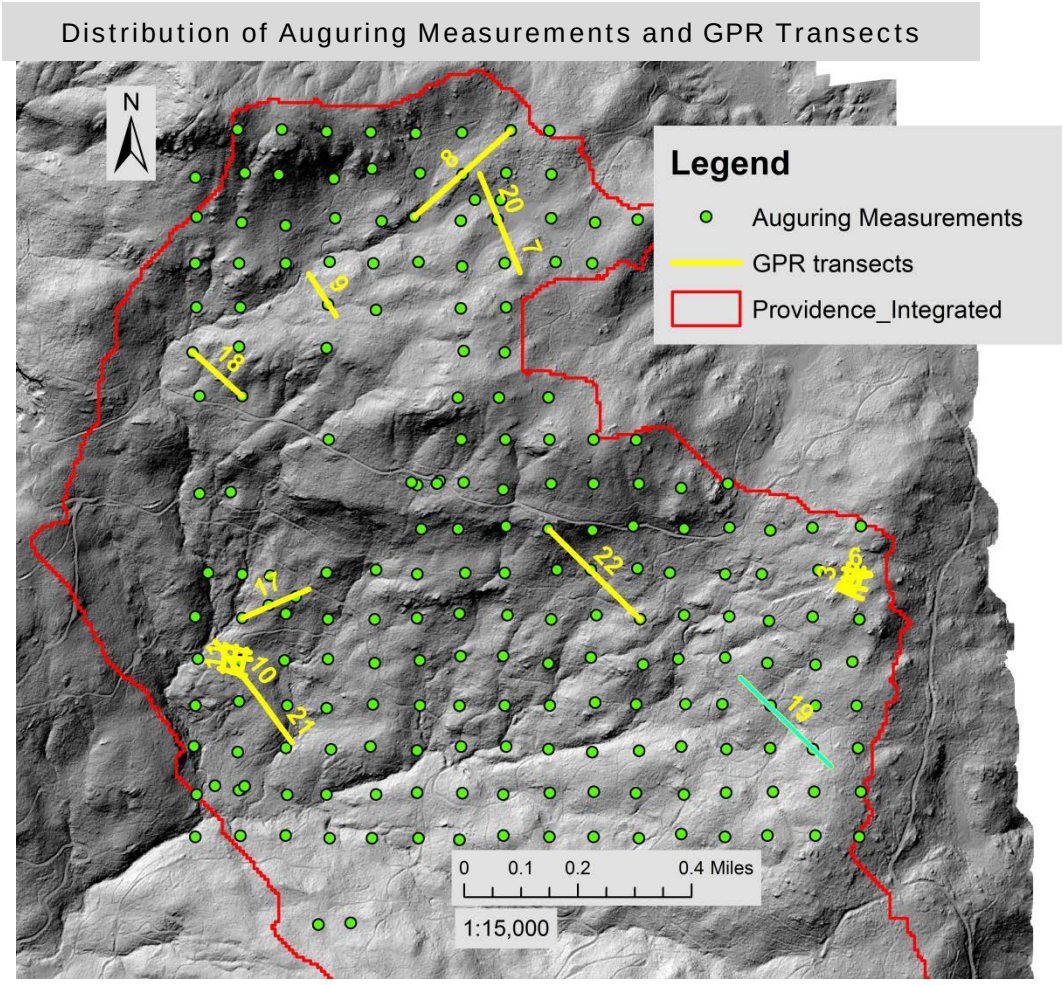

Figure 30. Survey locations of auguring measurements (green) and GPR transects (yellow). Boundaries of Providence catchment are shown in red. Numbers indicate the ID transects and clusters. Hillshaded raster is derived from a 1 meter resolution DEM. Scale: 1:15,000.

The survey was conducted during the summer (July 2013), when soil moisture was low compared with other time of the year. The area of study was remote enough to be free of noise. Position and direction of the transects (Figure 30) were selected with the purpose of capturing the cross-section geomorphological variability (i.e., landscape position, topographic curvature and slope), and to overlap with auguring measurements.

The beginning, the end, and each 10-m intervals of each transect were recorded using a GPS unit model Garmin GPSMAP 60CS®. The error of the GPR device in the field was between 5 to 7 m under the canopy. Exact places of hand auguring were marked in the field by the SSCZO in previous years, and some of these markers were used to locate the exactly location of auguring measurements, made in previous years. To counteract the field error of the GPS, the exact same trajectory was used for comparing results from the 100 and 200 Mhz antennas. The direction was defined with a compass. Before the survey, branches of trees and shrubs were removed from the GPR trajectory to avoid abrupt interruptions and protect the optical cable. A measuring tape was installed to reduce step-size distortion. The lines were surveyed by two operators, and in some deep slopes three operators were needed.

The sampling interval was 0.5 m and 0.25 m for the 100 Mhz and 200 Mhz antenna respectively. Sixteen traces at each survey position were made (i.e., stacking) to increase the signal-to-noise ratio. Stacking improved data quality counteracting noise by the presence of roots and soil moisture levels (Everett, 2011).

Processing of the Raw Data

Raw data collected in the field were processed following standard procedures to better visualize reflections (Cassidy, 2009), using the EKKO View 2® and EKKO View Deluxe R4® softwares. Simple filtering methods were preferred over advanced ones to avoid the loss of weak signals (Davis and Annan, 1989) and the introduction of subjective bias (Cassidy, 2009). This is especially important in a complex and heterogeneous environment as Providence Catchment.

Basic processing consisted of file reconciliation, trace editing (i.e., deletion of unusable data by equipment malfunctioning data and replacement by averaging immediate neighbor traces), dewowing (i.e., time filtering to remove low frequencies and preserve high frequencies), and time-zero correction (i.e., 5% of first peak amplitude in each trace) (Yelf, 2004). Background removal filtering was applied using a time window of ten traces around the original trace. In this way, some horizontal noise was removed avoiding the removal of the signature of soil horizons. Basic processing was followed by Spreading and Exponential Compensation (SEC) Gain. Unlike Automatic Gain Control (AGC), which enables visualization of shallower and deeper reflectors at similar display intensity (Everett, 2012). The attenuation value for the SEC was 3.0 (α) and a start function value of 1.

Point values of estimations of soil depth were recorded in a GIS using a spacing of 1 m apart. ArcMap-3D Analyst® was used to account for the topography in the location of point measurements in the GIS. A total of 6,645 estimations were recorded.

Determination of Velocity

Three methods to calibrate (i.e., obtain the velocity of the wave propagation) GPR data exist: common midpoint surveys (CMP) (Aranha et al., 2002; Laamrani et al., 2013; McClymont et al., 2010; Mysaiah et al., 2011), burying a target at a known depth (Sucre et al., 2011), and hyperbola fitting (Cassidy, 2009; Lunt et al., 2005; Moorman, 2001). CMP is a frequent method found in the literature. Nonetheless, CMP is not suitable for this study. Huisman et al. (2003) suggest that multiple offset measurements disadvantages result in (1) difficults in distinguishing the direct wave from refracted/reflected events, (2) difficults in selecting an appropriate antenna separation for rapid reconnaissance mapping; and (3) excessive attenuation of the ground wave resulting in uncertainties (Slater and Comas, 2009). For all these reasons, the methods of burying a target at a known depth and hyperbola fitting were preferred. A metal disc was buried at a 25 cm depth in three of the transects (i.e., the assumption was that the ability to resolve the details of a target or separately detect two targets is proportional to the size or spacing of the target in relation to the wavelength of the incident radiation). Also, hyperbola fitting was estimated in all transects using the EKKO View Deluxe R4® software. Several fittings were performed in the first and bottom layers of the profiles and a mean value was calculated to validate the method comparing it with the buried object results.

Results of velocity estimations were then used to obtain values of thickness of A horizon and total depth. The relationship between depth and velocity for homogeneous and isotropic materials are derived from (Davis and Annan, 1989):

$$d = v_r \frac{t}{2}$$

Where d is the depth of the homogeneous material in meters, v_r is the calculated velocity in meters by nanoseconds, and t is the two way travel-time in nanoseconds.

Interpretation of Radar Profiles

The continuity of reflections was observed in each profile, discriminating true subsurface signals from horizontal reverberations caused by noise. The A horizon was identified by the continuous reflection observed after the ground coupling (Figure 31). Once identified, minimum values of amplitude in the section were extracted by using a macro built in Excel (Microsoft Office®).

Total depth was estimated observing strong reflections that were assumed to come from the abrupt increment of bulk density by the presence of either saturated bedrock, soft bedrock, or unweathered bedrock. The eleven drilling descriptions were used to relate signal signatures with thickness of the A horizon and total depth. This is an essential steps for associate reflections with real features in the subsurface (Cassidy, 2009; Everett, 2012; Riebe and Chorover, 2014).

Validation of Estimations

Statistical validation of the results were made by analyzing the correlations between (1) the auguring and GPR estimations at the exactly same location (N= 17), and (2) GPR estimations and corresponding mean values of auguring measurements in the

coincident homogeneous units of a composite map (N=6,645 for thickness of the A horizon and N= 2,284 for total depth).

Because of the differences of spatial resolution between auguring and GPR methods, a small number of auguring measurements overlap exactly in the same locations of the survey lines. To validate the GPR results using a large sampling, a method of extrapolation of the values of soil depth from auguring was applied. The method involves the creation of a composite map from the terrain attributes that better explain the variability of soil and the assignment of a number of auguring measurements equivalent to the number of GPR estimations, respecting the variability of soil depth of each unit. Slope and wetness index are the two terrain attributes better correlated with the values of the A horizon whereas wetness and mean curvatures are better correlated with total depth measurements (i.e., discussed in Chapter III). Four classes are used in each variable (Table 7). Basic statistics were obtained from each one of the resulting units of the composite map, and frequency from the histograms was transformed in a set of weighted coefficients for the correlation (Table 8). The result is a set of modelled auguring measurements that is equal in number to the GPR estimations. Finally, a Pearson product- moment correlation was computed between these simulated auguring measurements and all GPR data.

Table 7. Classification of the terrain attributes used in the composite map. The range of values for each variable is specified.

Slope Classes		Wetness Index Classes		Mean Curvature	
ID	(Slope %)	**ID**	CTI, (Beven and Kirkby, 1979)	**ID**	Curvature (ArcMap 10)
1	0 - 9.48	**1**	0-1.10	**1**	0-5.454
2	9.48-17.32	**2**	1.10-1.96	**2**	5.454-5.488
3	17.32-27.44	**3**	1.96-2.97	**3**	5.488-5.522
4	27.44-83.31	**4**	2.97-12.64	**4**	5.522-6.202

Table 8. Basic statistics are given for each of the homogeneous units of the resulted raster by combining wetness and curvature terrain attributes.

GIS Value	Wetness	Curvature	Mean Total Depth	GPR Values Histogram	Univariate statistics or analysis
10	1	5	121.55	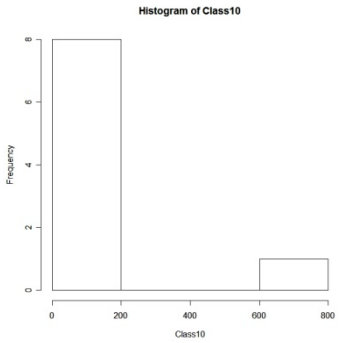	n= 9 stdev 230.56 max 722 min 0 Median 43.50 1st Qu. 13 3rd Qu. 61
6	2	5	93.60	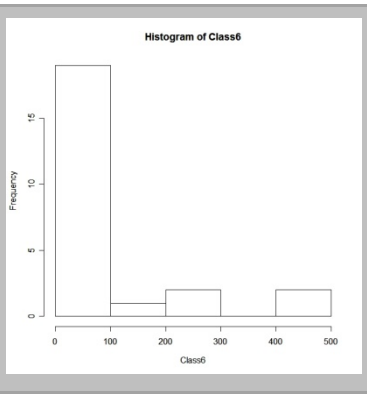	n= 24 stdev 125.51 max 460 min 0 Median 43.50 mfv 27/32/37 "most frequent number" 1st Qu. 59.60 3rd Qu. 66.62

Table 8 Continued

GIS Value	Wetness	Curvature	Mean Total Depth	GPR Values Histogram	Univariate statistics or analysis
1	3	5	78.95	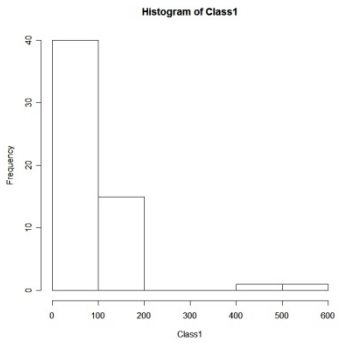	n= 57 stdev 90.20 max 525 min 0 Median 30.5 mfv 101 1st Qu. 59.60 3rd Qu. 101
7	4	5	143.62	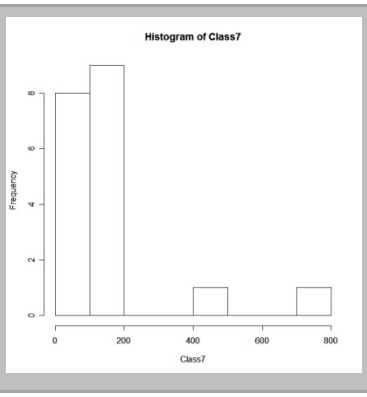	n= 19 stdev 163.75 max 728 min 0 Median 101 mfv 101 1st Qu. 72 3rd Qu. 120
9	5	5	142.51	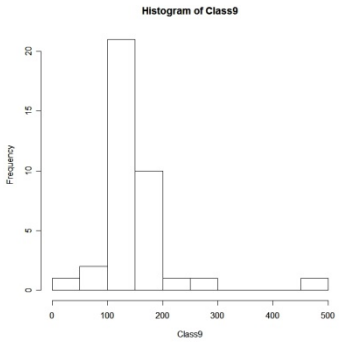	n= 37 stdev 75.36 max 465 min 0 Median 109 mfv 101 1st Qu. 101 3rd Qu. 185

Table 8 Continued

GIS Value	Wetness	Curvature	Mean Total Depth	GPR Values Histogram	Univariate statistics or analysis
5	6	5	201.16	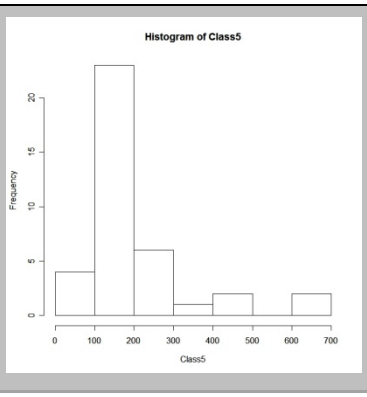	n= 38 stdev 143.38 max 700 min 45 Median 163 mfv 101 1st Qu. 114.5 3rd Qu. 205
2	7	5	225.88	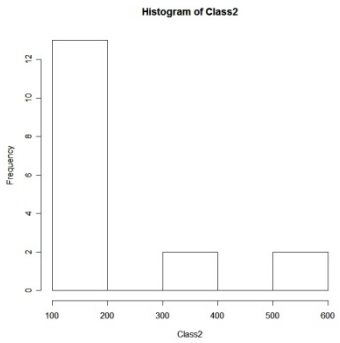	n= 17 stdev 146.37 max 581 min 101 Median 180 mfv 101/180 1st Qu. 59.60 3rd Qu. 101
3	8	5	407	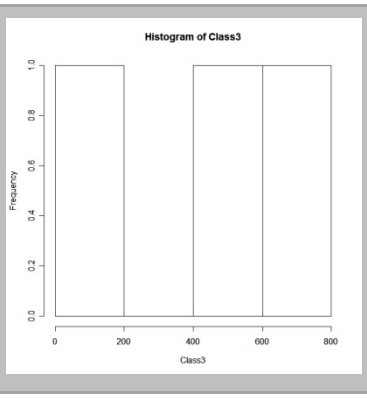	n= 3 stdev 217.51 max 623 min 188 Median 410 1st Qu. 299 3rd Qu. 516.5

Correlation between Results and Terrain Attributes

Terrain attributes were derived from the DEM (Chapter II) and plotted against estimations of depth of soils to assess if a potential relationship between the variables

exists. A partial correlation matrix was built to identify the best correlations, and the relationship was further explored using a stepwise linear regression (Moore et al., 1993).

Results and Discussion

Interpretation of the Radar Profiles

Estimations obtained using the 100 Mhz and 200 Mhz antennas were statistically similar ($N=100$, $r=0.92$, $p<0.01$). Estimations of thickness of the A Horizon were obtained from the 200 Mhz antenna with better resolution. The results of the 100 and 200 Mhz antennas were used for estimations of total depth.

After processing, visual inspection of the data shows the presence of stratification in all profiles. Hence, it was assumed that different velocities according to different conductivity values are present. Chaotic reflections, typical of corestones and erratic blocks of bedrock (Moorman, 2001), are present throughout all profiles.

Ground coupling caused by the interaction between the emitted EM wave and the ground (Laamrani et al., 2013) was seen in the top of radar profile (Figure 31). To remove the ground coupling effect, a time-zero adjustment was performed in each trace.

Estimations of A Horizon and total depth were calculated after the velocity of the radar wave in each profile was determined. The computed velocity, using a metallic object at a known depth, coincided with the results obtained by using the method of hyperbola fitting. Hyperbola fitting was, therefore, used to measure velocity in all profiles in shallow and deep horizons. Measurements of mean velocity in the horizon A

are estimated in 0.08 m/ns if data were collected using the 200 Mhz antenna, and 0. 069 m/ns if the 100 Mhz antenna was used. Mean velocity at the deeper horizon was determined as 0.1 m/ns for both antennas. The results of velocity are in agreement with values reported for granite (0.12-0.13 m/ns) (Neal and Roberts, 2000) and organic soils (between 0.042 and 0.038 m/ns) (Emili et al., 2006; Laamrani et al., 2013).

Soil moisture conditions in the field enabled the experiments to reach 10 to 12 m deep using the 100 Mhz antenna, and 5 to 7 m using the 200 Mhz antenna. Nevertheless, all transects lost range and resolution with depth, possibly caused by the presence of conductive material and saturated soft bedrock. The occurrence of fine interbedding restricts the penetration depth of radar waves as energy is lost at each reflecting horizon (Everett, 2012).

The high number of hyperbolas in all profiles is evidence of an irregular shape of bedrock (Cassidy, 2009), and variations of soil moisture are visualized as internal reflections in the profiles (Laamrani et al., 2013). Although in granitoid rocks weathering profile is particularly well-ordered in comparison with other type of rocks. Localized weathering occurs in the pre-existing zones of weakness. This phenomenon makes the geometry of the weathering front highly irregular (Migon, 2006). Therefore, instead of a clear boundary between saprolite and fresh bedrock, a gradient exists (Figure 32b). This finding is not surprising, and this topic remains as a continued object of investigation (Riebe and Chorover, 2014).

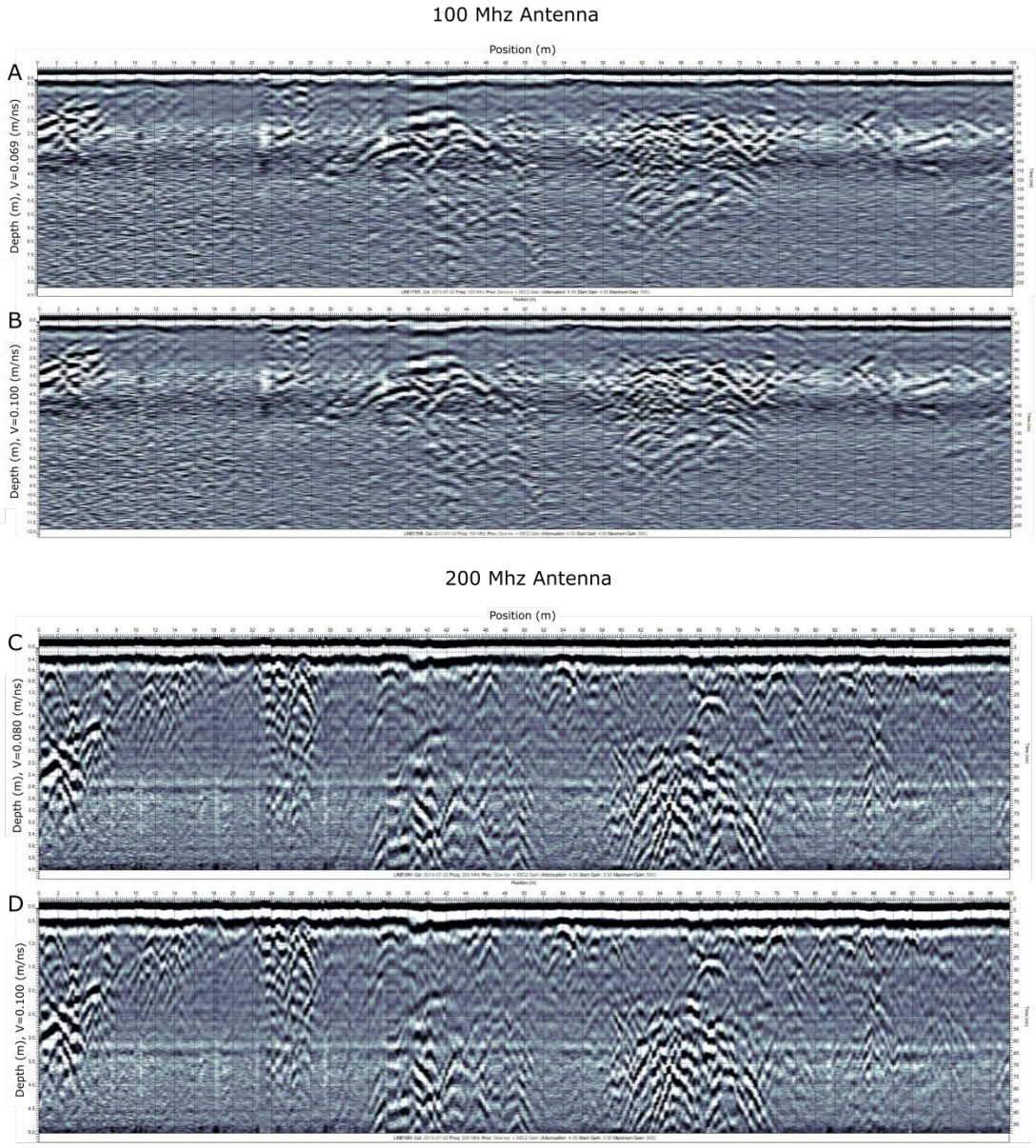

Figure 31. Transect 18 after processing was performed. The 100 Mhz antenna reached to 8 m deep, but at the cost of resolution. Differences of velocity in the top and bottom of the profile were taken into the account for interpret bedrock interface in B and D. Horizon A was calculated using the velocity obtained in the first meter of the profile in A and C. The Y axes show the depth (m) obtained converting time of wave travel, and the X axis shows the position (m) along the transect. SEC Gain was applied (Attenuation:4.00, Start Gain:3.50, Maximum Gain:500).

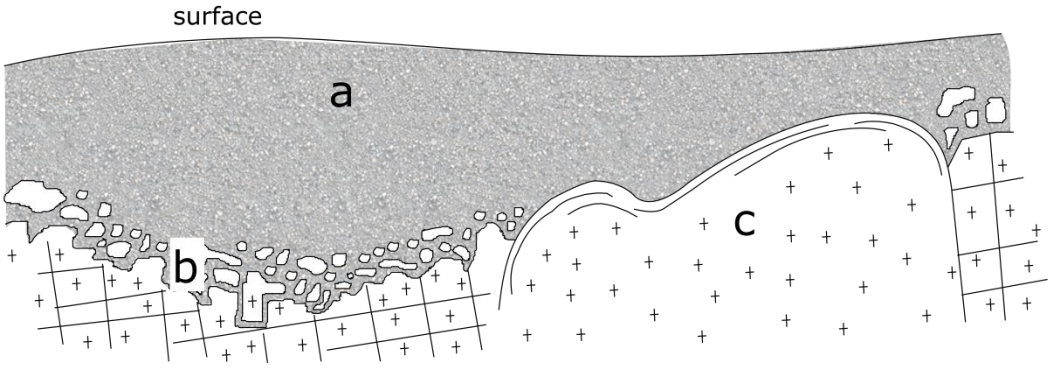

Figure 32. The classical profile of granitic rocks (Migon, 2006). A fuzzy boundary exists between fresh, fractured bedrock and saprolite. Organic and mineral soil (a) is followed by random blocks and cores of bedrock (b) before reaching the fresh bedrock(c).

In all transects, a continuum reflector is observed at three m of depth. Below this depth the signal is attenuated. And, even small amount of clay in the subsurface is enough to reduce the penetration depth (Doolittle and Collins, 1998). Generally, argillic horizons provide smooth, continuous reflectors because of the abrupt and substantial increase in clay content and bulk density (Doolittle and Butnor, 2009).

Fine-textured pedogenic layers have been reported in the Central Sierra Nevada Mountains at the same ranges of elevation as Providence (Figure 33), where clay translocation occurs below 1,600 m (Dahlgren et al., 1997). According to Dahlgren et al. (1997), the thickness of argillic horizons at 34 to 56 cm of depth increases until this elevation threshold, reaching a maximum at 1,390 m. Dahlgreen et al. (1997) hypothesized that the existence of this threshold is a result of active leaching by rainfall in areas below the winter snow line located at the elevation of 1,594 to 1,962 m

(Dahlgren et al., 1997) and 1,750 m to 2,008 m (Roos and Sahota, 2010), which coincides with the position of Providence.

This idea is reinforced by the described presence of clay during the drilling, after the 60 cm of depth, reaching a thick, argillic horizon at the 332 cm, in which an abrupt change of color occurs (i.e., from HUE10 to HUE 11 and 12). This description coincides with the location where the continuous reflection in the GPR profiles occurs (Figure 34). Also, roots were present until 342 cm of depth, close to the described argillic boundary.

All these reasons lead one to suggest that the reflection present in the profiles, along with the decrease of GPR signal below this depth, would correspond to a horizon a higher content of clay. The signal is not completely attenuated, however, because at this elevation, kaolinite is the dominant clay mineral in the surface horizons, and halloysite in the deepest ones (Dahlgren et al., 1997). These minerals, that are abundant in the Southern Sierra Nevada (Birkeland and Janda, 1971), have low cation-exchange capacity and low base saturation[2], producing less attenuation, if compared with minerals such as smectitic and vermiculitic (Doolittle and Butnor, 2009). Indeed, the abundance of kaolinite in the weathering mantle is usually associated with significant loosening of the rock fabric and an increase percentage of clay fraction. Clayed mantles dominated by kaolinite and residual quartz are typical products of very advanced weathering of granites (Migon, 2006). This is evident by the deep weathering mantle found by Holbrook et al., (2013) and the present investigation.

[2] Amount of basic cations that occupy the cation exchange sites, divided by the total cation exchange capacity.

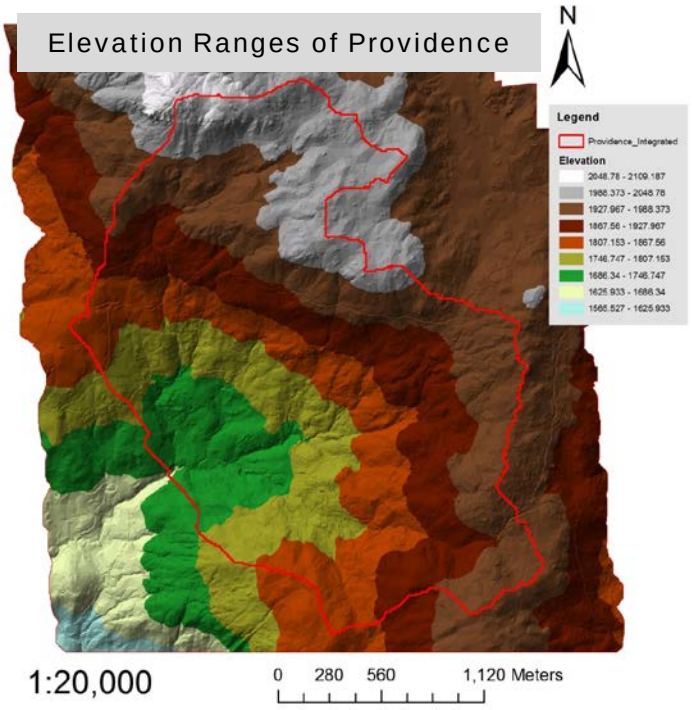

Figure 33. Ranges of elevation in Providence Catchment.

Horizontal variations of soil depth are pronounced at each profile, even in transects of 75 m long. Patterns of highly variable soil depths seen in Providence, changing by tens of meters over distances of a few hundred to tens of meters, has been observed in other granite environments in the world, such as the Jos Plateau in Nigeria, Sierra do Mar in Brazil and the Kowloon Peninsula, in Hong Kong (Migon, 2006).

Validation of Results

Estimation of Horizon A Soil Depths

A statistical summary between estimations made with auguring and the GPR technique is presented in Table 9.

Table 9. Comparison of descriptive statistics of estimations of thickness of Horizon A and total soil depths using auguring and GPR techniques.

	Thickness of the A Horizon		*Total Soil Depth*	
Method of estimation	**Augur**	**GPR**	**Augur**	**GPR**
Average (cm)	*24.95*	*34*	139.94	319.03
SD (cm)	*12.86*	*15*	138.21	192.17
Min (cm)	*0*	*0*	0	0
Max (cm)	*78*	*133*	728	900
N	*73*	*6645*	204	2,233
Skew	*1.45*	*-0.22*	2.22	0.33
Kurtosis	*6.1*	*2.9*	5.29	-0.6

Where: SD=Standard deviation, min= minimum value, max=maximum value and n= number of observations.

GPR overestimated the thickness of the A Horizon in all measurements (Figure 35). The first reflection that follows the effect of ground coupling, were interpreted as the maximum depth of the A Horizon. The resolution of the 100 Mhz and 200 Mhz antennas, however, were insufficient to differentiate subtle changes in soil properties in the topsoil. According to a USDA Report (2013), however, the Horizon A of families Gerle-Cagwin and Shaver have typical development of a A horizon of 33 cm to 76 cm, respectively (Soil Survey Staff, 2013), and GPR measurements do not escape from this range (Table 9). Further investigation with unified criteria of A Horizon interpretation would confirm the lack of correlation found.

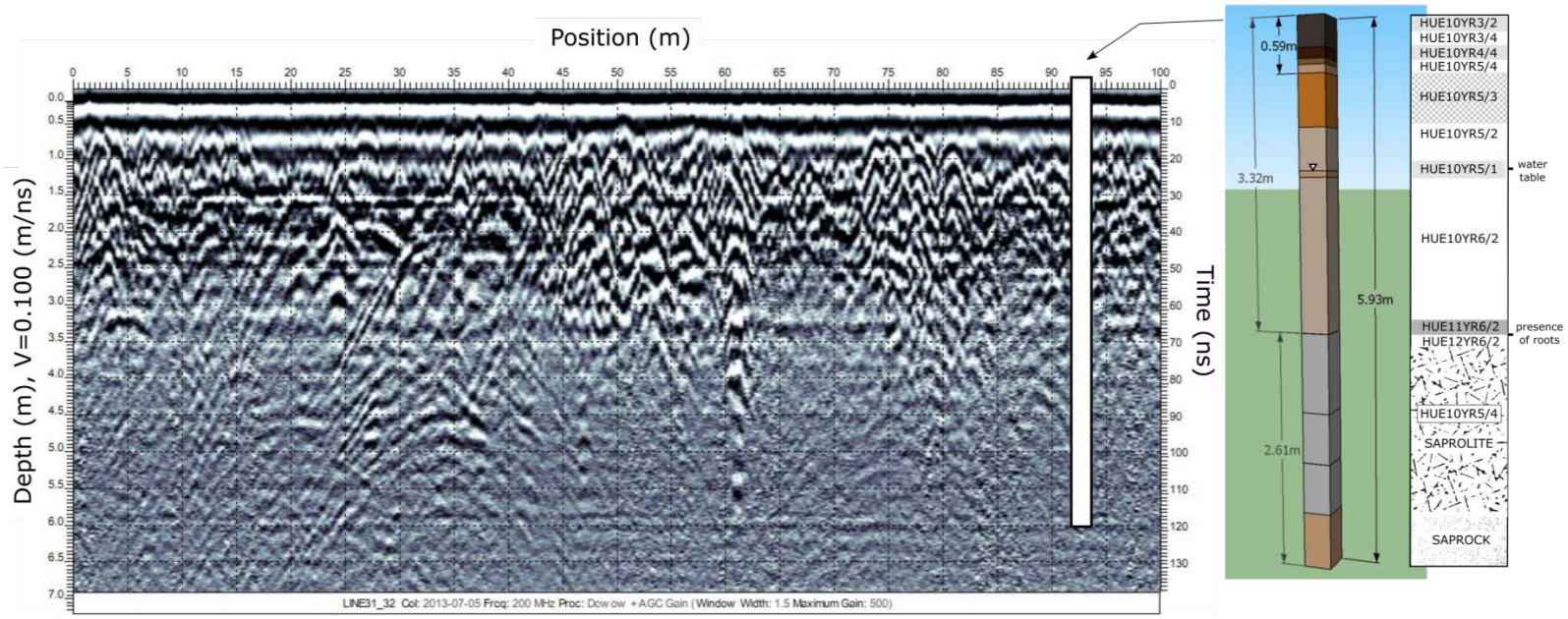

Figure 34. Transect 31 and the position and description of the coincident measurement made with the augur. Water table was observed at the 176 cm of depth and root were present were abrupt change of color occurs, at the 320 cm of depth.

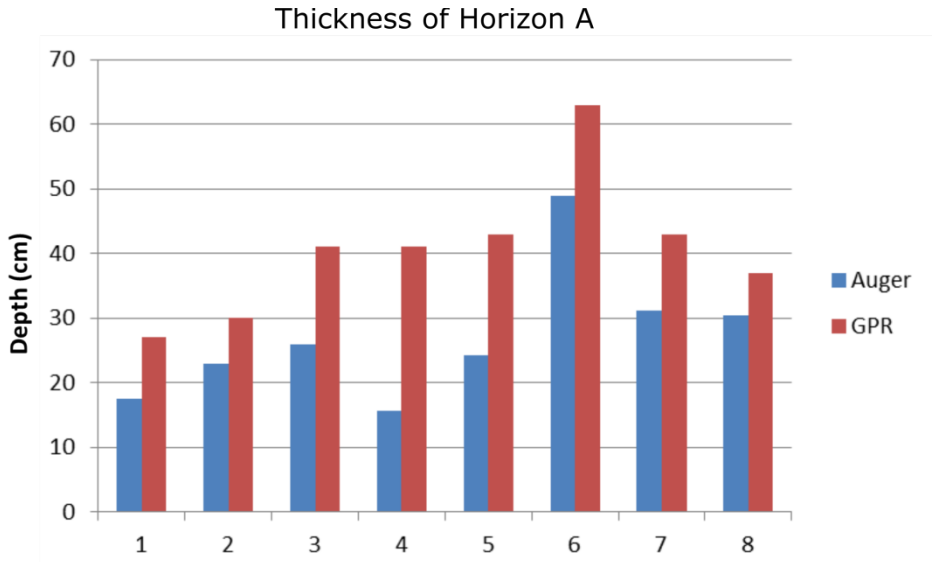

Figure 35. Comparison between the estimations of thickness of the horizon A made by auger and GPR methods.

The results of the correlation between estimations from auguring and from GPR by classes are shown in Figure 36. This result confirms the lack of meaningful relationship between values.

Total Soil Depth

Values of total depth estimations from auguring that overlap with any of the GPR transects are shown in Table 10.

When the overlap between the GPR estimations and auguring measurements of points of soil depth are compared, GPR exceeds auguring in all values (Figure 37). This finding is not surprising and is supported in the literature because the limitations of auguring measurements are known (Harrison et al., 2011; Jayawickreme et al., 2014; Sucre et al., 2011). Considering the eight hand-auguring measurements, five were not

drilled until refusal. Table 10 shows the comparison between estimation from the two methods. Asterisks show measurements where the soils are potentially deeper. Drilling in the presence of erratic blocks led to sub-estimation in measurements. Still, when overlapped measurements from auguring and GPR are compared, changes of color of the qualitative descriptions (i.e., Munsell color book) coincide with reflections of GPR profiles. And although GPR has some degree of subjectivity in the interpretation of features (Cassidy, 2009), the overlapping between color change and position of reflections were assumed as a validation of the use of the geophysical technique. That being said, the position of the last strongest reflection in the profiles was interpreted as the total depth value at that particular position. The assumption is that a strong reflection is related with a dramatic decrease in bulk density, where the interface between saprolite and saprock is located. A comparison between reflections from deep bedrock and exposed corestones facilitated the interpretation of these strong reflections.

Despite the differences in the total depth, the mean augur measurements by classes and the equivalent GPR measurements were well correlated ($r=0.9$, $P<0.001$) (Figure 38).

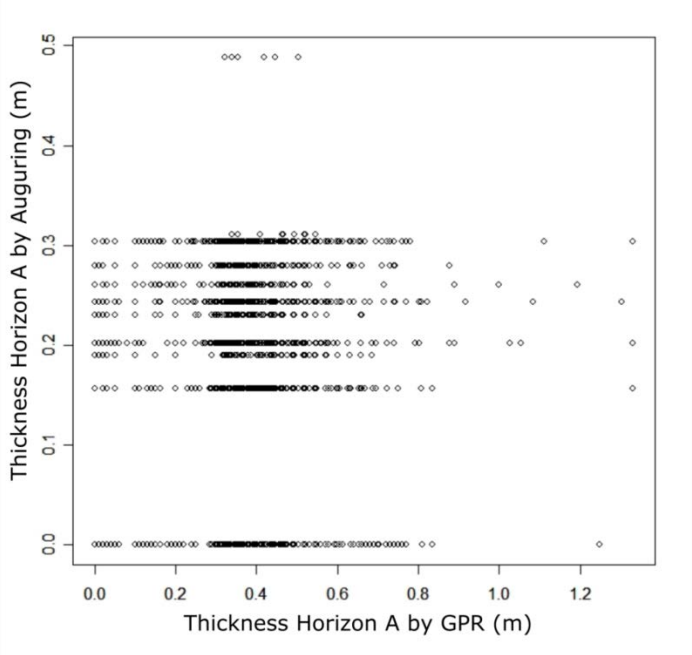

Figure 36. Graph showing the lack of correlation of thickness of A Horizon between estimations obtained from GPR and hang auguring. The test of relationship was made based in mean soil depth values by classes of a map composed by a combination of wetness and slope terrain attributes derived from a 4m resolution DEM.

Table 10. Comparison of total soil depth estimations obtained from auguring and GPR.

Augur ID	Estimated Depth using hand auger (cm)	GPR ID	Estimated Depth using GPR (cm)
G1	**101***	**Line 20**	**260**
190	**345**	**Line 19**	**380**
H3	**101***	**Line 17**	**200**
H2	**101***	**Line 17**	**250**
G1	**101***	**Line 20**	**250**
D3	**109**	**Line 21**	**250**
A6	**30**	**Line 36**	**100**
I9	**101***	**Line 35**	**300**

Table 10 Continued

Augur ID	Estimated Depth using hand auger (cm)	GPR ID	Estimated Depth using GPR (cm)
P10	**106**	**Line 11**	**120**
201	**150**	**Line 26**	**102**
201	**581**	**Line 30**	**600**

* Measurements were soils are potentially deeper. Drilling was stopped before refusal.

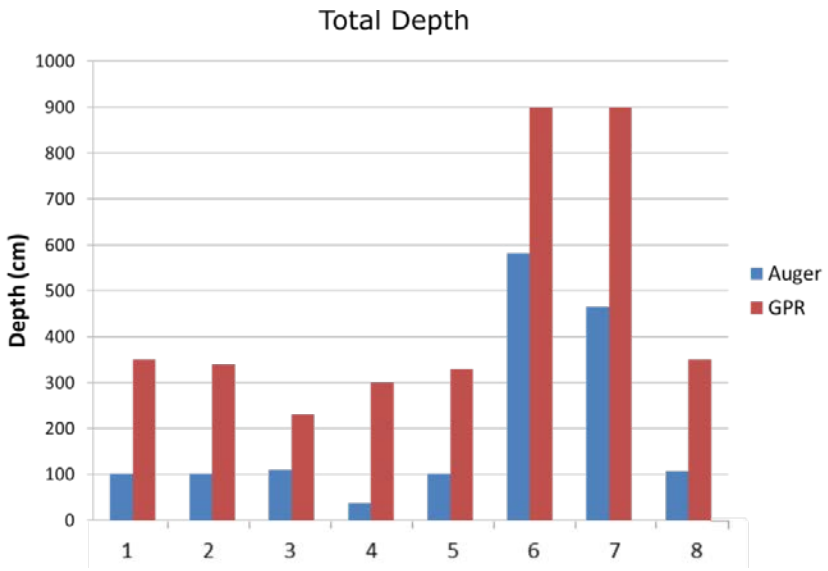

Figure 37. Comparison between the eight estimations of total depth made with the hand auger and GPR. These eight soil point measurements are located exactly along the transects.

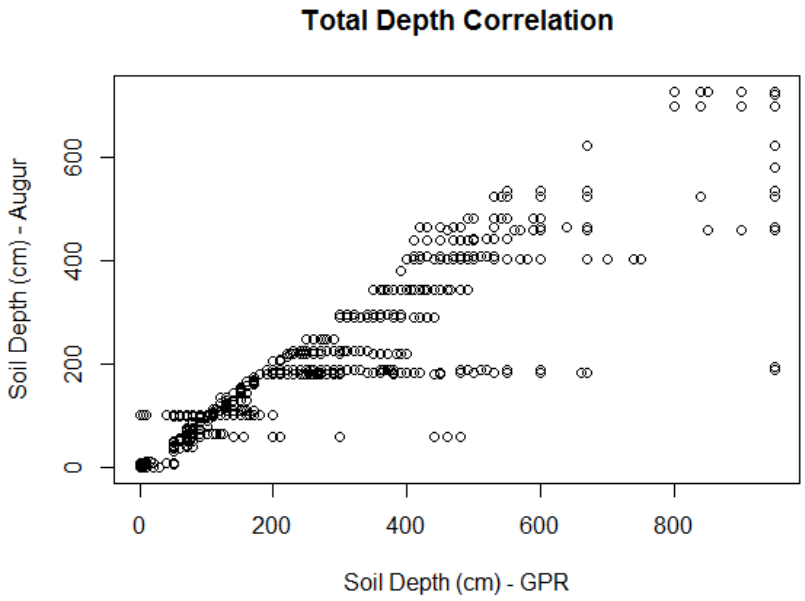

Figure 38. Graph showing the correlation between total soil depth estimations obtained from GPR and hang auguring. Values obtained of auguring measurements were obtained from classes of a map composed were the values were weighted by a combination of curvature and slope terrain attributes derived from a 4m resolution DEM (r=0.9, P<0.001, n=2,004).

Correlation between Terrain Attributes and Soil Depth

Univariate Correlation

Figure 39 presents the results of univariate correlation between terrain attributes and soil depths as a preliminary analysis. Although all terrain attributes developed in Chapter II were tested, the subset that presented some degree of correlation are presented. It can be assumed that terrain attributes that are absent in Figure 39 do not represent meaningful, statistical significance.

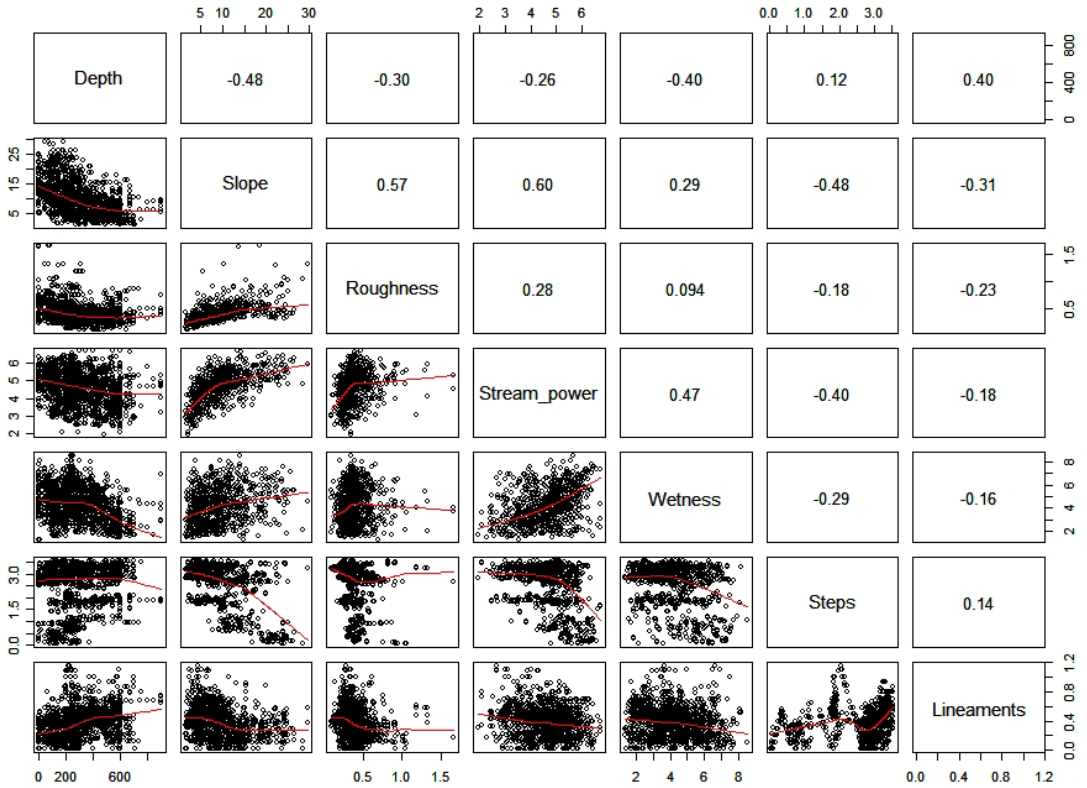

Figure 39. Results of correlation. P<0.001.

Modeling Soil Depth with Linear Multiple Regressions

The three terrain attributes that are better correlated with soil depth are selected for further analysis: slope (r=-0.48), wetness (r=-0.40) and lineaments (r=0.40) (Figure 38). Multiple regression modeling, using GPR data and three terrain variables (i.e., wetness, slope and lineaments), explains 36% of the variance in values of total soil depth in Providence (Table 11). Modeling using GPR data had a better performance if compared with the results shown using auguring measurements in Chapter III (i.e., adjusted R^2=0.1573). This better performance may be explained by the higher density of

samples (Li and Heap, 2011), covering the entire catchment, and by the method of designing values of weight according to the spatial variability inside classes.

Table 11. Multiple-regression coefficients relating total soil depth and significant terrain attributes.

Residuals					
	Min (cm)	**1Q**	**Median**	**3Q**	**Max (cm)**
Two variables	-397.79	-124.72	5.49	121.39	653.84
Three variables	-412.07	-113.78	-0.64	107.56	578.42
Coefficients					
		Two Variables		**Three Variable**	
(Intercept)					
Regression		606.2484		479.9477	
Wetness		-37.0023		-34.3991	
Slope		-13.9284		-11.3260	
Lineaments		-		239.1523	
Adjusted R^2		**0.3032**		0.3625	
F-statistic		485.3		423	

Note: P<0.001. Values without asterisk mean that results are not significant.

Conclusions

GPR was applied in twenty transects in different places along Providence Catchment to estimate the thickness of A horizons and total soil depths. The results of this study are: (1) GPR is a feasible tool to obtain depth to saprock in Providence Catchment. Compared with other geophysical techniques, GPR using 100 Mhz and 200 Mhz antennas requires only two operators, who can carry the instrument throughout the field where automobile accessibility is not possible. One of the challenges of using the

method in a forested mountainous region is to transverse the region to be sampled at a constant speed to avoid uncertainty in the sampling between markers. This is specially limiting on steep slopes. The results suggest that the use of the 200 Mhz antenna did not have the adequate resolution for identifying A horizons. A good correlation ($r=0.9$, $p<0.001$) was found, however, between GPR and auguring measurements on estimations of total depth.

(2) A gradient of changes in bulk density are seen in the GPR profiles, observed as layers of different materials. It was assumed that the strong reflection seen at approximately 3 m deep in all profiles is related with an argillic horizon reported in previous works to coincide with a snow line at the elevation in which Providence is located (Dahlgren et al., 1997).

Although it is known that deeper soil exists (Holbrook et al., 2013), the resolution of GPR allows it to discriminate details of the first meter of soil that are essential for hydrological studies (Weiler and McDonnell, 2004). (3) Terrain attributes that are better correlated with GPR estimations of depths of soil are slope, wetness and lineaments. This finding differs from the best correlations related auguring measurements (Chapter III), where curvature, wetness and slope showed a significant relationship. It is not surprising, however, that lineaments (i.e., joints and fractures) are related with soil depth, because preferential flow through fractures enhance weathering processes (Pacheco and Alencoão, 2006)

CHAPTER V

MODEL OF SOIL DEPTH OF THE PROVIDENCE CATCHMENT

This chapter describes the model of soil depth, which combines the geomorphology map developed in Chapter II and the investigation of the relationship between soil depth and terrain attributes described in Chapters III and IV.

Synopsis

Information about soil depth at the catchment scale is important for hydrological and hazard studies. Few studies exist, however, reporting the spatial variation of the depth of the soil, especially in areas such as the Sierra Nevada Mountains, where the landscape is not affected by agriculture, but instead is highly forested. Commonly used soil-landscape models were developed to predict values of the soil depth at the catchment scale, such as linear regressions or co-kriging, which depend on a structured sampling design or autocorrelation assumptions. This is a limitation because today geophysical surveys have been replacing conventional and expensive auguring methods to obtain the depth of soil. Here, a test the proposed method developed by Dahlke et al., (2009) using GPR transect information for soil depth combined with auguring measurements is undertaken. The RMSE (Root-mean-square deviation) between predicted and modelled values shows that better prediction occurs using the combination of four-terrain classes and the geomorphology map. The performance of the model (R=0.51) is in agreement with previous findings in this landscape. Thus, it can be shown

that descriptive geomorphology maps in combination with geomorphometry are valid tools for addressing the spatial heterogeneity of soil parameters in natural, complex terrains.

Introduction

Spatial models that capture the heterogeneity of the thickness of the soil are important inputs of spatially distributed hydrological and ecohydrology models (Arnold et al., 2012; Tague and Band, 2004; Wigmosta et al., 1994). Information on the depth of soil is also necessary in studies of slope stability (Dietrich et al., 1995; Guzzetti et al., 2012) and seismic hazards (Shafique et al., 2011), and to understand why heterogeneity exists in the first place (McDonnell et al., 2007). Then, the level of success of predictions of these models still depends of the development of good soil-landscape models that can capture the heterogeneity of surface data without exhaustive surveys of soil measurements.

Although the importance of this variable in the studies of the critical zone have been recognized by different disciplines (Riebe and Chorover, 2014), few quantitative studies exist about the horizontal variation of the depth of the soil, especially in areas such as the Sierra Nevada Mountains, where the landscape is not affected by agriculture, but instead is highly forested (Riebe and Chorover, 2014; Tesfa et al., 2010; Vanwalleghem et al., 2010). Challenges to obtain the measurements of soil depth in highly forested and little intervened areas are accessibility, the irregular topography, and

the technical difficulties obtaining auguring measurements because it is expensive, inaccurate and laborious.

In all cases - natural and highly disrupted landscapes – different models that allow the extrapolation of a few soil measurements to a higher extent have been proposed to account for the spatial variability of soil parameters (Scull et al., 2003). Existing approaches to obtain a continuous spatial representation of the values of soil depth are: (1) physically-based landform evolution models (Dietrich et al., 1995; Heimsath et al., 2005; Nicótina et al., 2011; Saco et al., 2006), (2) interpolation by using auxiliary terrain information and statistical techniques as linear regression (Moore et al., 1993), (3) regression trees (McKenzie and Ryan, 1999), (4) moving window regression (Laffan and Lees, 2004), kriging and co-kriging (Hengl et al., 2004; Kuriakose et al., 2009; Odeh et al., 1995; Ryan et al., 2000), (5) general linear models (McKenzie and Ryan, 1999), (6) general additive models (Tesfa et al., 2010), (7) Bayesian expert systems (Skidmore et al., 1996), (8) fuzzy logic (Zhu et al., 2010; Zhu et al., 2001), and (9) empirical-based geomorphological approaches (Catani et al., 2010; Dahlke et al., 2009; Shafique et al., 2011).

Three concerns exist about all of the mentioned methods: scaling, requirement of technical expertise, and the need of a certain sampling structure to ensure statistically desired coverage. The latter is an especially important limitation because geophysical techniques are increasingly replacing extensive and expensive auguring to obtain information about the depth of soil (Holbrook et al., 2013), and geophysical surveys are obtained in transects and not necessarily in a uniform grid distribution.

Also, simple soil-landscape models may be preferred over complicated approaches because hydrologists wants to avoid over-parameterization of (eco)hydrological models that are already complex (McDonnell et al., 2007). And, along with simplicity, it also desired that the input model match the resolution of the main model through spacing, extent and support (Blöschl and Sivapalan, 1995), while being independent of autocorrelation assumptions of measurements.

One of the models that answer all those limitations is proposed by Dahlke et al. (2009). In this model, terrain attributes are used as auxiliary variables and are overlain with the geomorphological information of the area to obtain mean measurements of soil depth that are representative of the final user-defined entities. The user has the advantage of choosing the final resolution and scale when a critical amount of soil-depth measurements are available in each entity. The idea of reclassified entities resulted from an overlay of terrain attributes is close to the idea of landform segmentation (Martin and Timmer, 2006). Terrain attributes used in the model varies from site to site because the degree of correlation between terrain parameters and depth of soil varies accordantly.

The goal of this study is to validate the model proposed by Dahlke et al. (2009) and to obtain a model of soil depth for Providence Watershed. The aim is to contribute to the understanding of the variability of soil depth in a forested mountain region with low human impact. Two types of data are used in the model: a grid, in which auguring measurements are spread 123 m apart throughout the entire catchment, and GPR transects that collected information of soil depth 1 m apart. An examination if the use of combined data will actually improve the prediction capability of the model in a 2.3 km^2

catchment, using terrain attributes that better correlate with this area of study: slope, lineaments and wetness index is undertaken. This work is supported by the availability of high-resolution DEMs from LiDAR remote sensing and measurements of soil depth that are adequate to the model assumption that the extent of the explanatory variables is greater than or equal to the spatial extent of the point observations, and the spacing between the point observations is smaller than the minimum size of the smallest spatial entity of any explanatory variable (Dahlke et al., 2009).

Area of Study

The area of study is the Providence Catchment, Southern Sierra Nevada Mountains, CA. Description of the catchment can be found in Chapter II - Area of Study.

Materials and Methods

Materials

Inputs for the model are obtained from results presented in previous chapters. The automated classification of landforms based on the methodology proposed by Iwahashi and Pike (2007) is used with a ten-factor level of aggregation (Chapter II), and it is referred to in this chapter as the geomorphology map. Terrain attributes, computed by manipulation of the LiDAR-DEM and the respective correlation matrixes (Chapter III), were used as auxiliary variables. Results of auguring measurements (204 point

measurements, 120 m apart) and GPR transects (2,232 point measurements, 1 m apart) are the source of the values of soil depth.

Model Approach to Soil Depth

The model of soil depth aims to extrapolate point information about soil to catchment scale. The ability of the GPR survey alone to predict soil depth values in the entire Providence, in comparison with a combination of GPR and manual auguring soil depth values was tested. Point measurement accounts for variation of measurements along a structured grid 123 m apart in the entire catchment, whereas GPR measurements account for the continuity of measurements in a transect fashion, which is important to understand the spatial heterogeneity of the variable in the area.

The conceptual model, based on the work of Dahlke et al. (2009), has the advantage to generate continuous raster maps that are scale independent. The approach consists of using mean-training values of soil depth in the intersection between the geomorphology and maps of terrain attributes at desired levels of disaggregation (i.e., upscaling achieved by classifying terrain attributes in a certain number of classes), under the assumption that terrain attributes represent actual differences in soil depth. This assumption is supported by the selection of relevant attributes based on the correlation between soil depth and attribute values (Boer et al., 1996; Gessler et al., 1995; Moore et al., 1993; Odeh et al., 1995; Tesfa et al., 2009). The elaboration of the model consist of the following steps: (1) select terrain attributes and the number of classes that better represent the spatial variance of the entire catchment; (2) the application of the

bootstrapping technique for validation of the model, (3) generate maps of the predicted soil depths at different levels of disaggregation; and (4) calculate the RMSE to estimate the most suitable map of soil prediction.

All statistical data were computed using the open source software R, and all spatial analyses were made using Arcmap® 10.

Selection of Terrain Attributes and Terrain Classes

Terrain attributes highly correlated (i.e., Pearson product-moment correlation coefficients) with values of soil depth are slope (r=0.48), wetness index (r=0.40) and lineaments index (r=0.40) (Chapter III and IV). These are the terrain attributes selected as explanatory variables used for the prediction.

The desired scale of work and prediction performance is affected by the number of explanatory variables and the level of disaggregation (McBratney et al., 2003). Therefore, as suggested by Dahlke et al. (2009), a combination of the three highly correlated variables at different levels of disaggregation (i.e., from two to eight classes) were obtained to evaluate prediction performance at different scales. The method for disaggregation was adapted to better represent the variability of soil depth in the catchment, instead of using only the statistical differences in topography (Dahlke et al., 2009). To this purpose, the range of values for soil depth for each class were obtained by observing the clutter distributions of the scattered plots in the correlation matrix developed in Chapter III and IV.

Finally, to determine how representative the variance is of the distribution of values of soil depth in the units with respect to the distribution of the values of soil depth in the entire catchment, ANOVA statistics were computed for each terrain attributes and combinations of terrain attributes, comparing classes from two to eight (Table 12) (Dahlke et al., 2009).

Model Fitting and Validation

To validate the model, the measurements of soil depth were divided into training and testing points. The number of training and testing data sets for the GPR data alone is 1,116 points, and the data set that combines auguring and GPR is 1,218 soil depths for each data set.

An overlay of the terrain attributes and the geomorphology map classes resulted in unique entities of intersection. For each unit, prediction is made by computing the harmonic mean using the Spatial Statistics toolbox available on Arcmap® 10.1. Harmonic means were used to avoid the bias of predicted soils in areas with bedrock exposure, which has zero values (Dhalke et al., 2009).

To calculate the RMSE between training and testing data sets and evaluate the confidence interval of predictions, the statistical method bootstrapping was applied. This method is preferred over split-sample and cross-validation because it has been found that bootstrapping provided stable estimates with lower bias (Steyerberg et al., 2001). Bootstrapping estimates standards of error by sampling the data set, where samples are repeatedly replaced (Dahlkle, 2009). This technique is non-parametric, where the data

set is taken as the population, and sampling is performed to preserve the structure of the sample. The reliability of the method improves with the higher number of iterations (Canty, 2002). Because this technique depends on the random distribution of the sample, a comparison between the results from GPR transects versus GPR and auguring measurements is useful to validate the proposed approach of Dahlke et al (2009) in the area of study. The spatial distribution of the data sets can be seen in Figure 40.

Bootstrapping sampling was computed in R with 10,000 iterations. RMSE was calculated according to the equation 1:

$$RMSE = \sqrt{\left(\frac{1}{n}\sum_{i=1}^{n}(x_i - y_i)^2\right)}$$

where x_i is the estimated soil depth using the training data set, and y_i is the value of each soil depth values of the testing set for the respective class combination (Dahlke et al., 2009).

Although the number of data points is sufficient to obtain values for soil depth in all classes of terrain combinations, the large range of values of soil depth in each class influences RMSE depending on the values picked during the bootstrapping (Dahlke et al., 2009).

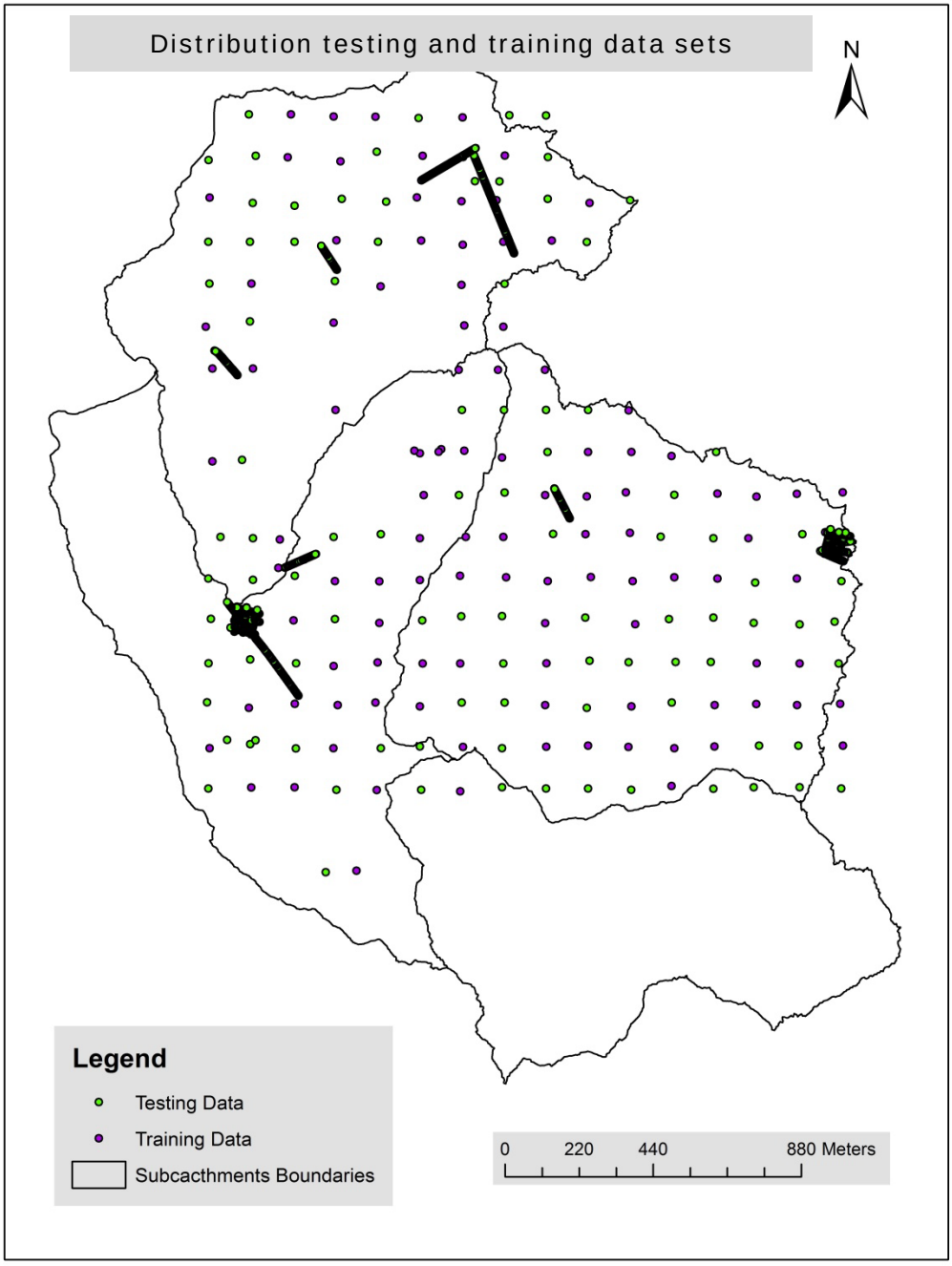

Figure 40. Spatial distribution of training and testing data sets used in the model of soil depth. Auguring measurements are distributed in a systematic grid while GPR measurements are grouped in transects.

Prediction Maps

For each scenario (i.e., GPR alone and GPR combined with auguring data sets) prediction maps are obtained for different levels of disaggregation, from two to eight classes. RMSE is calculated between cells of each map, and the measurements of soil depths of the entire data set to estimate the best prediction map.

Results

Selection of Terrain Attributes

Results of F-values for each one of the combinations are shown in Table 12 for the values of soil depth obtained from the GPR survey alone and Table 13 for the values of soil depth obtained from GPR and manual auguring. The selection of parameters and classes are made under the assumption that higher numbers of F-values are indicators of the capability of each terrain attribute with a particular number of classes to represent actual differences in the soil depth. The highest F-values on each number of classes were selected to develop the model of soil depth, which are indicated in bold Table 12 and Table 13. The combination of terrain parameters combinations selected are: lineaments index with the three, seven and eight classes; the combination of slope and lineaments with two and six classes; and the combination of slope, wetness and lineaments index with four and five classes.

Table 12. Summary of F-values obtained for the combination of terrain parameters using auguring and GPR data. In bold are the selected combinations of parameters as inputs in the model of soil depth. The level of significance is 0.001.

	Terrain Parameter	Number of Classes						
	Combinations*	2	3	4	5	6	7	8
1	slope	27.35	25.70	27.54	22.35	26.69	27.47	28.44
	wetness	5.02	10.98	8.71	10.97	12.20	9.05	13.49
	lineaments	17.82	**84.68**	56.93	42.69	39.11	**76.82**	**70.61**
2	slope/wetness	8.55	10.67	13.33	10.11	6.80	12.78	12.61
	slope/lineaments	**38.04**	36.40	45.73	39.351	**40.83**	44.74	36.51
	wetness/lineaments	1.00	4.35	1.61	2.6857	2.42	9.50	5.22
3	slope/wetness/lineaments	26.88	31.92	**57.68**	**48.35**	27.42	27.90	42.93

Table 13. Summary of F-values obtained for the combination of terrain parameters using only GPR data. In bold are the selected combinations of parameters as inputs in the model of soil depth. The level of significance is 0.001.

	Terrain Parameter	Number of Classes						
	Combinations*	2	3	4	5	6	7	8
1	slope	27.11	27.46	25.66	26.73	22.99	20.61	22.87
	wetness	4.80	9.47	9.10	10.58	12.16	10.45	12.23
	lineaments	19.55	**50.72**	56.23	45.85	35.18	**63.13**	**56.70**
2	slope/wetness	8.555	10.667	13.326	10.112	6.7969	12.78	12.606
	slope/lineaments	**34.75**	34.54	43.51	42.35	**39.99**	42.78	38.49
	wetness/lineaments	3.27	7.57	3.24	5.64	7.81	12.46	10.31
3	slope/wetness/lineaments	30.26	36.70	**47.27**	**43.84**	26.32	27.19	44.07

Validation of the model

The total available number of measurements of soil depth (i.e., training and testing data set) for each terrain/class combination is summarized in Table 14 (GPR values) and Table 15 (GPR and auguring measurements combined. Some classes have a low number of soil depths (e.g., 38 points in lineaments at the 8th class of Table 4) but all classes contain measurements, which imply that it is possible to infer prediction values in the entire catchment. Once the overlay between selected terrain combinations and the geomorphology map is completed, however, the number of values of soil depths available in each unit is lower, as is shown in Tables Table 16 and Table 17. The testing data set does not cover the entire spectrum of classes for all terrain combinations (i.e., empty cells shown in grey in Tables 5 and 6). Therefore, some classes do not have values for testing and cannot be included in the final prediction maps.

The 204 auguring measurements of soil depth range from 0 to 700 cm whereas the 2,232 measurements values of the GPR range from 0 to 900 cm. Also, auguring measurements cover more area of the watershed compared to the isolated transects of the GPR survey. It is hypothesized, therefore, that RMSE values reflect differences between results. The Figure 41, however, shows that no significant differences occur between the mean RMSE using all measurements compared with GPR measurements alone. Overall, the mean values of RMSE decrease to less than 70 cm for the combination of the 8-classes of the terrain map. This result is in agreement with findings from Dahlke et al. (2009).

Table 14. Number of values of soil depths for each selected terrain attribute and the geomorphology map when only GPR values are considered.

Number	Selected	Class Id								Total
Classes	Terrain attributes	1	2	3	4	5	6	7	8	
2	slope/lineaments	1214	1018							2232
3	lineaments	753	782	697						2232
4	slope/wetness/lineaments	602	573	621	436					2232
5	slope/wetness/lineaments	470	439	552	423	348				2232
6	slope/lineaments	270	388	563	375	323	313			2232
7	lineaments	329	397	302	360	336	453	55		2232
8	lineaments	280	338	324	291	288	328	360	23	2232
8	geomorphology map	68	160	322	167	746	127	444	198	2232

Table 15. Number of values of soil depth for each selected terrain attributes and the geomorphology map when the combination of GPR and auguring values are considered.

Number	Selected	Class Id								Total
Classes	Terrain attributes	1	2	3	4	5	6	7	8	
2	slope/lineaments	1307	1129							2436
3	lineaments	821	849	766						2436
4	slope/wetness/lineaments	646	620	694	476					2436
5	slope/wetness/lineaments	520	479	581	459	397				2436
6	slope/lineaments	295	410	602	408	384	337			2436
7	lineaments	341	434	351	385	389	464	72		2436
8	lineaments	303	365	331	303	343	356	397	38	2436
8	geomorphology map	82	182	64	181	890	148	680	209	2436

Table 16. Maximum available number of points of training and testing data sets for each one of the overlapping classes between the geomorphology map and terrain attributes, when GPR measurements are used alone.

N Class	Terrain Maps	Class ID	Number data points	Maximum available number of points of the training data set								Maximum number of points of testing data set exactly located in the same class combination							
				Geomorphology Map Classes								Geomorphology Map Classes							
				1	2	3	4	5	6	7	8	1	2	3	4	5	6	7	8
				68	*160*	*322*	*167*	*746*	*127*	*444*	*198*								
2	sl	1	1214	1282	1374	1536	1381	1960	1341	1658	1412	75	65	82	204	354	153	221	60
		2	1018	1086	1178	1340	1185	1764	1145	1462	1216	53	44	83	211	251	175	138	63
3	l	1	753	821	913	1075	920	1499	880	1197	951	14	50	62	136	120	222	137	12
		2	782	850	942	1104	949	1528	909	1226	980	3	13	39	124	155	203	233	12
		3	697	765	857	64	181	890	148	680	209	8	47	11	98	187	166	127	53
4	swl	1	602	670	762	924	769	1348	729	1046	800			98	104	167	101	49	83
		2	573	641	733	895	740	1319	700	1017	771	5	105	50	32	144	112	45	80
		3	621	689	781	943	788	1367	748	1065	819	13	22	98	112	137	139	74	26
		4	436	504	596	758	603	1182	563	880	634	1		21	52	161	184	17	
5	swl	1	470	538	630	792	637	1216	597	914	668		4	12	48	201	24	45	136
		2	439	507	599	761	606	1185	566	883	637	2	7	14	77	104	203	22	10
		3	552	620	712	874	719	1298	679	996	750	1	5	100	98	87	172	87	2
		4	423	491	583	745	590	1169	550	867	621	41	39	77	46	87	112	21	
		5	348	416	508	670	515	1094	475	792	546				98	133	23	94	
6	sl	1	270	338	430	592	437	1016	397	714	468		5	7	45	102	73	22	16
		2	388	456	548	710	555	1134	515	832	586	8	15	34	43	228	60		
		3	563	631	723	885	730	1309	690	1007	761	36	24	40	150	181	30	70	32
		4	375	443	535	697	542	1121	502	819	573		24	79	7	184	32	22	27
		5	323	391	483	645	490	1069	450	767	521		30	25	25	136	22	26	59
		6	313	381	473	635	480	1059	440	757	511			43	20	77	111	54	8
7	l	1	329	397	489	651	496	1075	456	773	527	22	41	27	30	121	67	21	
		2	397	465	557	719	564	1143	524	841	595	53	34	65	93	76	10	66	
		3	302	370	462	624	469	1048	429	746	500			32	45	124	42	28	31
		4	360	428	520	682	527	1106	487	804	558	11	74	26	29	72	66	76	6
		5	336	404	496	658	503	1082	463	780	534		20	76	77	89	22	52	
		6	453	521	613	775	620	1199	580	897	651	1	1	27	34	175	122	13	80
		7	55	123	215	377	222	801	182	499	253			13	5	22	8	7	
8	l	1	280	348	440	602	447	1026	407	724	478	14	53	22	14	98	15	38	26
		2	338	406	498	660	505	1084	465	782	536	1	13	16	59	162	44	10	33
		3	324	392	484	646	491	1070	451	768	522	5	11	2	42	144	67	20	33
		4	291	359	451	613	458	1037	418	735	489		24	12	93	85	33	32	12
		5	288	356	448	610	455	1034	415	732	486	23	25	15	23	90	41	41	30
		6	328	396	488	650	495	1074	455	772	526	10	22	58	30	88	97	21	2
		7	360	428	520	682	527	1106	487	804	558	33	45	12	100	113	42	10	5
		8	23	91	183	345	190	769	150	467	221				5	5	10	3	

Note: Cells highlighted in grey indicate combinations of classes that cannot be included in the final prediction maps because soil depth cannot be directly validated. Nomenclature of terrain attributes are: (l) lineament index (sl) combination of slope and lineaments index (swl) combination of slope, wetness and lineament index.

Table 17. Maximum available number of points of training and testing data sets for each one of the overlapping classes between the geomorphology map and terrain attributes, when GPR and auguring values are combined.

N Class	Terrain Maps	Class ID	Number data points	Maximum available number of points of the training data set								Maximum number of points of testing data set exactly located in the same class combination							
				Geomorphology Map Classes								Geomorphology Map Classes							
				1	2	3	4	5	6	7	8	1	2	3	4	5	6	7	8
				82	*182*	*64*	*181*	*890*	*148*	*680*	*209*								
2	sl	1	1307	1389	1489	1371	1488	2197	1455	1987	1516	102	78	89	240	362	153	222	61
		2	1129	1211	1311	1193	1310	2019	1277	1809	1338	56	45	86	248	283	175	160	76
3	l	1	821	903	1003	885	1002	1711	969	1501	1030	30	65	63	145	126	240	139	13
		2	849	931	1031	913	1030	1739	997	1529	1058	5	21	46	126	179	217	234	21
		3	766	848	948	64	181	890	148	680	209	20	65	21	109	190	167	134	60
4	swl	1	646	728	828	710	827	1536	794	1326	855		1	103	104	171	132	50	85
		2	620	702	802	684	801	1510	768	1300	829	7	108	53	42	152	115	55	88
		3	694	776	876	758	875	1584	842	1374	903	22	28	109	131	147	150	76	31
		4	476	558	658	540	657	1366	624	1156	685	5		30	62	179	187	19	
5	swl	1	520	602	702	584	701	1410	668	1200	729		5	13	65	204	32	56	145
		2	479	561	661	543	660	1369	627	1159	688	7	12	22	82	109	212	23	12
		3	581	663	763	645	762	1471	729	1261	790	2	5	100	98	87	200	87	2
		4	459	541	641	523	640	1349	607	1139	668	42	59	72	46	99	120	21	
		5	397	479	579	461	578	1287	545	1077	606				105	150	38	104	
6	sl	1	295	377	477	359	476	1185	443	975	504		5	7	60	107	77	23	16
		2	410	492	592	474	591	1300	558	1090	619	17	17	35	43	238	60		
		3	602	684	784	666	783	1492	750	1282	811	49	30	38	150	203	30	70	32
		4	408	490	590	472	589	1298	556	1088	617		37	79	12	187	38	22	33
		5	384	466	566	448	565	1274	532	1064	593		50	32	31	149	22	34	66
		6	337	419	519	401	518	1227	485	1017	546			48	22	78	113	64	12
7	l	1	341	423	523	405	522	1231	489	1021	550	23	41	27	30	123	67	30	
		2	434	516	616	498	615	1324	582	1114	643	54	34	72	100	87	20	67	
		3	351	433	533	415	532	1241	499	1031	560			32	45	132	55	45	42
		4	385	467	567	449	566	1275	533	1065	594	12	74	27	29	67	72	76	28
		5	389	471	571	453	570	1279	537	1069	598	1	37	98	78	95	22	53	5
		6	464	546	646	528	645	1354	612	1144	673	1	2	27	34	184	123	13	80
		7	72	154	254	136	253	962	220	752	281			13	8	36	8	7	
8	l	1	303	385	485	367	484	1193	451	983	512	16	54	24	14	104	16	39	36
		2	365	447	547	429	546	1255	513	1045	574	6	22	17	61	167	44	14	34
		3	331	413	513	395	512	1221	479	1011	540	5	13	2	43	145	67	22	34
		4	303	385	485	367	484	1193	451	983	512	3	25	12	93	85	36	35	14
		5	343	425	525	407	524	1233	491	1023	552	48	28	27	23	94	42	41	40
		6	356	438	538	420	537	1246	504	1036	565	11	25	58	37	97	103	23	2
		7	397	479	579	461	578	1287	545	1077	606	33	45	12	123	120	49	10	5
		8	38	120	220	102	219	928	186	718	247	3			9	7	12	7	

Note: Cells highlighted in grey indicate the combinations of classes that cannot be included in the final prediction maps because soil depths cannot be directly validated. Nomenclature of terrain attributes are: (l) lineament index (sl) combination of slope and lineaments index (swl) combination of slope, wetness and lineament index.

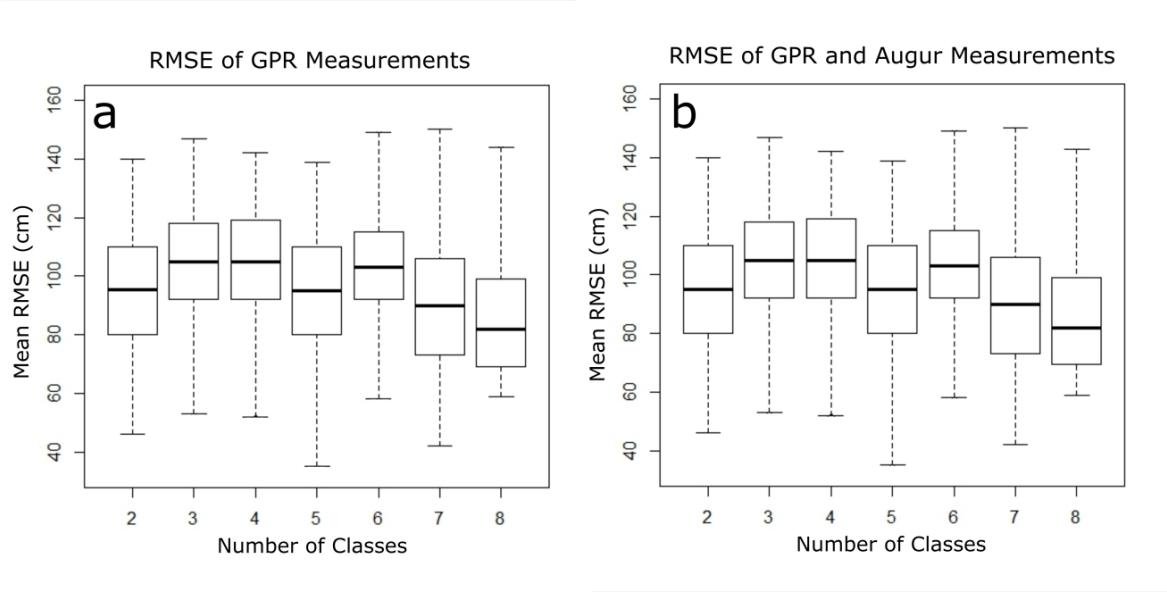

Figure 41. Boxplots comparing the mean values of RMSE (cm) by number of classes per terrain combination using only GPR measurements (a), and using all GPR and auguring measurements (b).

Prediction Maps of Soil Depth

Figure 42 shows maps generated using the results of model prediction. The maps spatially represent the values of harmonic mean that resulted from the overlay between the geomorphological map (i.e., fixed eight classes) and terrain attributes with a different number of classes (from two to eight classes). The lower the number of classes of terrain attributes, the lower the correspondent spatial disaggregation is. This is because the number of entities resulted in the overlay decreases from 732 (eight classes) to 183 (two classes), and consequently decreasing the size of the areas of each entity. As shown in Table 16 and Table 17, some of the classes do not have testing points to validate the predictions; therefore, those values were predicted, for mapping purposes, interpolating by ordinary kriging, assuming spatial correlation of data. The area of the interpolated

values corresponds to 1.3 to 1.9% of the total area of the Providence Catchment, respectively.

To know the best level of disaggregation of the prediction maps, the RMSE were calculated between all measurements of soil depth and the cells of the predicted values. Although the difference between the prediction maps using all depth measurements and only GPR measurements cannot be visually appreciated. RMSE calculations suggest a better overall performance in GPR and auguring measurements combined (Table 18). In both cases, the four-terrain classes maps have the best coefficient combinations, with less than 10% error in the predictions.

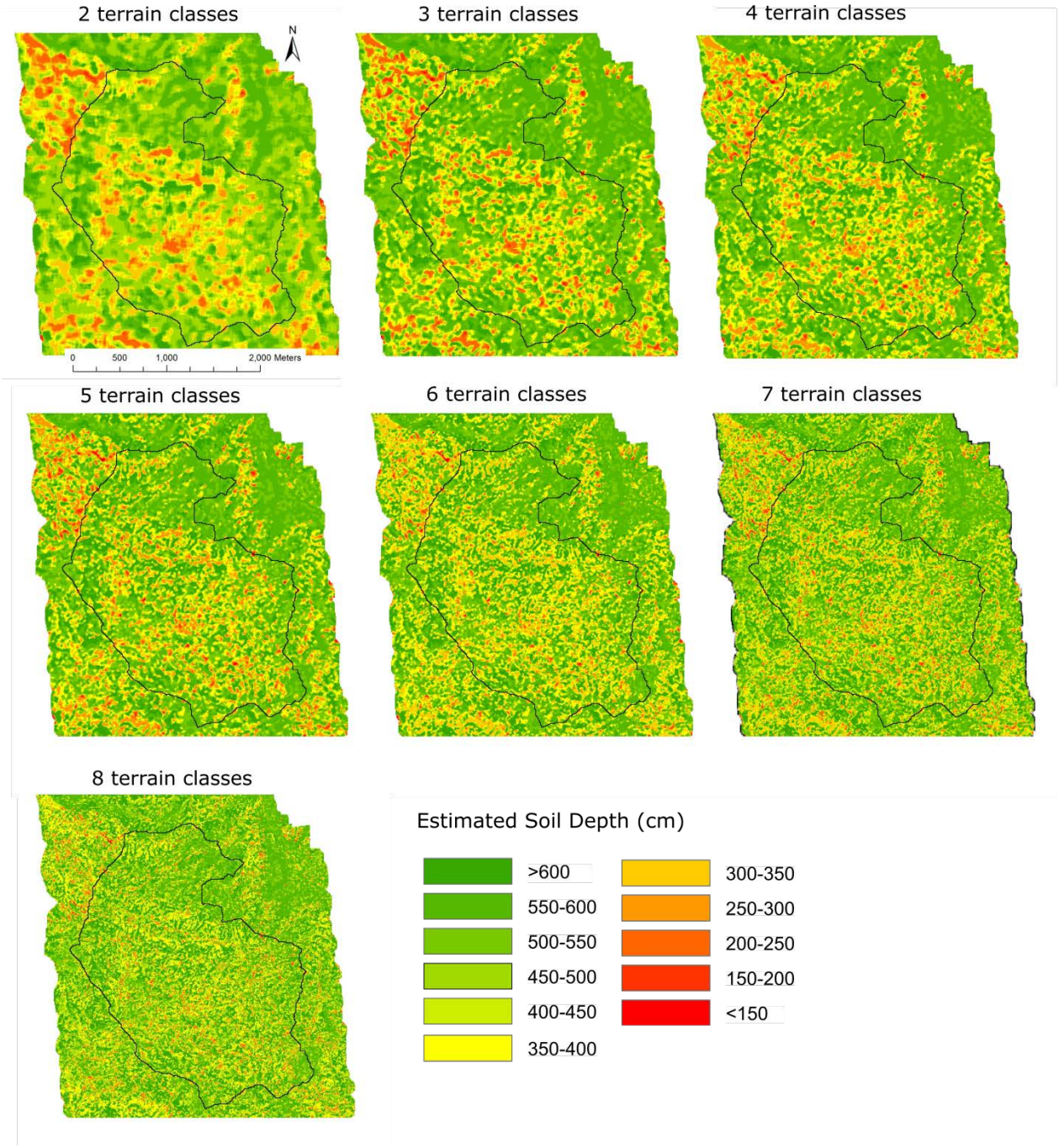

Figure 42. Maps generated with model predictions of soil depth. Values for soil depths were obtained by the overlay between terrain attributes and the geomorphology map. Number of classes of terrain attributes used in each overlay is indicated above the maps. Green values correspond to deeper soils, whereas red values indicate shallow and rocky areas.

Table 18. RMSE between (A) all measurements of soil depths or (B) GPR alone measurements and the correspondent cells of the predictions maps. In bold are the best coefficients combinations, indicating the best performance.

	Number of Classes						
A.	2	3	4	5	6	7	8
RMSE (cm)	57	65	**54**	88	92	96	101
Error (%)	8.7	9.0	**8.3**	12.7	13.4	24.8	23.7
R2	0.24	0.43	**0.51**	0.23	0.12	0.02	0.01
B.							
RMSE (cm)	64	77	**78**	103	131	152	177
Error (%)	9.1	9.8	**9.9**	13.3	16.2	30.5	32.6
R2	0.11	0.27	**0.37**	0.2	0.05	0.01	0.008

Discussion and Conclusions

Discussion

Although a weak correlation exist among the three terrain attributes used in the model and the measurements of soil depths, the results using the geomorphology map of Providence with the method proposed by Dahlke et al. (2009) are satisfactory, with a percentage of error or less than 10% for the four-terrain/geomorphology map combination in both results (i.e., GPR combined with auguring measurements and GPR measurements alone).

Compared with kriging and linear regression, this method does not depend on a uniform grid of measurements and does not depend on auto correlation assumptions. Also, although the development of the technique in a GIS platform is laborious, the statistical procedures do not require more than a personal laptop for computation (i.e., R open source was used). Some modifications were applied to the methodology to better

reflect actual differences in the variability of soil depths for each spatial entity. Instead of using a K-means clustering algorithm to group the values of soil depths in classes, which resulted in reflecting only differences in the statistics of the terrain, the ranges of soil depth by each class were obtained from central tendency analysis of the correlations between values of soil depths and the user defined classes.

This modification led to better reflect the actual variations of soil depth inside of each class. Also, instead of using the terrain attributes of vertical distance to channel network, elevation above channel and profile curvature, the terrain attributes that better correlate with soil depth in this are: lineaments, slope and wetness index (Chapter III and IV). The use of slope and wetness index can be found in other investigations (McKenzie and Ryan, 1999; Moore et al., 1993), but distance from lineaments has not been used as an auxiliary variable in previous studies. Lineaments are associated with differential weathering and preferential vertical flow. Migon (2006) explains why it is a good indicator of variation in soil depths variation in this granitic environment.

Kriging was used as a post-processing interpolation technique to complete the empty areas in which prediction was not possible because of the lack of testing points. Kriging alone would not be possible using only the measurements of soil depths because the assumption of spatial autocorrelation is not met either for auguring or GPR transects.

Observing the results of RMSE between the training and testing data sets, the use of the GRP data set alone did not show a significant difference when compared with the results of the combination with auguring measurements. Differences in the final RMSE, which measure error between field measurements and the analogous cells of prediction

map, however, show a better performance of the model when auguring measurements were combined with GPR. This can be explained by the larger sample product of a better resolution of GPR measurements alone, compared with sparse 123 m apart auguring measurements. Also, the number of entities covered by the extent of GPR measurements is lower, which suggests that a more extensive GPR sampling design that covers more combination entities of the catchment would improve the performance of the model. This would occur if the conditions in the field would allow access to the entire catchment.

Conclusions

The model of soil depth based on the method developed by Dahlke et al. (2009) is tested to compare the results between GPR and all depth measurements. The RMSE between predicted and modelled values showed that better prediction occurs using the combination of four-terrain classes and the geomorphology map. The level of disaggregation of terrain attributes (i.e., eight classes divisions) affected the level of disaggregation of the final prediction maps, and consequently affected resolution. If a different level of disaggregation is desired to meet the scale requirements of a (eco)hydrology model, the design of GPR sampling can be adjusted to cover the entire spectrum of entities to ensure coverage in all classes and therefore improve the performance of the model at the desired resolution.

The model suggested by Dahlke et al. (2009) is a simple soil-landscape model that satisfactorily predicts (RMSE=54 cm and R^2= 0.51) soil depths under the assumption that a relationship exists between soil depth and surface expression. Although the level of correlation between predicted and measured values is not optimal, the results are in agreement with other investigations in natural, non-agricultural landscapes (Dahlke et al., 2009; Tesfa et al., 2010; Vanwalleghem et al., 2010; Verstappen, 2011) and granitic landscapes (Birkeland and Janda, 1971; Migon, 2006). The inherent randomness of horizontal distribution of soil depth in these landscapes would explain why a better R^2 is not hypothesized. Besides, the accumulation of measurement error of the technique used to perform the auguring is not negligibly. This reason would explain similar poor relationships between soil and landscape parameters in publications using the same method of sampling (Pennock, 2003; Vanwalleghem et al., 2010). Harrell (2013) suggests to avoid model uncertainty by using subject matter knowledge (Harrell, 2013). Geomorphological description along with digital terrain analysis could provide such knowledge.

In forested, natural landscapes, soil redistribution by erosion and deposition has been identified as one of the key processes controlling total variation in soil depths (Dalsgaard et al., 1981; Rejman et al., 2014; Vanwalleghem et al., 2010; Vreeken, 1975). Therefore, and along with the results of this work, it can be suggested that descriptive geomorphology maps in combination with geomorphometry are valid tools for addressing the spatial heterogeneity of soil parameters in natural, complex terrains. Although the correlation between landform and soil attributes is weak in these

environments (Vanwalleghem et al., 2010; Verstappen, 1983; Verstappen, 2011), it is suggested that traditional, descriptive geomorphological maps help explain heterogeneity and better discriminate landforms that automated geomorphometry cannot (e.g., discrimination of roads against lineaments and meadows), and consequently improving the predictions of the model.

CHAPTER VI

CONCLUSIONS AND FUTURE DIRECTIONS

In this chapter, I discuss major conclusions and indicate recommendations for future research.

Conclusions

Soil depth, defined as the portion of subsurface that extends from horizon O to the contact between saprolite and saprock, is an important parameter for modelling studies in the critical zone. A consensus about the delimitation of the bottom boundary of the critical zone is needed, although a limited amount of literature engages in such discussion. Soil depth and weathering profile delimitation are still developing areas of research, and the present study was motivated to add data and to be part of this discussion.

In granite environments, the use of the hand auguring technique underestimates the values of depth of soil, and an exhaustive amount of point measurements are necessary to account for the spatial variability of the variable at the catchment scale. Therefore, mapping the depth of soil, which is an important input for spatially distributed hydrological models, turns out to be an especially expensive and inaccurate in granitic environments. The use of traditional geomorphological mapping, combined with the GPR technique is presented as an alternative. Discussion about the advantages and limitation follows.

Is Geomorphological Information Useful for Investigation of Soils?

Geomorphological processes occurring locally affect the thickness of soils (Birkeland, 1999). Pedogenesis is interrupted by geomorphological processes, which occur at rates many times higher than the formation of soils (Verstappen, 1983). Accordingly, the assumption of the present study is that a relationship between soil depth and surface expression exists in the first place. It is argued that, although geomorphological analysis would not solve the puzzle of soil depth alone, it is an important input to set assumptions and boundary conditions, along with defining research logistics. The geomorphology map presented is proposed to investigate the relationship between surface and subsurface properties, and also as an interdisciplinary tool for the SSCZO team to integrate investigation efforts at the local scale to the processes occurring at the catchment scale.

It is emphasized that the combination of automated and manual classification of landforms converged to a more comprehensible description of the features and processes, compared with the use of geomorphometry alone is necessary. T is suggested that, the technological advance of the geographic information system that has led to automation does not yet completely matured to explain the complexity of landscapes. Therefore, for now, traditional geomorphological techniques are still necessary to obtain more realistic representation of the landscapes, and to capture the whole vision of the processes and patterns occurring in a certain area. Verstappen (1983, p.49) is correct when he argues that linking soil patterns only to topographic characterization – as in the case of automated classification techniques – is unsatisfactory because the correlation

between soils and landforms is based on the intensity of geomorphological processes and in the age of chronology of landforms. It is known that only in relative rare cases the parent material *in situ* provides the parent material for soil development. In many cases this is a Quaternary sediment, which distribution pattern, characteristics and origin can only be revealed through geomorphological analysis and field observations (Anderson et al., 2012; Phillips, 2008; Verstappen, 1983; Verstappen, 2011). Providence Catchment provides an example, where geomorphological analysis led to a hypothesis that grus present in the northern area comes from periglacial movements of past important glaciations. This observation may explain the abundance of debris flows in this portion of the catchment, compared with the southern portion of the catchment. Also, lineaments, which are significant correlated ($P<0.001$) with total depth estimated from GPR, were identified manually. In this case, lineaments could not be identified with automated classification because it would lead to mistakenly identify roads as joints.

Similarly, differences in sediment load in the main channels (Hunsaker and Neary, 2012), hypsometric analysis, and distribution of areas with susceptibility to erosion are evidences of the role of the geological heterogeneity in explaining differences in the mean values of soil depth among sub-catchments. Automated classification of landforms, however, did not discriminate geological information, putting different morphogenetically different zones under the same classes.

Geomorphological analysis led to the identification of homogeneous units that were used in the soil depth model. Similar to the concept of hydrologic landscapes (Winter, 2001), 'pedological landscapes' is proposed as homogeneous spatial units that

share similar relationships between geomorphology and soils. In particular, homogeneous units defined from the relationships between depth of soil and terrain attributes is proposed as the foundation for a data network in critical zone research, helping the comparison of processes occurring in different locations.

The main argument for the use of soil depth as the fundamental soil attribute is the dependence of several hydrological models of the definition of this variable (Arnold et al., 2012; Beven and Kirkby, 1979; Quinn et al., 1991; Tague and Band, 2004; Wigmosta et al., 1994).

Finally, geomorphological information was used to develop a simple soil-landscape model that satisfactory predicted (RMSE=54 cm and R^2= 0.51) soil depths in the Providence Catchment. Although the level of correlation between predicted and measured values is not optimal, the results are in agreement with other investigations in natural, non-agricultural landscapes (Dahlke et al., 2009; Tesfa et al., 2010; Vanwalleghem et al., 2010; Verstappen, 2011) and granitic landscapes (Birkeland and Janda, 1971; Migon, 2006). The inherent randomness of horizontal distribution of soil depth in these landscapes and the error in the measurements would explain why a higher R^2 is not common.

Terrain Attributes Related with Soil Depth

Terrain attributes that are best correlated with soil depth in Providence Catchment are curvature ($r=0.32$, $p<0.01$), lineaments ($r=0.40$, $p<0.001$), slope ($r=0.48$, $p<0.001$), and wetness ($r=0.47$, $p<0.001$). These results were obtained by exploratory

analysis using univariate linear regression. The spacing and density of sampling prohibit the use of multiple linear regressions for reliable predictions, although a demonstration was presented as a preliminary result. The model presented in Chapter that combines a geomorphology map and terrain attributes was proposed instead, to capture the spatial heterogeneity of soil depth considering the amount of sampling available.

It was hypothesized that the positive correlation between curvature and soil depth is related to the highly forested character of the landscape. In forested, natural landscapes, soil redistribution by erosion and deposition has been identified as one of the key processes controlling total variation in soil depths (Dalsgaard et al., 1981; Rejman et al., 2014; Vanwalleghem et al., 2010; Vreeken, 1975). Heimsath et al. (1999) have argued through long-term modelling that a depth-curvature relationship exists if land use change has not occurred, and the local steady state is the product of long-term processes. Hypsometric analysis has shown, indeed, that the catchment is approaching a steady state, and, therefore, is the process of balance between soil production and transport of materials.

Correlation between depth of soil and lineaments ($r=0.40$, $p=0.001$) is an indicator of the influence of the underlying geology in explaining the variability of values of depth throughout the catchment. In other granitic environments of the world, the highest gradients in thickness are also associated with joints and fault lines, in which alteration is enhanced (Migon, 2006).

The negative correlation of soil attributes and slope and wetness are related with the influence of slopes in a state of erosion, sedimentation and horizonation (Moore et

al., 1993). This finding is in agreement with previous investigations (Akumu et al., 2015; Gessler et al., 2000; Gillin et al., 2015; Goovaerts, 1999; Hengl et al., 2004; Martin and Timmer, 2006; McKenzie and Ryan, 1999; Moore et al., 1993; Odeh et al., 1995; Young and Hammer, 2000; Zebarth et al., 2002). In other forested regions, however, a lack of a relationship between these variables and soil attributes was observed (Vanwalleghem et al., 2010).

Terrain attributes, used as auxiliary variables for the modelling of soil depth at catchment scale, are an example of the benefits of combining qualitative and quantitative approaches to study the spatial distribution of soil properties. Whereas slope, wetness index and curvature can be extracted by geomorphometry, lineaments and surface outcrops still need manual identification.

In the literature, a site-specific difference between the level of correlation between terrain attributes and soil depth is reported. Mainly, natural and agricultural sites are differentiated according to the level of landscape irruption by human activities. Whereas in non-forested landscapes, the influence of water flow contributes to spatial patterns of soil (Landi et al., 2004; Manning et al., 2001; Pennock et al., 1994); in forested regions, tree canopy and litter interception reduce the impact of water flow, and therefore, mass movement may be more important for heterogeneity compared with terrain attributes (Banwart et al., 2012; Martin and Timmer, 2006). Under this consideration, the levels of correlation observed in the present investigation are an argument to confirm that although a correlation exists, the values of the correlation coefficients show that the relationship is weak. Other variables, such as tree throw and

bioturbation, may play an important role in explaining these results (Dietrich et al., 1995).

The Use of GPR in the Investigation of Soil Properties

Among all geophysical techniques that have been extensively studied, GPR relates to the objectives of this study and it is pertinent to the characteristics of Providence Catchment. GPR had an adequate scale of penetration versus resolution, and the instrument could be carried by two people, to reach inaccessible locations of the catchment on foot.

The geological conditions of the subsurface (i.e., granite and its disintegration to sandy residuum) enabled the penetration of GPR radar waves, but attenuation was observed at the three meter of depth. It is hypothesized that this reflection corresponds to an argillic horizon reported in Dahlgren et al. (1997) and coincides with the snow line of the Sierra Nevada Mountains (Dahlgren et al., 1997). Deep-weathered granite, reported to be at 20 to 30 m (Holbrook et al., 2013; Wahrhaftig, 1965) was not reached because the maximum depth of penetration of the instrument using a 100 Mhz antenna was 10 m. Nevertheless, the contact with saprock, which is defined in this identification as total soil depth, was identified. The interpretation of saprock layer on the radar signature was validated using auguring measurements that overlapped with the survey transects.

GPR was applied in twenty transects overlapping geomorphological units of the Iwahashi classification to ensure proper coverage for the purpose of extrapolation of measurements. GPR successfully estimated total soil depth (i.e., depth to saprock), but

estimations of the Horizon A thickness did not correlate with direct measurements (i.e., through auguring). Previous investigations found that GPR can successfully identify top soil horizons in forested regions (Laamrani et al., 2013; Sucre et al., 2011), and, therefore, further investigation may elucidate if a mistmatch in the criteria of A horizon definition between the auguring measurements (Johnson et al., 2011) and GPR would be a possible cause of the lack correlation found here.

Patterns of Soil Depth of Providence Catchment

Prediction maps show a pronounced spatial variability of depths of soil also observed in other forested regions (Da Fonseca et al., 2006; Gillin et al., 2015; Wigmosta et al., 1994). The main implication of this finding is that this variability cannot be ignored while changing the scale of work (Turner, 2010). To accurately represent the heterogeneity of the catchment, the sampling design should be adjusted to meet the objectives of the investigation. In the modeling applied in the present investigation, the level of disaggregation of terrain attributes (i.e., eight classes division) affected the level of disaggregation of the final prediction maps, and consequently affected resolution. If a different level of disaggregation is desired to meet the scale requirements of a (eco)hydrology model, the design of GPR sampling can be adjusted to cover the entire spectrum of entities with a statistically adequate number of samples to ensure coverage in all classes, and in this way, improve the performance of the model at the desired resolution.

Considering the sampling design of auguring and GPR measurements presented here, the RMSE between predicted and modelled values showed that better prediction occurs using the combination of four-terrain classes and the geomorphology map. Even if hypothetically, a lower resolution or larger scale is desired, and only mean values by sub catchments would be considered, according to the models results in Chapter V, mean values of soil depth differ among sub catchments (P301=250 cm, P302=175 , P303=116 cm, P403= 131 cm in 2,000 samples). This implies that even at these coarse resolutions, the values of soil depth may affect hydrological simulation results (Franchini et al., 1996; Quinn et al., 1991), identifying the spatial heterogeneity as an important component to consider in studies conducted in this critical zone observatory.

Future Directions

Weathering Patterns

Description of geochemical and mineralogical evolution of weathered rock, identifying transitions and end products of weathering exists (Anderson, 2010; Brantley et al., 2007; Migon, 2006). Landscape analysis, including the variations of weathering front at hillslope and catchment scale, is more scarce (Dahlgren et al., 1997; Jessup et al., 2011; Wahrhaftig, 1965). If preferential weathering occurs in pre-existing zones of weakness, it would be interesting to investigate, with more detail, the correlation between lineaments and subsurface patterns of weathering.

It has been suggested that most of the weathering solute flux at the catchment scale is sourced from bedrock fracture zones, and fracture spacing combined with mineral dissolution may largely control watershed topography in many watersheds (Buss and Moore, 2013).

Bioturbation

Several authors have suggested that in mountain, forested regions, bioturbation processes may explain the highly variable distribution of the first horizons of soil (Dietrich et al., 1995; Šamonil et al., 2010; Vanwalleghem et al., 2010; Wilkinson et al., 2009), but the causality is still not proven. In this forest, dominated by conifers, 40 to 60 m in height, tree fall is likely to produce mechanical disruption of soils, along with burrowing from fauna. It is proposed that a comparison be made between the first soil layers in the SSCZO and the Cordillera de la Costa in Central Chile, where a similar granodiorite batholith is present under similar Mediterranean climate conditions. In La Campana National Park, the same elevation and snow/rainfall patterns are present. The vegetation, however, is dominated by sclerophyllous shrubs and trees from 0.5 to 10 m in height. It is hypothesized that in Chile, where tree fall and the significant animal disruption of soils is absent, soil layers will show better correlation, compared with the Sierra Nevada Mountains. In Chile, it is hypothesized that the distribution of the thickness of horizons is influenced by topography and geomorphology. The results of this investigation have the potential to contribute to the understanding of bioturbation in the random character of soil thickness in forested regions.

To elucidate the relationship between pedogenesis and bioturbation is important, because the role of vegetation in water availability is commonly confined to its outputs of the water balance equation in the vadose zone. The results are relevant for decisions about land-use and hydrological modeling.

Sensitivity of Hydrology Models to Soil Depth in Providence Catchment

Spatial patterns of depth of soils is one of the controlling factors influencing the water balance (Nicótina et al., 2011). Local soil measurements of soil depth or estimates may be necessary if land use change is being planned. In that case, the mean soil depth would change over time: deposition and mass movement will be higher in production, which will decrease the thickness of the soil depth and water-holding capacity by the section of the catchment and affecting the overall all the interconnected system.

The magnitude of the importance of soil depth values, however, across different hydroclimatic regions and scale is not clear. In well-drained watersheds, where sensitivity models have been applied, spatial variability does not influence quality of discharge predictions (Saulnier et al., 1997). In those cases, runoff predictions are mostly controlled by topographic indices rather than effective soil depths. Small variations in the depth of the soil are often ignored and its real influence is still not well understood (Tromp-van Meerveld and McDonnell, 2006). Because the influence of depth of soil cannot be isolated from other variables such as topography, texture, and structure of soil, Hopp and McDonnell (2009) suggest virtual experiments for characterizing the hillslope interaction between different hydrological environments.

To conduct a virtual experiment in Providence Catchment, in addition to the data obtained in the present investigation, the design of a sensitivity hydrological model needs to consider measurements of subsurface stormflow in several events in the contact between soil and saprock, detailed saprock-soil contact topography, and pressure head readings at the hillslope scale. This will validate simulations of subsurface stormflow and actual measurements.

The scrutiny of the hypothesis that hydrological response is highly influenced by soil depth will contribute to the understanding of the role and interplay of soil depth with other variables affecting hydrological response, such as slope and bedrock permeability (Hopp and McDonnell, 2009). The determination of the role of soil depth in a hydrological response has important consequences for decision making in the critical zone (Lin, 2010), because changes in parameterization will affect the results of hydrological modeling (Quinn et al., 1991). And, accurate hydrological modeling is a high priority in the determination of effects of climate and land-use change (Bales et al., 2011b).

REFERENCES

Abella, S.R., Denton, C.W., Steinke, R.W., Brewer, D.G., 2013. Soil development in vegetation patches of Pinus ponderosa forests: Interface with restoration thinning and carbon storage. Forest Ecology and Management, 310, 632-642.

Akumu, C.E., Johnson, J.A., Etheridge, D., Uhlig, P., Woods, M., Pitt, D.G., McMurray, S., 2015. GIS-fuzzy logic based approach in modeling soil texture: Using parts of the Clay Belt and Hornepayne region in Ontario Canada as a case study. Geoderma, 239–240, 13-24.

Anbazhagan, S., Sajinkumar, K., 2011. Geoinformatics in terrain analysis and landslide susceptibility mapping in parts of Western Ghats, India. Geoinformatics in applied geomorphology. CRC Press, USA, 291-315.

Anderson, R.S., Anderson, S., Aufdenkampe, A.K., Bales, R., Brantley, S., Chorover, J., Duffy, C.J., Scatena, F.N., Sparks, D.L., Troch, P.A., Yoo, K. , 2010. Future Directions for Critical Zone Observatory (CZO) Science.

Anderson, R.S., P.Anderson, S., 2010. Geomorphology. The mechanics and chemistry of landscapes. Cambridge University Press, Cambridge.

Anderson, S.P., Anderson, R.S., Tucker, G.E., 2012. Landscape scale linkages in critical zone evolution. Comptes Rendus Geoscience, 344(11), 586-596.

Anderson, S.P., Dietrich, W.E., Brimhall, G.H., 2002. Weathering profiles, mass-balance analysis, and rates of solute loss: Linkages between weathering and erosion in a small, steep catchment. Geological Society of America Bulletin, 114(9), 1143-1158.

Aranha, P.R.A., Augustin, C.H.R.R., Sobreira, F.G., 2002. The use of GPR for characterizing underground weathered profiles in the sub-humid tropics. Journal of Applied Geophysics, 49(4), 195-210.

Arnold, J., Moriasi, D., Gassman, P., Abbaspour, K., White, M., Srinivasan, R., Santhi, C., Harmel, R., Van Griensven, A., Van Liew, M., 2012. SWAT: Model use, calibration, and validation. Transactions of the ASABE, 55(4), 1491-1508.

Bales, R., 2011. CZO: Critical Zone Observatory - Snowline Processes in the Southern Sierra Nevada, University of California - Merced, Merced.

Bales, R., Hopmans, J.W., T.O'Geen, A., Meadows, M., Hartsough, P.C., Kirchner, P., Hunsaker, C.T., Beaudette, D., 2011a. Soil Moisture Response to Snowmelt and

Rainfall in a Sierra Nevada Mixed-Conifer Forest. Vadose Zone Journal, 10, 786-799.

Bales, R.C., Battles, J.J., Chen, Y., Conklin, M.H., Holst, E., O'Hara, K.L., Saksa, P., Stewart, W., 2011b. Forests and Water in the Sierra Nevada: Sierra Nevada Watershed Ecosystem Enhancement Project.

Banwart, S., Menon, M., Bernasconi, S.M., Bloem, J., Blum, W.E.H., Souza, D.M.d., Davidsdotir, B., Duffy, C., Lair, G.J., Kram, P., Lamacova, A., Lundin, L., Nikolaidis, N.P., Novak, M., Panagos, P., Ragnarsdottir, K.V., Reynolds, B., Robinson, D., Rousseva, S., de Ruiter, P., van Gaans, P., Weng, L., White, T., Zhang, B., 2012. Soil processes and functions across an international network of Critical Zone Observatories: Introduction to experimental methods and initial results. Comptes Rendus Geoscience, 344(11–12), 758-772.

Bateman, P.C., Wones, D.R., 1972. Huntington Lake Quadrangle, Central Sierra Nevada, California:--analytic Data. US Government Printing Office.

Beven, K., Kirkby, M., 1979. A physically based, variable contributing area model of basin hydrology/Un modèle à base physique de zone d'appel variable de l'hydrologie du bassin versant. Hydrological Sciences Journal, 24(1), 43-69.

Bian, L., Butler, R., 1999. Comparing effects of aggregation methods on statistical and spatial properties of simulated spatial data. Photogrammetric Engineering and Remote Sensing, 65, 73-84.

Bierman, P.R., 1994. Using in situ produced cosmogenic isotopes to estimate rates of landscape evolution: A review from the geomorphic perspective. Journal of Geophysical Research: Solid Earth (1978–2012), 99(B7), 13885-13896.

Birkeland, P., 1999. Soils and Geomorphology. Oxford University Press, New York.

Birkeland, P.W., Janda, R.J., 1971. Clay mineralogy of soils developed from Quaternary deposits of the eastern Sierra Nevada, California. Geological Society of America Bulletin, 82(9), 2495-2514.

Blöschl, G., Sivapalan, M., 1995. Scale issues in hydrological modelling: A review. Hydrological Processes, 9(3-4), 251-290.

Bocco, G., Mendoza, M., Velázquez, A., 2001. Remote sensing and GIS-based regional geomorphological mapping—a tool for land use planning in developing countries. Geomorphology, 39(3–4), 211-219.

Boer, M., Del Barrio, G., Puigdefábres, J., 1996. Mapping soil depth classes in dry Mediterranean areas using terrain attributes derived from a digital elevation model. Geoderma, 72(1–2), 99-118.

Bolger, B.L., Park, Y.J., Unger, A.J.A., Sudicky, E.A., 2011. Simulating the pre-development hydrologic conditions in the San Joaquin Valley, California. Journal of Hydrology.

Brantley, S.L., Goldhaber, M.B., Ragnarsdottir, K.V., 2007. Crossing disciplines and scales to understand the critical zone. Elements, 3(5), 307-314.

Bremer, H., Sander, H., 2000. Inselbergs: Geomorphology and Geoecology. In: S. Porembski, W. Barthlott (Eds.), Inselbergs. Ecological Studies. Springer Berlin Heidelberg, pp. 7-35.

Brinson, M.M., Rheinhardt, R., 1996. The role of reference wetlands in functional assessment and mitigation. Ecological Applications, 69-76.

Bue, B.D., Stepinski, T.F., 2006. Automated classification of landforms on Mars. Computers & Geosciences, 32(5), 604-614.

Burcar, S., Miller, W., Johnson, D., Tyler, S., 1994. Seasonal preferential flow in two Sierra Nevada soils under forested and meadow cover. Soil Science Society of America Journal, 58(5), 1555-1561.

Buss, H.L., Moore, O.W., 2013. Beyond the Regolith: A Deep Critical Zone Drilling Perspective on Weathering Profiles. School of Earth Sciences, University of Bristol, UK, Denver, Colorado

Canty, A.J., 2002. Resampling methods in R: the boot package. R News, 2(3), 2-7.

Cassidy, N.J., 2009. Ground penetrating radar data processing, modelling and analysis. Elsevier, Amsterdam.

Catani, F., Segoni, S., Falorni, G., 2010. An empirical geomorphology-based approach to the spatial prediction of soil thickness at catchment scale. Water resources research, 46(5).

Chamorro, A., Giardino, J.R., Granados-Aguilar, R., Price, A.E., 2015. A Terrestrial Landscape Ecology Approach to the Critical Zone. In: J.R. Giardino, C. Houser (Eds.), Principles and Dynamics of the Critical Zone. Elsevier.

Chernicoff, S.F., Venkatakrishnan, H.A., 1997. Essentials of geology.

Clark, M.K.a.M., Saleeby, G.a., Farley, J.a., A., K., 2005. The non-equilibrium landscape of the southern Sierra Nevada, California. GSA Today, 15(9), 4-10.

Collins, M., Doolittle, J., 1987. Using ground-penetrating radar to study soil microvariability. Soil Science Society of America Journal, 51(2), 491-493.

Craigg, T.L., Adams, P.W., Bennett, K.A., 2015. Soil Matters: Improving Forest Landscape Planning and Management for Diverse Objectives with Soils Information and Expertise. Journal of Forestry, 113(3), 343-353.

Da Fonseca, A.V., Carvalho, J., Ferreira, C., Santos, J., Almeida, F., Pereira, E., Feliciano, J., Grade, J., Oliveira, A., 2006. Characterization of a profile of residual soil from granite combining geological, geophysical and mechanical testing techniques. Geotechnical & Geological Engineering, 24(5), 1307-1348.

Dahlgren, R., Boettinger, J., Huntington, G., Amundson, R., 1997. Soil development along an elevational transect in the western Sierra Nevada, California. Geoderma, 78(3), 207-236.

Dahlke, H.E., Behrens, T., Seibert, J., Andersson, L., 2009. Test of statistical means for the extrapolation of soil depth point information using overlays of spatial environmental data and bootstrapping techniques. Hydrological Processes, 23(21), 3017-3029.

Dalsgaard, K., Baastrup, E., Bunting, B.T., 1981. The influence of topography on the development of Alfisols on calcareous clayey till in Denmark. Catena, 8(1), 111-136.

Davis, J.L., Annan, A.P., 1989. Ground-penetrating Radar for High-Resolution Mapping of Soil and Rock Stratigraphy. Geophysical Prospecting, 37, 531-551.

De Benedetto, D., Castrignano, A., Sollitto, D., Modugno, F., Buttafuoco, G., Papa, G.l., 2012. Integrating geophysical and geostatistical techniques to map the spatial variation of clay. Geoderma, 171–172(0), 53-63.

Dedkov, A., Moszherin, V., 1992. Erosion and sediment yield in mountain regions of the world. Erosion, debris flows and environment in mountain regions, 209, 29-36.

DeGraff, J.V., 1994. The geomorphology of some debris flows in the southern Sierra Nevada, California. Geomorphology, 10(1–4), 231-252.

Demek, J., 1972. Manual of detailed geomorphological mapping. Academia.

Dietrich, W.E., Reiss, R., Hsu, M.-L., Montgomery, D.R., 1995. A process-based model for colluvial soil depth and shallow landsliding using digital elevation data. Hydrological Processes, 9(3-4), 383-400.

Dikau, R., Brabb, E., Mark, R.K., Pike, R.J., 1995. Morphometric landform analysis of New Mexico. Zeitschrift Fur Geomorphologie Supplementband, 109-126.

Dikau, R., Brabb, E.E., Mark, R.M., 1991. Landform classification of New Mexico by computer. US Department of the Interior, US Geological Survey.

Doolittle, J.A., Butnor, J.R., 2009. Soils, peatlands, and biomonitoring. Ground Penetrating Radar: Theory and Applications, 524.

Doolittle, J.A., Collins, M.E., 1998. A comparison of EM induction and GPR methods in areas of karst. Geoderma, 85(1), 83-102.

Dragut, L., Blaschke, T., 2006. Automated classification of landform elements using object-based image analysis. Geomorphology, 81(3-4), 330-344.

Dramis, F., Guida, D., Cestari, A., 2011. Nature and Aims of Geomorphology Mapping. In: M.J. Smith, P. Paron, J.S. Griffiths (Eds.), Geomorphological Mapping. Methods and Applications. Developments in Earth Surface Processes. Elsevier, Oxford.

Earl, R., Taylor, J., Wood, G., Bradley, I., James, I.T., Waine, T., Welsh, J., Godwin, R., Knight, S., 2003. Soil factors and their influence on within-field crop variability, part I: field observation of soil variation. Biosystems engineering, 84(4), 425-440.

Emili, L.A., Price, J.S., Fitzgerald, D.F., 2006. Hydrogeological influences on forest community type along forest-peatland complexes in coastal British Columbia. Canadian journal of forest research, 36(8), 2024-2037.

Everett, M., 2012. GEOP: Near-Surface Geophysics. Teaching Material. Texas A&M University

Field, J.P., Breshears, D.D., Law, D.J., Villegas, J.C., López-Hoffman, L., Brooks, P.D., Chorover, J., Barron-Gafford, G.A., Gallery, R.E., Litvak, M.E., Lybrand, R.A., McIntosh, J.C., Meixner, T., Niu, G.-Y., Papuga, S.A., Pelletier, J.D., Rasmussen, C.R., Troch, P.A., 2015. Critical Zone Services: Expanding Context, Constraints, and Currency beyond Ecosystem Services. gsvadzone, 14(1), -.

Florinsky, I.V., 2012. Digital terrain analysis in soil science and geology. Academic Press.

Franchini, M., Wendling, J., Obled, C., Todini, E., 1996. Physical interpretation and sensitivity analysis of the TOPMODEL. Journal of Hydrology, 175(1–4), 293-338.

Gessler, P.E., Chadwick, O.A., Chamran, F., Althouse, L., Holmes, K., 2000. Modeling Soil–Landscape and Ecosystem Properties Using Terrain Attributes. Soil Science Society of America Journal, 64(6), 2046-2056.

Gessler, P.E., Moore, I.D., McKenzie, N.J., Ryan, P.J., 1995. Soil-landscape modelling and spatial prediction of soil attributes. International Journal of Geographical Information Systems, 9(4), 421-432.

Giger, D., Schmitt, G., 1993. Soil Survey of Sierra National Forest, California. USDA Forest Service, University of California Agricultural Experiment Station, Soil Conservation Service.

Gillin, C.P., Bailey, S.W., McGuire, K.J., Gannon, J.P., 2015. Mapping of hydropedologic spatial patterns in a steep headwater catchment. Soil Science Society of America Journal, 79(2), 440-453.

Gleeson, T., Novakowski, K., 2009. Identifying watershed-scale barriers to groundwater flow: Lineaments in the Canadian Shield. Geological Society of America Bulletin, 121(3-4), 333-347.

Goovaerts, P., 1999. Using elevation to aid the geostatistical mapping of rainfall erosivity. Catena, 34(3), 227-242.

Goudie, A., Anderson, M., Burt, T., Lewin, J., Richards, K., Whalley, B., Worsley, P. (Eds.), 1990. Geomorphological Techniques Routledge.

Grayson, R.B., Blöschl, G., Western, A.W., McMahon, T.A., 2002. Advances in the use of observed spatial patterns of catchment hydrological response. Advances in Water Resources, 25(8–12), 1313-1334.

Guo, Q., 2011. Critical Zone Observatory LiDAR, NCALM, Merced.

Gustavsson, M., Seijmonsbergen, A.C., Kolstrup, E., 2008. Structure and contents of a new geomorphological GIS database linked to a geomorphological map—With an example from Liden, central Sweden. Geomorphology, 95(3), 335-349.

Guzzetti, F., Mondini, A.C., Cardinali, M., Fiorucci, F., Santangelo, M., Chang, K.-T., 2012. Landslide inventory maps: New tools for an old problem. Earth-Science Reviews, 112(1–2), 42-66.

Gyssels, G., Poesen, J., Bochet, E., Li, Y., 2005. Impact of plant roots on the resistance of soils to erosion by water: a review. Progress in Physical Geography, 29(2), 189-217.

Hahm, W.J., Riebe, C.S., Lukens, C.E., Araki, S., 2014. Bedrock composition regulates mountain ecosystems and landscape evolution. Proceedings of the National Academy of Sciences, 111(9), 3338-3343.

Hammond, E.H., 1964. Analysis of Properties in Landform Geography: An Application to Broad-scale Landform Mapping. Annals of the Association of American Geographers, 54(1), 11-19.

Harrell, F.E., 2013. Regression modeling strategies: with applications to linear models, logistic regression, and survival analysis. Springer Science & Business Media.

Harrison, R., Richter, D., Fox, T., 2011. Deep soils. Forest Science, 57(1), 1.

Heimsath, A.M., Dietrich, W.E., Nishiizumi, K., Finkel, R.C., 1997. The soil production function and landscape equilibrium. Nature, 388(6640), 358-361.

Heimsath, A.M., E. Dietrich, W., Nishiizumi, K., Finkel, R.C., 1999. Cosmogenic nuclides, topography, and the spatial variation of soil depth. Geomorphology, 27(1–2), 151-172.

Heimsath, A.M., Furbish, D.J., Dietrich, W.E., 2005. The illusion of diffusion: Field evidence for depth-dependent sediment transport. Geology, 33(12), 949-952.

Hengl, T., Heuvelink, G., Stein, A., 2004. A generic framework for spatial prediction of soil variables based on regression-kriging. Geoderma, 120(1), 75-93.

Holbrook, W.S., Riebe, C.S., Elwaseif, M., Hayes, J., Reeder, K., Harry, D., Malazian, A., Dosseto, A., Hartsough, P., Hopmans, J., 2013. Geophysical constraints on deep weathering and water storage potential in the Southern Sierra Critical Zone Observatory. Earth Surface Processes and Landforms, n/a-n/a.

Hopp, L., McDonnell, J.J., 2009. Connectivity at the hillslope scale: Identifying interactions between storm size, bedrock permeability, slope angle and soil depth. Journal of Hydrology, 376(3–4), 378-391.

Horn, B.K., 1981. Hill shading and the reflectance map. Proceedings of the IEEE, 69(1), 14-47.

Huisman, J., Hubbard, S., Redman, J., Annan, A., 2003. Measuring soil water content with ground penetrating radar. Vadose zone journal, 2(4), 476-491.

Hunsaker, C.T., Neary, D.G., 2012. Sediment loads and erosion in forest headwater streams of the Sierra Nevada, California, Proceedings of a workshop for the International Association of Hydrological Sciences, General Assembly in

Melbourne. Revisiting Experimental Catchment Studies in Forest Hydrology. Wallingford, United Kingdom, pp. 195-204.

Hunsaker, C.T., Whitaker, T.W., Bales, R.C., 2012. Snowmelt Runoff and Water Yield Along Elevation and Temperature Gradients in California's Southern Sierra Nevada1. JAWRA Journal of the American Water Resources Association, no-no.

Irvin, B.J., Ventura, S.J., Slater, B.K., 1997. Fuzzy and isodata classification of landform elements from digital terrain data in Pleasant Valley, Wisconsin. Geoderma, 77(2), 137-154.

Iwahashi, J., Pike, R.J., 2007. Automated classifications of topography from DEMs by an unsupervised nested-means algorithm and a three-part geometric signature. Geomorphology, 86(3), 409-440.

James, L.A., Watson, D.G., Hansen, W.F., 2007. Using LiDAR data to map gullies and headwater streams under forest canopy: South Carolina, USA. CATENA, 71(1), 132-144.

Jayawickreme, D.H., Jobbágy, E.G., Jackson, R.B., 2014. Geophysical subsurface imaging for ecological applications. New Phytologist, 201(4), 1170-1175.

Jenson, S.K., Domingue, J.O., 1988. Extracting topographic structure from digital elevation data for geographic information system analysis. Photogrammetric engineering and remote sensing, 54(11), 1593-1600.

Jessup, B.S., Jesse Hahm, W., Miller, S.N., Kirchner, J.W., Riebe, C.S., 2011. Landscape response to tipping points in granite weathering: The case of stepped topography in the Southern Sierra Critical Zone Observatory. Applied Geochemistry, 26, Supplement(0), S48-S50.

Johnson, D., Hunsaker, C., Glass, D., Rau, B., Roath, B., 2011. Carbon and nutrient contents in soils from the Kings River Experimental Watersheds, Sierra Nevada Mountains, California. Geoderma, 160(3), 490-502.

Johnson, D.W., Curtis, P.S., 2001. Effects of forest management on soil C and N storage: meta analysis. Forest Ecology and Management, 140(2–3), 227-238.

Katsuyama, M., Ohte, N., Kabeya, N., 2005. Effects of bedrock permeability on hillslope and riparian groundwater dynamics in a weathered granite catchment. Water Resources Research, 41(1), W01010.

Kneisel, C., Lehmkuhl, F., Winkler, S., Tressel, E., Schröder, H., 1998. Legende für geomorphologische Kartierungen in Hochgebirgen (GMK Hochgebirge). Geographische Ges.

Knighton, D., 2014. Fluvial forms and processes: a new perspective. Routledge.

Kottek, M., Grieser, J., Beck, C., Rudolf, B., Rubel, F., 2006. World Map of the Köppen-Geiger climate classification. Meteorologische Zeitschrift, 15(3), 259-263.

Kristensen, T., Ohlson, M., Bolstad, P., Nagy, Z., 2015. Spatial variability of organic layer thickness and carbon stocks in mature boreal forest stands—implications and suggestions for sampling designs. Environmental monitoring and assessment, 187(8), 1-19.

Krüger, J., Franko, U., Fank, J., Stelzl, E., Dietrich, P., Pohle, M., Werban, U., 2013. Linking geophysics and soil function modeling—An application study for biomass production. Vadose Zone Journal, 12(4).

Kuriakose, S.L., Devkota, S., Rossiter, D.G., Jetten, V.G., 2009. Prediction of soil depth using environmental variables in an anthropogenic landscape, a case study in the Western Ghats of Kerala, India. CATENA, 79(1), 27-38.

Laamrani, A., Valeria, O., Cheng, L.Z., Bergeron, Y., Camerlynck, C., 2013. The use of ground penetrating radar for remote sensing the organic layer–mineral soil interface in paludified boreal forests. Canadian Journal of Remote Sensing, 39(1), 1-15.

Laffan, S.W., Lees, B.G., 2004. Predicting regolith properties using environmental correlation: a comparison of spatially global and spatially local approaches. Geoderma, 120(3–4), 241-258.

Landi, A., Mermut, A., Anderson, D., 2004. Carbon distribution in a hummocky landscape from Saskatchewan, Canada. Soil Science Society of America Journal, 68(1), 175-184.

Langbein, W.B., 1947. Topographic characteristics of drainage basins. US Government Printing Office.

Li, J., Heap, A.D., 2011. A review of comparative studies of spatial interpolation methods in environmental sciences: performance and impact factors. Ecological Informatics, 6(3), 228-241.

Lin, H., 2010. Earth's critical zone and hydropedology: Concepts, characteristics, and advances. Hydrology and Earth System Sciences, 14, 25-45.

Liu, F., Hunsaker, C., Bales, R.C., 2012. Controls of streamflow generation in small catchments across the snow–rain transition in the Southern Sierra Nevada, California. Hydrological Processes, n/a-n/a.

Lockwood, J.P., Moore, J.G., 1979. Regional deformation of the Sierra Nevada, California, on conjugate microfault sets. Journal of Geophysical Research: Solid Earth (1978–2012), 84(B11), 6041-6049.

Lunt, I., Hubbard, S., Rubin, Y., 2005. Soil moisture content estimation using ground-penetrating radar reflection data. Journal of Hydrology, 307(1), 254-269.

MacMillan, R., Pettapiece, W., Brierley, J., 2005. An expert system for allocating soils to landforms through the application of soil survey tacit knowledge. Canadian journal of soil science, 85(1), 103-112.

MacMillan, R., Pettapiece, W., Nolan, S., Goddard, T., 2000. A generic procedure for automatically segmenting landforms into landform elements using DEMs, heuristic rules and fuzzy logic. Fuzzy Sets and Systems, 113(1), 81-109.

MacMillan, R., Shary, P., 2009. Landforms and landform elements in geomorphometry. Developments in soil science, 33, 227-254.

Manning, G., Fuller, L., Eilers, R., Florinsky, I., 2001. Topographic influence on the variability of soil properties within an undulating Manitoba landscape. Canadian Journal of Soil Science, 81(4), 439-447.

Martin, W., Timmer, V., 2006. Capturing spatial variability of soil and litter properties in a forest stand by landform segmentation procedures. Geoderma, 132(1), 169-181.

McBratney, A.B., Mendonça Santos, M.L., Minasny, B., 2003. On digital soil mapping. Geoderma, 117(1–2), 3-52.

McClymont, A., Hayashi, M., Bentley, L., Muir, D., Ernst, E., 2010. Groundwater flow and storage within an alpine meadow-talus complex. Hydrology and Earth System Sciences, 14(6), 859-872.

McDonnell, J., Sivapalan, M., Vaché, K., Dunn, S., Grant, G., Haggerty, R., Hinz, C., Hooper, R., Kirchner, J., Roderick, M., 2007. Moving beyond heterogeneity and process complexity: A new vision for watershed hydrology. Water Resources Research, 43(7).

McKenzie, N.J., Ryan, P.J., 1999. Spatial prediction of soil properties using environmental correlation. Geoderma, 89(1–2), 67-94.

Migon, P., 2006. Granite landscapes of the world. Oxford University Press Oxford, New York.

Minasny, B., McBratney, A.B., 2006. Mechanistic soil–landscape modelling as an approach to developing pedogenetic classifications. Geoderma, 133(1), 138-149.

Mitasova, H., Hofierka, J., 1993. Interpolation by regularized spline with tension: II. Application to terrain modeling and surface geometry analysis.

Mohawesh, Y., Taimeh, A., Ziadat, F., 2015. Effects of land use changes and soil conservation intervention on soil properties as indicators for land degradation under a Mediterranean climate.

Moore, I.D., Gessler, P.E., Nielsen, G.A., Peterson, G.A., 1993. Soil Attribute Prediction Using Terrain Analysis. Soil Sci. Soc. Am. J., 57(2), 443-452.

Moorman, B., 2001. Ground-Penetrating Radar Applications in Paleolimnology. In: W. Last, J. Smol (Eds.), Tracking Environmental Change Using Lake Sediments. Developments in Paleoenvironmental Research. Springer Netherlands, pp. 23-47.

Morgan, J., Lesh, A.M., 2005. Developing landform maps using ESRI'S Model-Builder, ESRI International User Conference.

Musselman, K.N., Molotch, N.P., Margulis, S.A., Kirchner, P.B., Bales, R.C., 2012. Influence of canopy structure and direct beam solar irradiance on snowmelt rates in a mixed conifer forest. Agricultural and Forest Meteorology, 161, 46-56.

Mysaiah, D., Maheswari, K., Rao, M.S., Kumar, P.S., Seshunarayana, T., 2011. Ground-penetrating radar applied to imaging sheet joints in granite bedrock. Current science, 100(4), 473-475.

Neal, A., Roberts, C.L., 2000. Applications of ground-penetrating radar (GPR) to sedimentological, geomorphological and geoarchaeological studies in coastal environments. Geological Society, London, Special Publications, 175(1), 139-171.

Nicótina, L., Tarboton, D.G., Tesfa, T.K., Rinaldo, A., 2011. Hydrologic controls on equilibrium soil depths. Water Resour. Res., 47(4), W04517.

Odeh, I.O.A., McBratney, A.B., Chittleborough, D.J., 1995. Further results on prediction of soil properties from terrain attributes: heterotopic cokriging and regression-kriging. Geoderma, 67(3–4), 215-226.

Olaya, V., 2009. Basic land-surface parameters. Developments in Soil Science, 33, 141-169.

Ollier, C., 1971. Causes of spheroidal weathering. Earth-Science Reviews, 7(3), 127-141.

Otto, J.-C., Dikau, R., 2004. Geomorphologic system analysis of a high mountain valley in the Swiss Alps. Zeitschrift für Geomorphologie, NF, 323-341.

Otto, J.-C., Smith, M.J., 2013. Geomorphological mapping. British Society for Geomorphology.

Pacheco, F.A.L., Alencoão, A.M.P., 2006. Role of fractures in weathering of solid rocks: narrowing the gap between laboratory and field weathering rates. Journal of Hydrology, 316(1–4), 248-265.

Papadaki, E.S., Mertikas, S.P., Sarris, A., 2011. Identification of lineaments with possible structural origin using ASTER images and DEM derived products in Western Crete, Greece. EARSeL eProceedings, 10(1), 10.

Park, S.J., Burt, T.P., 2002. Identification and Caractherization of Pedogeomorphological Processes on a Hillslope. American Society of Agronomy, 66, 1897-1910.

Pennock, D., Anderson, D., De Jong, E., 1994. Landscape-scale changes in indicators of soil quality due to cultivation in Saskatchewan, Canada. Geoderma, 64(1-2), 1-19.

Pennock, D.J., 2003. Terrain attributes, landform segmentation, and soil redistribution. Soil and Tillage Research, 69(1–2), 15-26.

Pérez-Peña, J.V., Azañón, J.M., Azor, A., 2009. CalHypso: An ArcGIS extension to calculate hypsometric curves and their statistical moments. Applications to drainage basin analysis in SE Spain. Computers & Geosciences, 35(6), 1214-1223.

Phillips, J.D., 2008. Soil system modelling and generation of field hypotheses. Geoderma, 145(3–4), 419-425.

Pike, R., Evans, I., Hengl, T., 2009. Geomorphometry: a brief guide. Geomorphometry: concepts, software, applications, 33, 3-30.

Quinn, P., Beven, K., Chevallier, P., Planchon, O., 1991. The prediction of hillslope flow paths for distributed hydrological modelling using digital terrain models. Hydrological Processes, 5(1), 59-79.

Regmi, N.R., 2010. Hillslope Dynamics in the Paonia-McClure Pass Area, Colorado, USA, Texas A&M University.

Rejman, J., Rafalska-Przysucha, A., Rodzik, J., 2014. The Effect of Land Use Change on Transformation of Relief and Modification of Soils in Undulating Loess Area of East Poland. The Scientific World Journal.

Riebe, C.S., Chorover, J., 2014. Report on Drilling, Sampling, and Imaging the Depths of the Critical Zone, an NSF Workshop.

Roos, M., Sahota, S., 2010. Contrasting Snowpack Trends in the Sierra Nevada of California.

Ross, D.C., 1989. Air photo lineaments, southern Sierra Nevada, California, U.S. Geological Survey.

Ruszkiczay-Rüdiger, Z., Fodor, L., Horváth, E., Telbisz, T., 2009. Discrimination of fluvial, eolian and neotectonic features in a low hilly landscape: A DEM-based morphotectonic analysis in the Central Pannonian Basin, Hungary. Geomorphology, 104(3–4), 203-217.

Rutzinger, M., Maukisch, M., Petrini-Monteferri, F., Stötter, J., 2007. Development of algorithms for the extraction of linear patterns (lineaments) from airborne laser scanning data. na.

Ryan, P.J., McKenzie, N.J., O'Connell, D., Loughhead, A.N., Leppert, P.M., Jacquier, D., Ashton, L., 2000. Integrating forest soils information across scales: spatial prediction of soil properties under Australian forests. Forest Ecology and Management, 138(1–3), 139-157.

Saco, P.M., Willgoose, G.R., Hancock, G.R., 2006. Spatial organization of soil depths using a landform evolution model. Journal of Geophysical Research: Earth Surface (2003–2012), 111(F2).

Šamonil, P., Král, K., Hort, L., 2010. The role of tree uprooting in soil formation: a critical literature review. Geoderma, 157(3), 65-79.

Saulnier, G.M., Beven, K., Obled, C., 1997. Including spatially variable effective soil depths in TOPMODEL. Journal of Hydrology, 202(1-4), 158-172.

Schoeneberger, P.J., 2002. Field book for describing and sampling soils, Version 3.0. Government Printing Office.

Scull, P., Franklin, J., Chadwick, O., McArthur, D., 2003. Predictive soil mapping: a review. Progress in Physical Geography, 27(2), 171-197.

Shafique, M., Van der Meijde, M., Rossiter, D.G., 2011. Geophysical and remote sensing-based approach to model regolith thickness in a data-sparse environment. Catena, 87(1), 11-19.

Sharpnack, D.A., Akin, G., 1969. An algorithm for computing slope and aspect from elevations. Photogrammetric Engineering and Remote Sensing, 35(3), 247–248.

Shi, X., 2013. ArcSIE user's guide. Available in:< http://www. arcsie. com/index. htm> Acessed on: Jun, 4.

Skidmore, A.K., Watford, F., Luckananurug, P., Ryan, P., 1996. An operational GIS expert system for mapping forest soils. Photogrammetric Engineering and Remote Sensing, 62(5), 501-511.

Slater, L., Comas, X., 2009. The contribution of ground penetrating radar to water resource research. Ground Penetrating Radar: Theory and Applications, 203-246.

Smith, M.J., 2011. Digital mapping: Visualisation, interpretation and quantification of landforms. Geomorphological mapping, 15, 225-251.

Smith, M.J., Pain, C.F., 2009. Applications of remote sensing in geomorphology. Progress in Physical Geography, 33(4), 568-582.

Smith, M.J., Paron, P., Griffiths, J.S. (Eds.), 2011. Geomorphological Mapping. Methods and Applications. Developments in Earth Surface Processes, 15. Elsevier.

Soil Survey Staff, N.R.C.S., 2013. Websoil Survey - Available online at http://websoilsurvey.nrcs.usda.gov/. United States Department of Agriculture.

Stepinski, T.F., Ghosh, S., Vilalta, R., 2006. Automatic recognition of landforms on Mars using terrain segmentation and classification, Discovery Science. Springer, pp. 255-266.

Steyerberg, E.W., Harrell, F.E., Borsboom, G.J., Eijkemans, M., Vergouwe, Y., Habbema, J.D.F., 2001. Internal validation of predictive models: efficiency of some procedures for logistic regression analysis. Journal of clinical epidemiology, 54(8), 774-781.

Strahler, A.N., 1952. Hypsometric (area-altitude) analysis of erosional topography. Geological Society of America Bulletin, 63(11), 1117-1142.

Sucre, E.B., Tuttle, J.W., Fox, T.R., 2011. The use of ground-penetrating radar to accurately estimate soil depth in rocky forest soils. Forest Science, 57(1), 59.

Tague, C., 2008. Interacting controls on eco-hydrologic responses to warming in mountain ecosystems, AGU Fall Meeting Abstracts, pp. 02.

Tague, C.L., Band, L.E., 2004. RHESSys: Regional Hydro-Ecologica Simulation System- An Object Oriented Approach to Spatially Distributed Modelling of Carbon, Water, and Nutrient Cycling. Earth Interactions, 8(19), 1-42.

Tesfa, T., Tarboton, D., Chandler, D., McNamara, J., 2010. A Generalized Additive Soil Depth Model for a Mountainous Semi-Arid Watershed Based Upon Topographic and Land Cover Attributes. Digital Soil Mapping, 29-41.

Tesfa, T.K., Tarboton, D.G., Chandler, D.G., McNamara, J.P., 2009. Modeling soil depth from topographic and land cover attributes. Water Resour. Res., 45(10), W10438.

Theler, D., Reynard, E., 2011. Chapter Sixteen- A Geomorphological Map as a Tool for Assessing Sediment Transfer Processes in Small Catchments Prone to Debris-Flows Occurrence: A Case Study in the Bruchi Torrent(Swiss Alps). Developments in Earth Surface Processes, 15, 443-458.

Thornbury, W.D., 1965. Chapter 25: Sierra-Cascade Province, Regional geomorphology of the United States. John Wiley & Sons New York pp. 506:527.

Tromp-van Meerveld, H.J., McDonnell, J.J., 2006. On the interrelations between topography, soil depth, soil moisture, transpiration rates and species distribution at the hillslope scale. Advances in Water Resources, 29(2), 293-310.

Turner, M.G., 2010. Disturbance and landscape dynamics in a changing world. Ecology, 91(10), 2833-2849.

Twidale, C., 1982. Granitic landforms. Amsterdam.

Twidale, C.R., Romaní, J.R.V., 2010. Landforms and geology of granite terrains. CRC Press.

USDA, N., 2012. Custom Soil Resource Report for Sierra National Forest Areas Parts of Fresno, California - Providence Arriba, USDA, NRCS Web Soil Survey

Vanwalleghem, T., Poesen, J., McBratney, A., Deckers, J., 2010. Spatial variability of soil horizon depth in natural loess-derived soils. Geoderma, 157(1–2), 37-45.

Ventura, S., Irvin, B., 2000. Automated landform classification methods for soil-landscape studies. Terrain analysis: Principles and applications, 267-294.

Verstappen, H.T., 1983. Applied Geomorphology. Geomorphological Surveys for Environmental Development. Elsevier, New York.

Verstappen, H.T., 2011. Old and New Trends in Geomorphological and Landform Mapping. In: M.J. Smith, P. Paron, J.S. Griffiths (Eds.), Geomorphological Mapping. Methods and Applications. Developments in Earth Surface Processes. Elsevier, Oxford.

Vreeken, W., 1975. Variability of depth to carbonates in fingertip loess watersheds in Iowa. Catena, 2, 321-336.

Wahrhaftig, C., 1965. Stepped Topography of the Southern Sierra Nevada, California. Geological Society of America Bulletin, 76(10), 1165-1190.

Weiler, M., McDonnell, J., 2004. Virtual experiments: a new approach for improving process conceptualization in hillslope hydrology. Journal of Hydrology, 285(1–4), 3-18.

Weixelman, D., Hill, B., Cooper, D., Berlow, E., Viers, J., Purdy, S., Merrill, A., Gross, S., 2011. A field key to meadow hydrogeomorphic types for the Sierra Nevada and southern Cascade Ranges in California. US Forest Service, Pacific Southwest Region, Vallejo, California, USA.

Wigmosta, M.S., Vail, L.W., Lettenmaier, D.P., 1994. A distributed hydrology-vegetation model for complex terrain. Water Resour. Res., 30(6), 1665-1679.

Wilkinson, M.T., Richards, P.J., Humphreys, G.S., 2009. Breaking ground: Pedological, geological, and ecological implications of soil bioturbation. Earth-Science Reviews, 97(1–4), 257-272.

Wilson, J.P., Gallant, J.C., 2000. Digital terrain analysis. Terrain analysis: Principles and applications, 1-27.

Winter, T.C., 2001. The Concept of Hydrological Landscapes 1 JAWRA Journal of the American Water Resources Association, 37(2), 335-349.

Woodward, C., Johnson, D.W., Meadows, M.W., Miller, W.W., Hynes, M.M., Robertson, C.M., 2013. Nutrient hot spots in a Sierra Nevada forest soil: Temporal characteristics and relations to microbial communities. Soil Science, 178(11), 585-595.

Wu, W., Sidle, R.C., 1995. A distributed slope stability model for steep forested basins. Water Resources Research, 31(8), 2097-2110.

Yamakawa, Y., Kosugi, K.i., Masaoka, N., Sumida, J., Tani, M., Mizuyama, T., 2012. Combined geophysical methods for detecting soil thickness distribution on a weathered granitic hillslope. Geomorphology, 145–146(0), 56-69.

Yelf, R., 2004. Where is true time zero?, Ground Penetrating Radar, 2004. GPR 2004. Proceedings of the Tenth International Conference on. IEEE, pp. 279-282.

Young, F.J., Hammer, R.D., 2000. Defining Geographic Soil Bodies by Landscape Position, Soil Taxonomy, and Cluster Analysis Contribution from the Missouri Agric. Exp. Stn. J. Series No. 12,451. Soil Sci. Soc. Am. J., 64(3), 989-998.

Zebarth, B.J., Rees, H., Walsh, J., Chow, L., Pennock, D.J., 2002. Soil variation within a hummocky podzolic landscape under intensive potato production. Geoderma, 110(1–2), 19-33.

Zevenbergen, L.W., Thorne, C.R., 1987. Quantitative analysis of land surface topography. Earth Surface Processes and Landforms, 12(1), 47-56.

Zhao, Y., Peth, S., Krümmelbein, J., Horn, R., Wang, Z., Steffens, M., Hoffmann, C., Peng, X., 2007. Spatial variability of soil properties affected by grazing intensity in Inner Mongolia grassland. Ecological Modelling, 205(1), 241-254.

Zhu, A.-X., Qi, F., Moore, A., Burt, J.E., 2010. Prediction of soil properties using fuzzy membership values. Geoderma, 158(3), 199-206.

Zhu, A.X., Hudson, B., Burt, J., Lubich, K., Simonson, D., 2001. Soil Mapping Using GIS, Expert Knowledge, and Fuzzy Logic. Soil Sci. Soc. Am. J., 65(5), 1463-1472.

Zribi, L., Mouillot, F., Gharbi, F., Ourcival, J.-M., Hanchi, B., 2015. Warm and Fertile Sub-Humid Conditions Enhance Litterfall to Sustain High Soil Respiration Fluxes in a Mediterranean Cork Oak Forest. Forests, 6(9), 2918-2940.

APPENDIX

The structure of the Geomorphological GIS database